CCAP
Centre for the Clinical Application of Particles

Nuclear diagnostics and Magnetic Resonance Imaging

K. Long
Imperial College London/STFC
K.Long@Imperial.ac.uk

Drawing heavily on material prepared in 2018/19 by J. Pozimski

May 4, 2020

Contents

Section 1

Introduction

Aims

With the course I aim to:

- Provide students with a general overview of the physical principles that underlie nuclear diagnostics (ND) and magnetic resonance imaging (MRI);
- Allow students to appreciate the factors that influence the development of contrast in ND and MRI; and
- Give students the means to estimate the resolution, speed, and sensitivity of ND and MRI imaging modalities.

Objectives 1: radionuclides and gamma camera

At the end of the course students will be able to:

- Explain the principal methods used for the production of radionuclides;
- Explain and apply the definitions of activity, half-life and decay constant;
- Calculate the energies of the particles involved in radioactive decay in a given situation;
- Explain the principal radioactive decay pathways and the application of the radiation produced to medical imaging;
- Explain how a gamma camera operates and discuss the main parameters that affect its performance;
- Calculate the resolution and efficiency of a gamma camera in a particular situation; and
- Explain the different types of event that can be recorded by using a gamma camera and discuss how these affect the image.

Objectives 2: SPECT and PET

At the end of the course students will be able to:

- Explain how Single Photon Emission Computed Tomography (SPECT) is performed;
- Explain the methods typically used in the reconstruction of a SPECT images;
- Explain how a Positron Emission Tomography (PET) image is produced and discuss the principal limitations of PET;
- Discuss the different types of detection events recorded by a PET system and how they affect the image;
- Calculate the resolution, detection efficiency, detection rate, and coincidence rate for a particular PET scanner;
- Explain how to compensate for attenuation and unwanted random and scatter events in PET; and
- Describe and discuss the main differences between 2D and 3D PET image acquisition

Objectives 3: Magnetic resonance imaging

At the end of the course students will be able to:

- Describe the principles of nuclear magnetic resonance (NMR);
- Discuss how relaxation mechanisms contribute to the generation of contrast in magnetic resonance imaging (MRI);
- Describe techniques for spatial localisation of the NMR signals in MRI;
- Distinguish between phase and frequency encoding is used in MRI to enable the spatial localisation of the NMR signal;
- Use the Fourier-transform technique to exploit 'k-space' to describe MRI images in this space;
- Connect the receiver bandwidth, acquisition time, and sampling frequency to the field of view and resolution;
- Identify the causes of the most common image artefacts;
- Show how the signal-to-noise ratio (SNR) is affected by the choice of data acquisition parameters;
- Recall the major hardware components necessary for MRI;
- Recall, devise, and interpret typical MRI pulse sequences and discuss the changes in image contrast induced by changes in the pulse sequences; and
- Calculate the optimal 'TR' and 'TE' to maximise image contrast for 'proton density', 'T1', and 'T2' weighted imaging.

Recommended books

Physics in Nuclear Medicine
S. Cherry, J.A. Sorenson, M.E. Phelps
Central Library: 616.075 CHE

The Essential Physics of Medical Imaging
J. Bushberg, J. Seibert, E. Leidholdt, J. Boone
Central Library: 616.075 BUS

MRI: the basics
R. Hasgemi, W. Bradley, C. Lisanti
Central Library: 616.075 HAS

Section 2

Nuclear diagnostics

What is 'nuclear diagnostics'?

Imaging using radio-isotopes:

- Introduce radionuclide into the body:
  - A 'radiotracer' is usually introduced into the body on a 'radiophamaceutical';
  - Detectors external to body used to 'image' distribution of radiotracer within body;
  - Spatial distribution depends on 'take-up' of radiopharmaceutical in tissue.
- ND usually 'emission imaging' ...
  to be contrasted with conventional x-ray imaging which is 'transmission imaging'.

Sensitivity!

- Goal is to use such a small amount of radiotracer that biological system under investigation is not perturbed.

Radiopharmaceuticals

Enormous field! Beyond the scope of this course.

Consider the radiopharmaceutical as a means of delivering an isotope to a particular location:

- Compound tagged with a radionuclide;
- Accumulation, rate of uptake and clearance related to physiological, biochemical and/or molecular processes;
- Carrier molecule designed to target organ or function;
- Radionuclide required to produce emissions that can be detected outside the body;:
  - Require penetrating radiation: primary gammas, photons produced in positron annihilation;
- Radiouclides delivered in tiny amounts: nanograms:
  - Require sensitive detectors.
- Administration:
  - Intravenous, inhalation, subcutaneous, oral

Radiopharmaceuticals: an example

Delivering ^{18}F, and exploitation in diagnosis of Alzheimer's disease using PET.

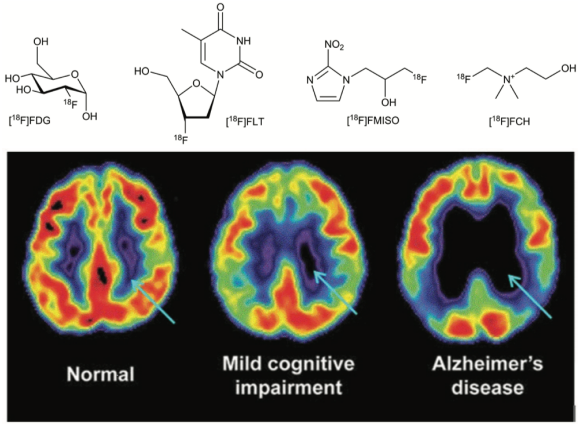

http://real.mtak.hu/41305/1/225_247_BRC_2015_Vol_2.pdf

Radioactivity '101'

- Radioactivity is an intrinsic property of unstable nuclei;
- Quantum-mechanical process: uniform probability of decay;
- Radioactive decays:
  - Electromagnetic: de-excitation yielding photons . . . gammas;
  - Weak:
    - $N \rightarrow N' + e^- + \bar{\nu}_e$
    - $N \rightarrow N' + e^+ + \nu_e$ $\leftarrow$ the basis of PET.
  - Strong: e.g. α-decay; not of use for ND.
- Isotopes have the same number of protons;
- Isotones have the same number of neutrons;
- Isobars have the same number of nucleons.

Nuclei and decay modes

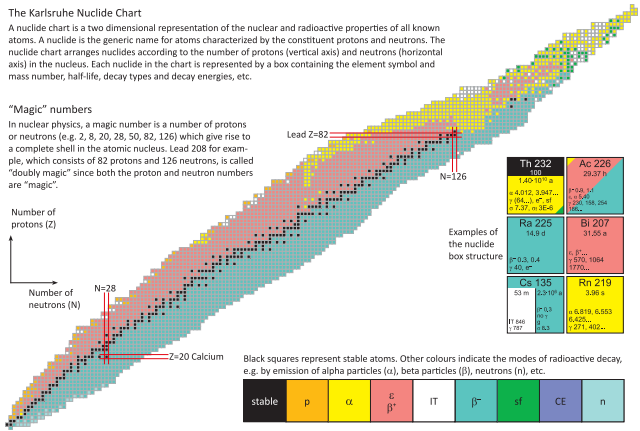

https://www.epj-n.org/articles/epjn/full_html/2019/01/epjn180014/epjn180014.html

Radioactive decay

For a single nucleus, probability of decay per unit time is constant:

$$\frac{dP}{dt} = -\lambda$$

So, probability that nucleus will eventually decay is 1.
If there are N nuclei at time t:

$$\frac{dN}{dt} = -\lambda N \qquad \ldots \text{and so} \ldots \qquad N(t) = N(0)\exp(-\lambda t)$$

λ is the decay constant. The 'halflife', $t_{\frac{1}{2}}$, is related to the 'lifetime', τ, and λ by:

$$t_{\frac{1}{2}} = \frac{\ln(2)}{2}\tau = \frac{\ln(2)}{2}\frac{1}{\lambda}$$

Activity

Activity: $A = \left|\frac{dN}{dt}\right| = \gamma N$

- SI unity of activity: Becquerel (Bq):
  - $1\,\text{Bq} = 1$ decay per second
- Curie (Ci):
  - $1\,\text{Ci} = 3.7 \times 10^{10}\,\text{Bq}$

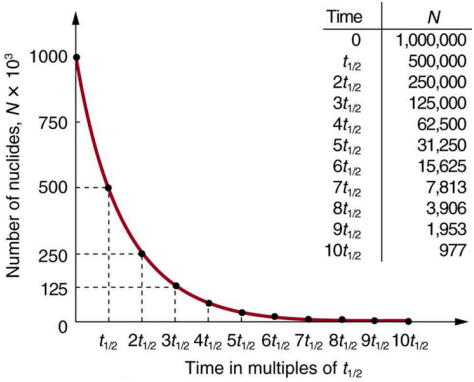

Time	N
0	1,000,000
$t_{1/2}$	500,000
$2t_{1/2}$	250,000
$3t_{1/2}$	125,000
$4t_{1/2}$	62,500
$5t_{1/2}$	31,250
$6t_{1/2}$	15,625
$7t_{1/2}$	7,813
$8t_{1/2}$	3,906
$9t_{1/2}$	1,953
$10t_{1/2}$	977

https://courses.lumenlearning.com/physics/chapter/31-5-half-life-and-activity/

β decay

Underlying process: $n \rightarrow p + e^- + \bar{\nu}_e$

$$ {}^{A}_{Z}X \xrightarrow{e^-(\beta^-)} {}^{A}_{Z+1}Y $$

$$ {}^{A}_{Z}X + e^- \rightarrow {}^{A}_{Z+1}Y + e^- + \bar{\nu}_e $$

Kinematics requires neutral atoms, hence e^- on LHS.

Continuous electron-energy spectrum due to 3-body decay.

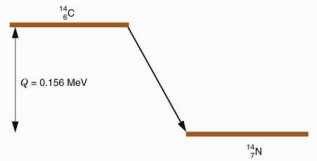

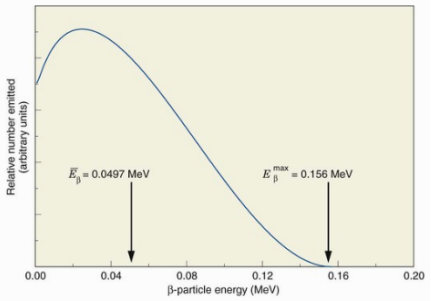

(β, γ) decay

β absorbed in short distance; no use for ND.
Exploit de-excitation γs.

$$ {}^{A}_{Z}X \xrightarrow{\beta^-} {}^{A}_{Z+1}Y^* \xrightarrow{\gamma} {}^{A}_{Z+1}Y $$

β-decay leaves Y in excited state—indicated by '*'.

Discrete photon energy or energies.

Electron from β decay absorbed in tissue.

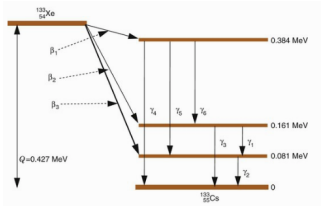

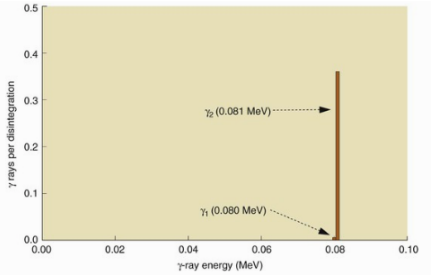

Isomeric transition (IT)

Daughter nuclide produced in long-lived, 'metastable' state.
Again, exploit de-excitation γs.

$$ {}^{A}_{Z}X \xrightarrow{\beta^-} {}^{Am}_{Z+1}Y \xrightarrow{\gamma} {}^{A}_{Z+1}Y $$

β-decay leaves Y in metastable excited state—indicated by 'm'.

Discrete photon energy or energies.

IT identical to decay by γ production, except that lifetime is much longer.

Important example:

$$ {}^{99}Mo \xrightarrow{\beta^-} {}^{99m}Tc \xrightarrow{\gamma} {}^{99}Tc $$

$\tau_{1/2}$ = 66 hrs $\tau_{1/2}$ = 6 hrs

Halflife of ^{99}Tc is 211 millenia:

- Decay rate of ^{99}Tc is low; but
- Clearly important to ensure 'waste' radionuclide is excreted.

Internal conversation (IC)

$$ {}^{A}_{Z}X^{*} \xrightarrow{\text{IC}} {}^{A}_{Z}X + e $$

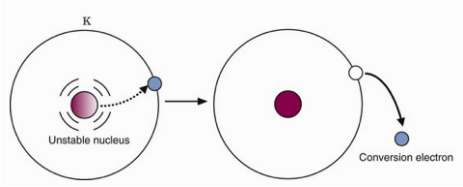

Nucleus in an excited state or a meta-stable excited state may decay such that:

- Energy from nuclear is transition transfered to orbital electron which is emitted;
- Electron emitted has an energy typical of a nuclear transition;
- Orbital vacancy is filled creating characteristic X-rays or Auger electrons.

In a sense, the γ that might have been emitted is 'internally converted' into an electron.

Positron emission

Underlying process: $p \rightarrow n + e^+ + \nu_e$

$$ {}^{A}_{Z}X \xrightarrow{e^+(\beta^+)} {}^{A}_{Z-1}Y $$

$$ {}^{A}_{Z}X \rightarrow {}^{A}_{Z-1}Y + e^- + e^+ + \nu_e $$

Kinematics requires neutral atoms,
hence e^- on RHS.
[Orbital electron 'lost' from atom after decay]

Continuous electron-energy spectrum due to 3-body decay.

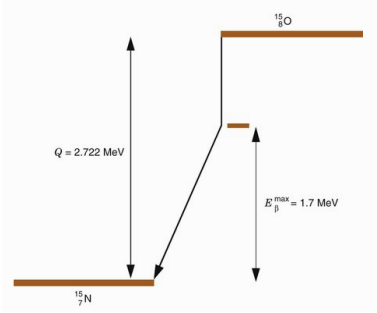

$$
\begin{aligned}
Q &= 2.72\,\mathrm{MeV} \\
&= 2m_e c^2 + E_\beta^{\max} \\
&= 1.022\,\mathrm{MeV} + 1.7\,\mathrm{MeV}
\end{aligned}
$$

Electron capture (EC) and (EC, γ)

Underlying process: $p + e^- \rightarrow n + \nu_e$
Orbital electron is captured by nucleus; transforms proton to neutron.

$$ {}^{A}_{Z}X \xrightarrow{\text{EC}} {}^{A}_{Z-1}Y $$

Orbital vacancy leads to the emission of characteristic X-rays.
Only useful for imaging if X-rays are of high enough energy.

γs or conversion electrons may be emitted: γs have 'MeV-scale' energies are are more likely to be of use for ND.

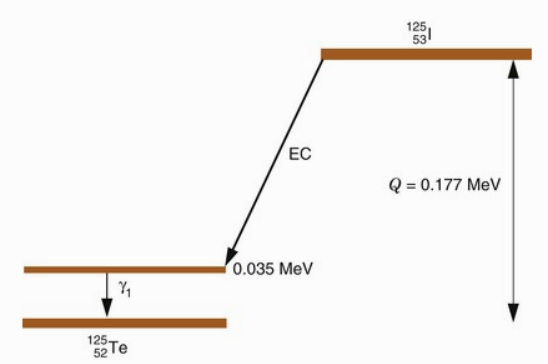

Commonly used radionuclides for imaging in ND

Nuclide	Decay mode	Principle photon emissions	Half-life	Imaging system	Comment
^{11}C	β^+	511 keV	20 min	PET	
^{13}N	β^+	511 keV	10 min	PET	
^{15}O	β^+	511 keV	2 min	PET	
^{18}F	β^+	511 keV	110 min	PET	80% of all PET imaging is of glucose metabolism (FDG)
^{67}Ga	EC	93, 185, 300 keV	3.3 days	γ-cam, SPECT	
^{82}Rb	β^+	511 keV	1.25 min	PET	
^{99m}Tc (Technetium)	IT	140 keV	6.0 hours	γ-cam, SPECT	70% of all gamma camera imaging
^{111}In (Indium)	EC	172, 247 keV	2.8 days	γ-cam, SPECT	Used for longer term studies
^{123}I (Iodine)	EC	159 keV	13 hours	γ-cam, SPECT	
^{201}Tl (Thallium)	EC	68-80 keV x-rays	3.0 days	γ-cam, SPECT	

A practical matter . . .

A "Goldilocks" problem:

- Lifetime: neither:
  Too long—too small a fraction of decays used for imaging;
  Too short—too small a fraction delivered for imaging
- Practical lifetimes for imaging: minutes (seconds) to days
  - Longer-lived isotopes have applications in therapy
- Decay products 'sufficiently' penetrating:
  - Imaging requires external detection of radiation
- Radiation must emerge from the body:
  - Without leaving an unacceptably large dose . . . and . . .
  - With properties that make it easy to detect . . . and . . .
  - Pointing back to the origin of the radiation

Desirable properties of radioisotopes

- α-emitters are not suitable for imaging;
  Range too small, deposit too much dose
- γ-emitters: γ energy in range $50 < E_\gamma < 600\,\text{keV}$;
  Low-energy photons have large interaction probability so unlikely to leave body, simply deposit dose
- Beta emitters: e^- absorbed or lose energy and scatter, not used for imaging;
  If absorbed, e^- simply deposits dose, reducing rate that could be detected.
  Energy loss and scattering of high-energy e^- destroys pointing accuracy and make e^- hard to detect.
- e^+ emitters exploited in positron-emission tomography;
  Signal (back-to-back photons) from e^+e^- annihilation.

Radiopharmaceuticals – examples

Nuclide	Compound	Measurement	Example of clinical use
^{99m}Tc	^{99m}Tc-methylene diphosphonate (MDP)	Bone metabolism	Metastatic spread of cancer
^{99m}Tc	Sestamibi, Tetrofosmin	Myocardial perfusion	Coronary artery disease
^{99m}Tc	MAG3, DTPA	Renal function	Kidney disease
^{99m}Tc	HMPAO, EDC	Cerebral blood flow	Neurologic disorders
^{131}I	Sodium Iodide	Thyroid function	Thyroid disease
^{67}Ga	Gallium citrate	Sequestered in tumours	Tumour localization
^{111}In	Labelled white blood cells	Sites of infection	Detecting inflammation
^{18}F	Fluorodeoxyglucose	Glucose metabolism	Cancer, neurological disorders and myocardial diseases
^{13}N	Ammonia	Myocardial perfusion	Coronary artery disease

Branching ratio

Decay constant, λ, determines the decay rate. The 'lifetime', τ is defined to be:

$$\tau = \frac{1}{\lambda} \qquad \ldots \text{and so} \ldots \qquad \lambda = \frac{1}{\tau}$$

The decay rate for the transition of X into Y may be calculated using "Fermi's Golden Rule":

$$\lambda_{X \to Y} = \eta \left| M_{X \to Y} \right|^2 \rho_f$$

Where η is a constant and ρ_f is the density of final states. $M_{X \to Y}$ is the quantum-mechanical 'matrix element' for the transition $X \to Y$. Some radionuclides may decay via more than one route. For such nuclei:

$$\frac{dP}{dt} = \frac{dP_{X \to Y}}{dt} + \frac{dP_{X \to Z}}{dt} + \cdots = \lambda_{X \to Y} + \lambda_{X \to Z} + \cdots = \sum_i \lambda_i = \lambda_T$$

λ_T is the 'total decay rate' (sometimes referred to as 'total width'). The λ_i are the 'partial' decay rates, or 'partial widths'.

Branching ratios; an additional constraint

'Branching ratio' (BR): fraction of all decays that result in a particular final state:

$$BR = \frac{\lambda_{X \to Y}}{\lambda_T}$$

Decay chain may include beneficial radiation, suitable for imaging, and harmful radiation.

Example: ^{131}I decay — $^{131}\mathrm{I}(e^-, \gamma)^{131}\mathrm{Xe}$

- Some γs in useful range for imaging, but
- e^- and low-energy γs simply deposit dose.

Has application in therapy, e.g., thyroid tumours.
Not widely used today for imaging.
So, consider ^{123}I, which decays via EC.

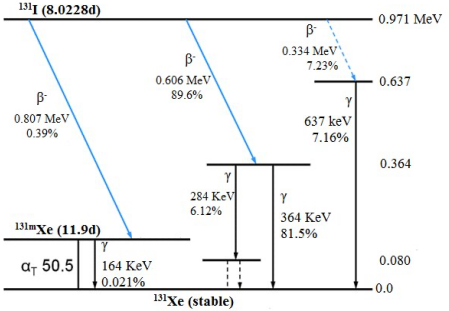

Figure from https://www.researchgate.net/publication/295919808_Radioiodine_I-131_for_Diagnosing_and_Treatment_of_Thyroid_Diseases

Parent-daughter decay chain

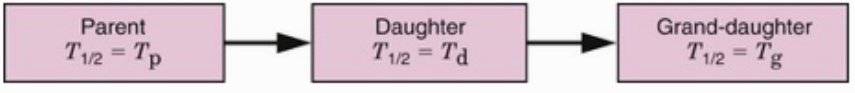

Branching ratio [Parent $\rightarrow$ Daughter] $= \beta$

Rate of 'decay'of daughter nuclei:

$$\begin{aligned} \frac{dN_D}{dt} &= \lambda_P N_P \beta - \lambda_D N_D \\ &= \lambda_P N_{P0} \beta \exp(-\lambda_P t) - \lambda_D N_D \end{aligned}$$

I.e.:

$$\frac{dN_D}{dt} + \lambda_D N_D - \lambda_P \beta N_{P0} \exp(-\lambda_P t) = 0\,.$$

Solution:

$$N_D = \frac{\lambda_P}{\lambda_D - \lambda_P} \beta N_{P0} \left[\exp(-\lambda_P t) - \exp(-\lambda_D t)\right] + N_{D0} \exp(-\lambda_D t)$$

Or in terms of activation:

$$A_D = \frac{\lambda_D}{\lambda_D - \lambda_P} \beta A_{P0} \left[\exp(-\lambda_P t) - \exp(-\lambda_D t)\right] + A_{D0} \exp(-\lambda_D t) \quad (1)$$

$T_P >> T_D$; secular equilibrium

$T_P >> T_D \Rightarrow \frac{\lambda_P}{\lambda_D} << 1$ and $\exp(-\lambda_P t) \sim 1$.

So, equation 2 becomes:

$$A_D = \beta A_{P0}\left[1 - \exp(-\lambda_D t)\right] + A_{D0}\exp(-\lambda_D t)$$

If $A_{D0} = 0$ and $\beta = 1$, then the build up of N_D reaches 'secular equilibrium after 5–6 T_D.

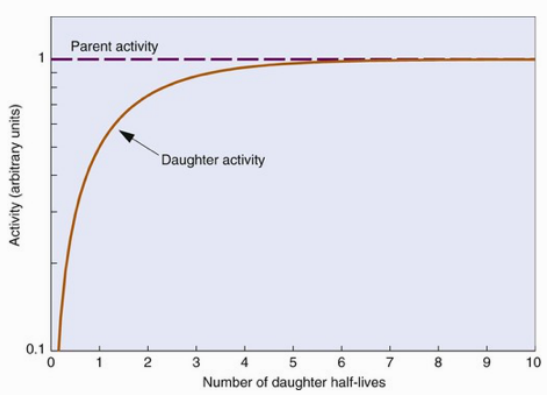

$T_P > T_D$; transient equilibrium

Transient equilibrium occurs at t_{eq} given by:

$$t_{\mathrm{eq}} = \frac{\ln\left[\frac{\lambda_P}{\lambda_D}\right]}{\lambda_P - \lambda_D}$$

At this time the activity of the daughter is a maximum, so one may write:

$$t_{\mathrm{max}} = t_{\mathrm{eq}} = \frac{1.44\,T_P\,T_D}{T_P - T_D}\ln\left[\frac{T_P}{T_D}\right]$$

If $A_{D0} = 0$, $\beta = 1$, and $T_P = 10\,T_D$, then build up and decay of N_D reaches 'transient equilibrium' after $\sim 3.5\,T_D$.

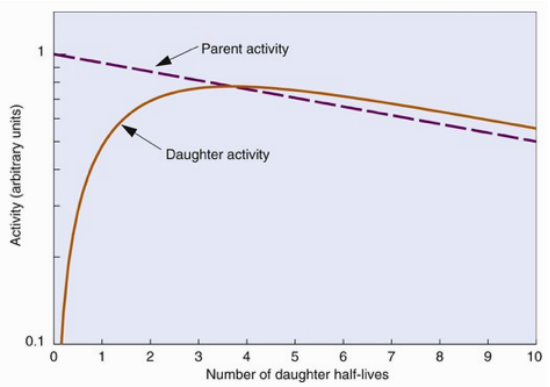

$T_D > T_P$; no equilibrium

Maximum activity of daughter is still given by:

$$t_{\max} = t_{\text{eq}} = \frac{1.44\, T_P\, T_D}{T_P - T_D} \ln\left[\frac{T_P}{T_D}\right]$$

The daughter activity grows until $t_{\max}$ and then decreases. The parent activity 'falls away' and therefore fails to replenish the daughter.

If $A_{D0} = 0$, $\beta = 1$, and $T_P = 10\, T_D$, then build up of N_D reaches maximum activity at $\sim 0.3\, T_D$.

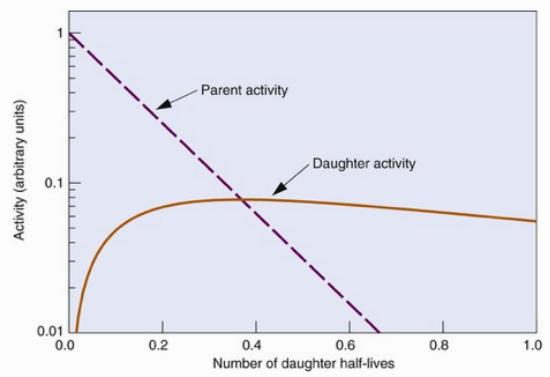

Methods for the production of radionuclides; overview

Nuclear reactor:

- Neutron capture
- Fission fragments

Radionuclide generators:

- Portable devices widely used in hospitals
- Require materials produced in nuclear reactors or accelerators

Accelerator:

- Cyclotron
- Active area of research; may return to this if there is time

Nuclear reactor; one-slide outline

- Graphite or D_2O moderator surrounds fissionable fuel cells
- Control rods, commonly boron, shield or expose fuel cells
- Position of fuel cells & control rods determine rate of chain reaction
- Ports in core allow insertion of samples for irradiation

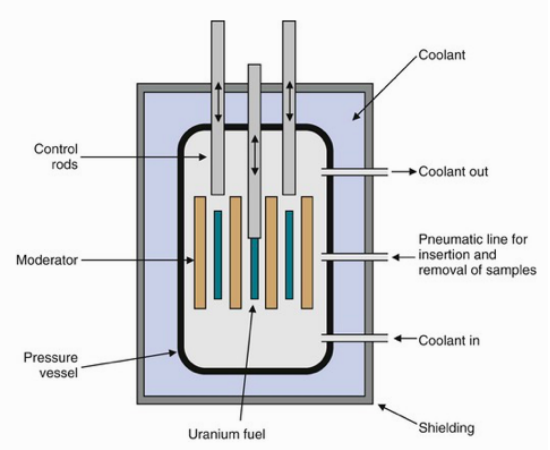

Used to generate fission products or perform neutron activation

Nuclear reactor: radionuclides produced by 'neutron activation'

Fission of ^{235}U produces neutrons which bombard samples introduced into the core.

Neutron activation produces:

- Neutron-rich radionuclides, which usually undergo beta decay
- Product is chemically identical to parent material:
  - Product therefore can not be separately chemically;
  - Results in lower purity and lower activity than other production methods

Example reactions:

- $^{31}\mathrm{P}(n,\gamma)^{32}\mathrm{P}$
  - Capture of n produces $^{32}\mathrm{P}^{*}$ which decays to $^{32}\mathrm{P}$ emitting a γ
- $^{50}\mathrm{Cr}(n,\gamma)^{51}\mathrm{Cr}$

Nuclear reactor: production of ^{125}I

^{125}I *is* produced via neutron activation and *can* be chemically separated, vis:

$$^{124}\mathrm{Xe}(n,\gamma)^{125}\mathrm{Xe} \underbrace{\xrightarrow{\mathrm{EC\ or\ }\beta^-}}_{T_{\frac{1}{2}}=17\,\mathrm{hr}} {}^{125}\mathrm{I}$$

Nuclear reactor: production via fission fragments

Fission fragments:

- Have bimodal distribution in A
- Excess of neutrons, hence tend to undergo β^- decay until stable nucleus is produced

If long-lived isotope is produced it can be chemically extracted, e.g.:

$$^{99}_{39}\mathrm{Y} \xrightarrow{\beta^-(1.5\,\mathrm{s})} {}^{99}_{40}\mathrm{Zr} \xrightarrow{\beta^-(21\,\mathrm{s})} {}^{99}_{41}\mathrm{Nb} \xrightarrow{\beta^-(15\,\mathrm{s})} {}^{99}_{42}\mathrm{Mo}$$

Halflife of ^{99}Mo is 65.9 hr, long enough to allow it to be extracted and incorporated in radionuclide generator to produce $^{99\mathrm{m}}$Tc

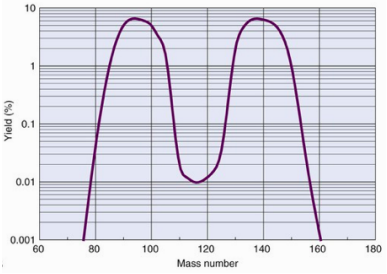

Radionuclide generators

Parent-daughter radionuclide pair in an apparatus that permits separation and extraction of the daughter from the parent

$T_P > T_D$ so that daughter product is replenished continuously by the decay of the parent and may be extracted repeatedly

Provides a local supply of short-lived radionuclides without needing a cyclotron or nuclear reactor

Radionuclide generator: ^{99m}Tc for imaging

$$^{99}\text{Mo} \xrightarrow{\beta^-;\ T_{\frac{1}{2}}=66\ hr} {}^{99m}\text{Tc} \xrightarrow{\gamma;\ T_{\frac{1}{2}}=6\ hr} {}^{99}\text{Tc}$$

- ^{99}Mo bound to an alumina column in form of molybdate ion (MoO_4^-)
- ^{99m}Tc, the decay product, is not bound to column; it is chemically different
- ^{99m}Tc is eluted from column with 5–25 ml saline
- 75–85% of available ^{99m}Tc can be extracted
- Typically used for one week
- Often refereed as a 'Molly' or a 'Cow'

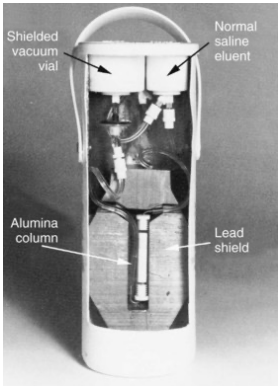

Accelerator: cyclotron

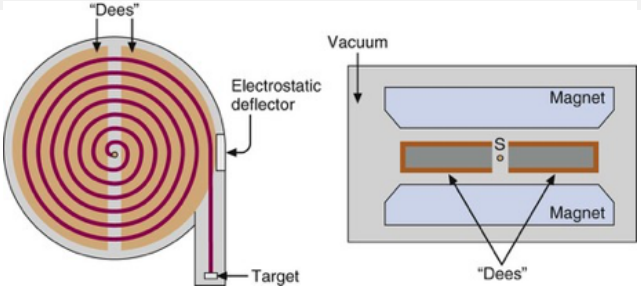

Cyclotron frequency, f:

$$f = \frac{qB}{2\pi m}$$

where q is ion charge, B the magnetic field strength, and m is ion mass.

Extraction is at a single, pre-determined, energy.

Accelerator: cyclotron

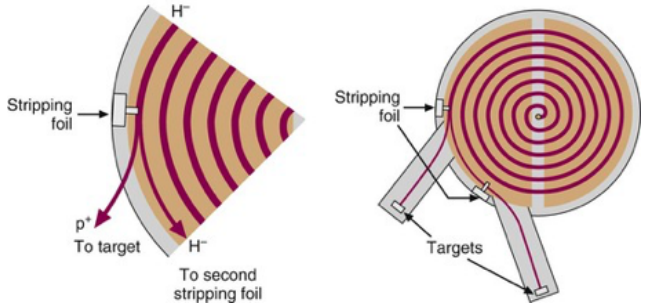

Schematic of H^- ion cyclotron showing stripping foils and targets.

Compact biomedical cyclotron

Medical cyclotrons usually located near PET scanner due to short lifetimes of radionuclides that are produced.

Examples of cyclotron-produced radionuclides

Product	Decay Mode	Common Production Reaction	Natural Abundance of Target Isotope* (%)	Energy Threshold (MeV)†
^{11}C	β^+, EC	^{14}N(p,α)^{11}C	99.6	3.1
		^{10}B(d,n)^{11}C	19.9	0
^{13}N	β^+	^{16}O(p,α)^{13}N	99.8	5.5
		^{12}C(d,n)^{13}N	98.9	0.35
^{15}O	β^+	^{14}N(d,n)^{15}O	99.6	0
		^{15}N(p,n)^{15}O	0.37	—
^{18}F	β^+, EC	^{18}O(p,n)^{18}F	0.20	2.57
		^{20}Ne(d,α)^{18}F	90.5	0
^{67}Ga	(EC,γ)	^{68}Zn(p,2n)^{67}Ga	18.8	5.96
^{111}In	(EC,γ)	^{109}Ag(α,2n)^{111}In	48.2	—
		^{111}Cd(p,n)^{111}In	12.8	—
^{123}I	(EC,γ)	^{122}Te(d,n)^{123}I	2.6	—
		^{124}Te(p,3n)^{123}I	4.8	—
^{201}Tl	(EC,γ)	^{201}Hg(d,2n)^{201}Tl	13.2	—

Radioisotopes produced using cyclotron beams.
Decay schemes and production reactions are given.

Overview

Exploit γs produced in decay of radiotracer, so, detectors must:

- Have good detection efficiency in range 80–300 keV
- Provide capability to measure γ energy:
  - To detect and reject γ that have undergone Compton scattering and so have lost pointing accuracy

"Gamma camera":

- Technique based on light production in a large-area crystal of sodium iodide (NaI)
- Scintillation light, produced by exciting atoms by absorption of radiation
- Light detection typically using 'photomultiplier tubes' (PMTs)

Generating scintillation light

Scintillation light is generated by relaxation of atomic electrons excited by ionising radiation.

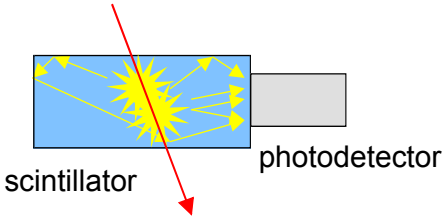

Properties of inorganic scintillators (e.g. NaI) include:

- Large range of Z and density; for medical application average and density Z of NaI and are favourable giving high probability that photon will be detected
- Large light yield; up to 40,000 photons per MeV
  - i.e. signal depends on energy of incident photon
- Single-decay times of from ns to μs

See for example Ambrosio, CERN Academic Training, April 2005

Generating scintillation light

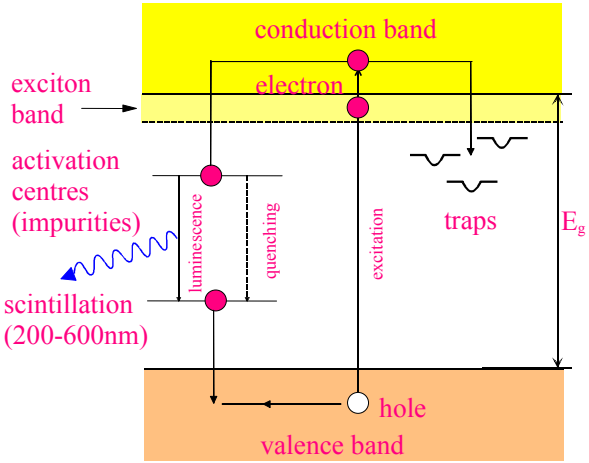

There can be more than one time constant:

- Fast recombination (ns–μs) from activation centres
- Delayed recombination due to trapping (μs–ms)
  - Traps arise due to dopants (wanted) and lattice imperfections (unwanted)

Chrystal preparation determines properties of scintillation light

See for example Ambrosio, CERN Academic Training, April 2005

Photon absorption in crystals

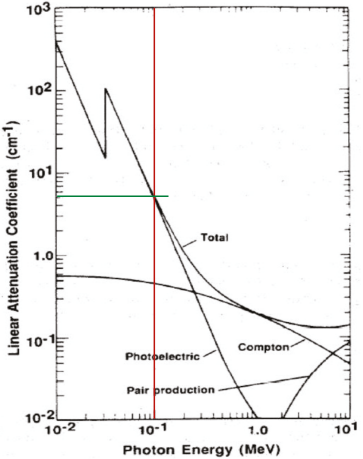

Intensity, I, function of depth traversed, d:

$$I = I_0 \exp(-\mu d)$$

μ is the "Linear attenuation coefficient"

For NaI, at the energies we are interested in, penetration depth is a few mm

DOI: http://dx.doi.org/10.5772/intechopen.8550

Detecting scintillation light

Photo-electric effect used to convert light into electronic signal that can be digitised

Detector requirements:

- High sensitivity; i.e. high "quantum efficiency", QE:

$$\mathrm{QE} = \frac{N_{\mathrm{pe}}}{N_{\gamma}}$$

  where N_{pe} is the number of photo-electrons generated by N_{γ} photons impinging on detector
- Low intrinsic noise
- Low gain fluctuations

See for example Gys, CERN Academic Training, April 2005

The photo-electric effect

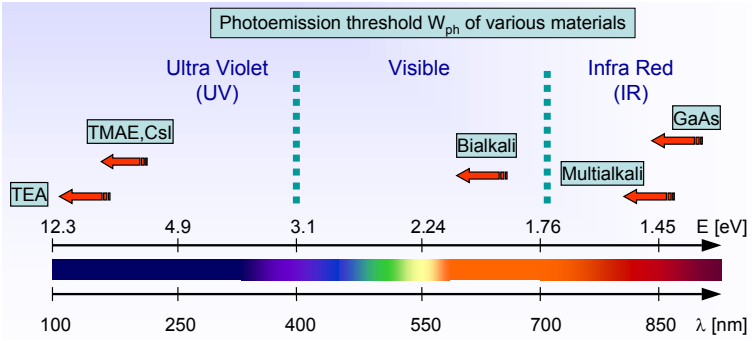

Photo-electric a 3-step process:

- Excite electrons in photocathode photon
- Excited electrons diffuse through material, losing some energy
- Electrons reaching surface with energy sufficient to escape may be detected

The photo-multiplier tube

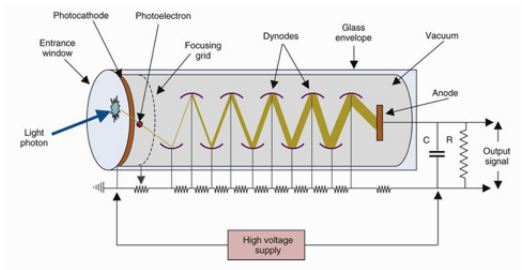

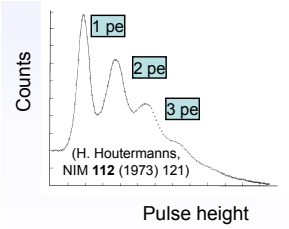

- Photo-emission from photo-cathode
- Secondary emission from subsequent dynodes
- Dynode gain, $g_i = \frac{N_e^{\rm sec}}{N_e^{prim}}$, usually between $g_i = 3$ and $g_i = 50$
- Total gain $\mathcal{G} = \Pi_1^{N_{\rm dynode}} g_i$

See for example Gys, CERN Academic Training, April 2005

The Gamma camera

"Imaging collimator" defines direction of detected γs

- Forms projected image on scintillator

Large, single-crystal NaI scintillator coupled to a clear plastic or glass light guide

Light detected using PMT array

PMT readout by pulse-height-sensitive electronics; events are recorded if energy falls within the desired window

Many events are required for an image to be built up image:

- x, y intensity map;
- γ-energy spectrum
- Possibly also the time evolution of the image

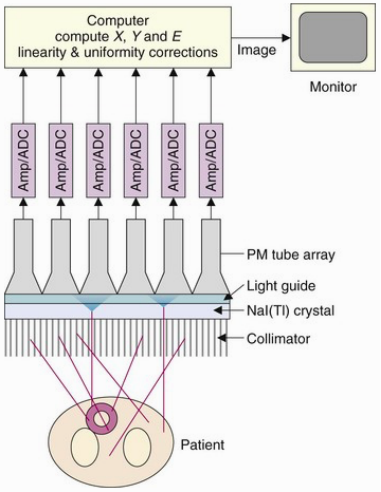

Example image

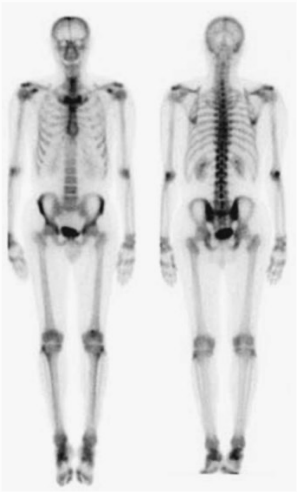

Example whole-body image taken using ^{99m}Tc-MDP

Resolution

Contributions to intrinsic resolution:

- Detector thickness (geometrical effect)
- Compton scattering on atomic electron:
  - $\gamma_i + e \rightarrow \gamma_o + e'$; γ_o not parallel to γ_i
  - Small effect: $< 10\%$ of γs displaced by $> 2.5\,\text{mm}$ in $6.4\,\text{mm}$ thick detector
- Statistical fluctuations in photon count:
  - Scintillation photons & photoelectrons Poisson distributed
  - If N photoelectrons expected, variance of number detected will be N
  - Consequence is that distribution of γs over surface of detector will fluctuate
- Intrinsic resolution degrades with decreasing E_γ:
  - Fewer scintillation photons expected for low-energy γs
  - So, RMS of fluctuations ($\propto \frac{\sqrt{N}}{N}$) grows as E_γ decreases

Intrinsic spatial resolution for 6.3 mm thick NaI(Tl) crystal.

Thallium (Tl) doping improves light production efficiency through recombination of electrons/holes at dopant site in lattice.

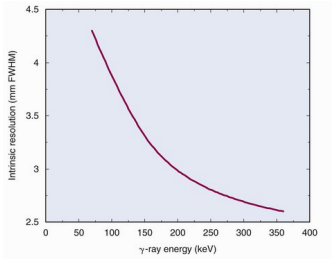

Trade off between resolution and efficiency

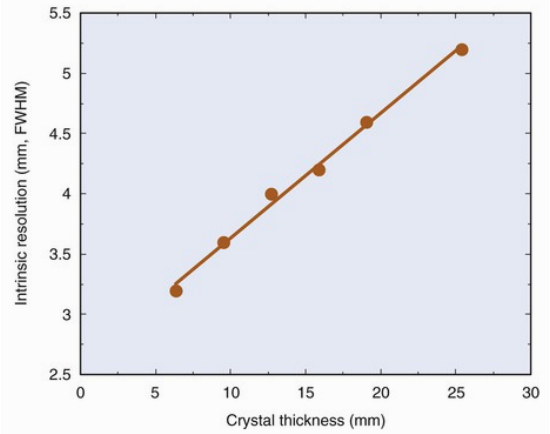

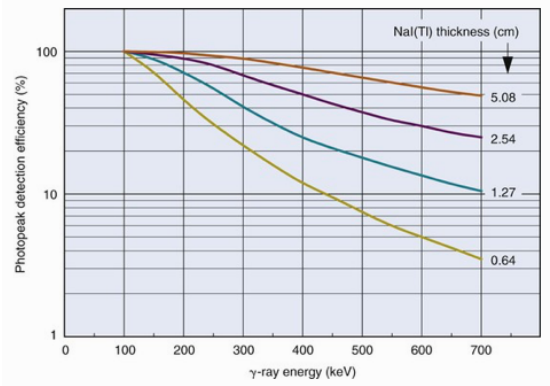

For practical sources (e.g. ^{99m}Tc), $100 \lesssim E_\gamma \lesssim 200\,\text{keV}$. Motivates thickness of 5–6 mm to get high efficiency and good resolution.

Decay γ selection

Compton-scattered photons have an energy lower than that of the decay photons.
Atomic transitions from electrons excited in the lead shield or the NaI detector also contribute low-energy photons.

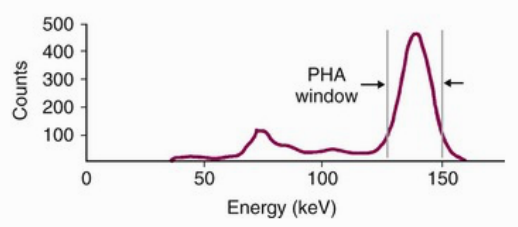

PHA: pulse height analyser

Exploit energy resolution to select γs that emerge without scattering:

- Energy resolution $\propto \frac{1}{E_\gamma}$.
- Typical energy resolution, $\frac{\Delta E_\gamma}{E_\gamma}$, is $\sim 10\%$ at 140 keV.

Types of event

A: Good event

B: Scatter in detector:

- Full energy is recorded, but
- Position information is distorted

C: Scatter in patient

- γ arriving at detector has reduced energy, but may still fall within the detection window
- Unwanted event

D: Septal penetration

- Unwanted event

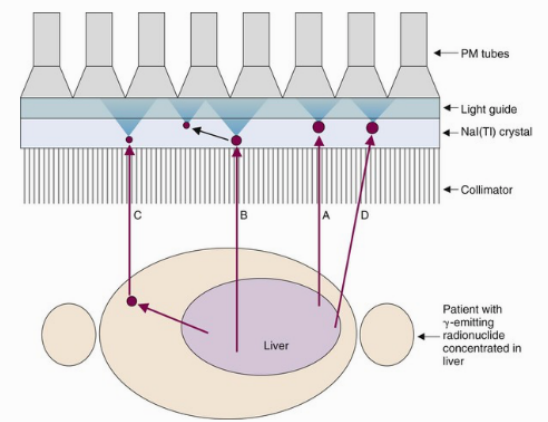

Image formation

Image is formed using an "absorptive" collimator:

- The collimator absorbs "unwanted" γs

Collimator selects direction of observed γs:

- This determines the "pointing geometry"
- Wasteful of γs, most are absorbed in collimator

Absorptive collimator made from lead or tungsten:

- High probability of absorption in moderate thickness of material

Four main types:

- Parallel, pin-hole, converging, diverging

Parallel-hole collimator

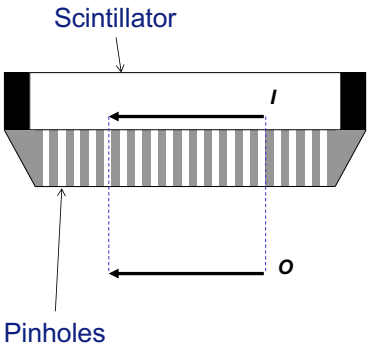

Magnification, M, given by:

$$M = \frac{I}{O} = 1$$

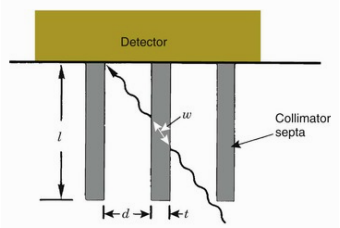

Septal thickness: $t = \frac{2dw}{l-w}$

To generate contrast, require low transmission of off-axis γs. Specify, septal penetration $< 5\%$. Then, for medium with linear attenuation coefficient, μ:

$$t \gtrsim \frac{6d}{\mu\,(\mu l - 3)} \approx 3\,\mathrm{mm} \text{ for Pb collimator and } E_\gamma = 140\,\mathrm{MeV}$$

Parallel-hole collimator: contribution to resolution

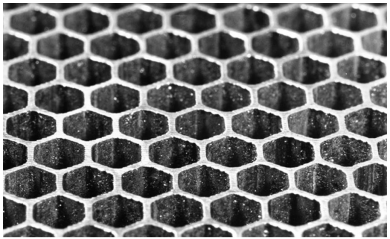

Example: hexagonal holes to maximise area of detector exposed

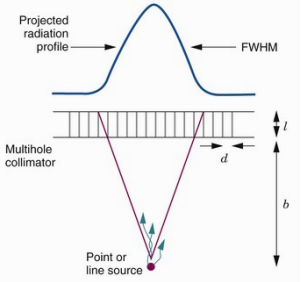

Resolution, δr_{col}, is FWHM spread of radiation from point source.

$$\delta r_{\mathrm{col}} \approx d\frac{l+b}{l}$$

Independent of t

Parallel-hole collimator: geometrical efficiency

Geometric efficiency, g, defined as fraction of emitted γs that are transmitted by collimator
Example, for square-hole collimator:

$$g = \frac{d^4}{12l^2\,(d+t)^2}$$

Independent of b, because:

- Efficiency for a particular hole falls as $\frac{1}{b^2}$, but
- Number of holes illuminated groups as b^2

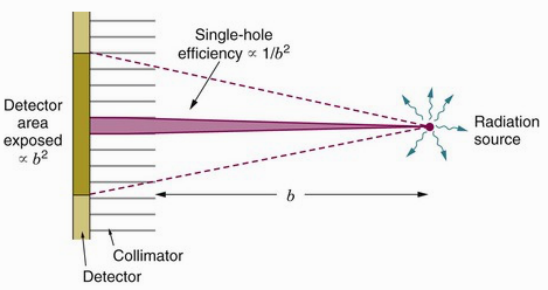

Parallel-hole collimator: summary

Collimator Type	Recommended Max. Energy (keV)	Efficiency, g	Resolution R_{coll} (FWHM at 10 cm)
Low-energy, high-resolution	150	1.84×10^{-4}	7.4 mm
Low-energy, general-purpose	150	2.68×10^{-4}	9.1 mm
Low-energy, high-sensitivity	150	5.74×10^{-4}	13.2 mm
Medium-energy, high-sensitivity	400	1.72×10^{-4}	13.4 mm

Diverging collimator

Focal point typically 40–50 cm behind collimator

Large field of view

Reduced image that is not inverted

Image size depends on distance (z) leading to distortion

Magnification:

$$M = \frac{I}{O} = \frac{f - l}{f + z} < 1$$

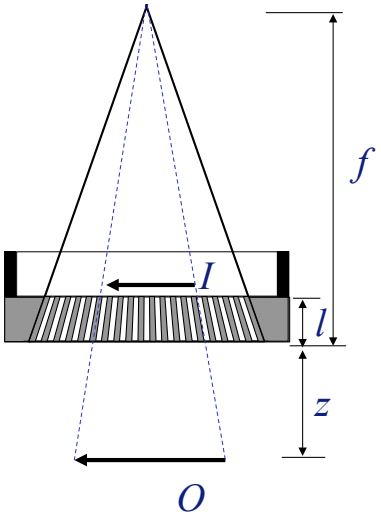

Converging collimator

Focal point typically 40–50 cm in front of collimator

Reduced field of view

Magnified image that is:

- Not inverted if $z < f$
- Inverted if $z > f$

Image size depends on distance (z) leading to distortion

Magnification:

$$M = \frac{I}{O} = \frac{f + l}{f - z} > 1$$

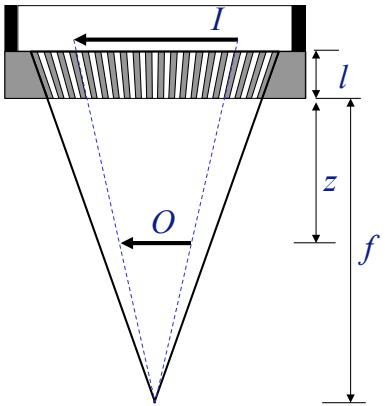

Pinhole collimator

Pinhole size $\sim$ mm

Field of view depends on z

Image is:

- Magnified and inverted if $z < f$
- Reduced and inverted if $z > f$

Image size depends on distance (z) leading to distortion

Magnification:

$$M = \frac{I}{O} = \frac{f + I}{f - z} > 1$$

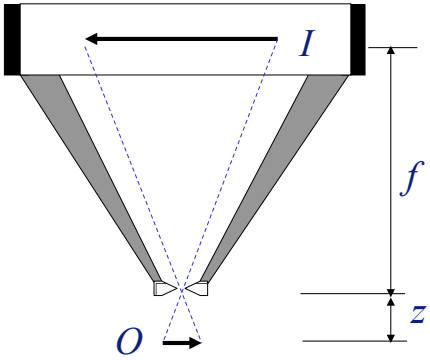

Crystal assembly

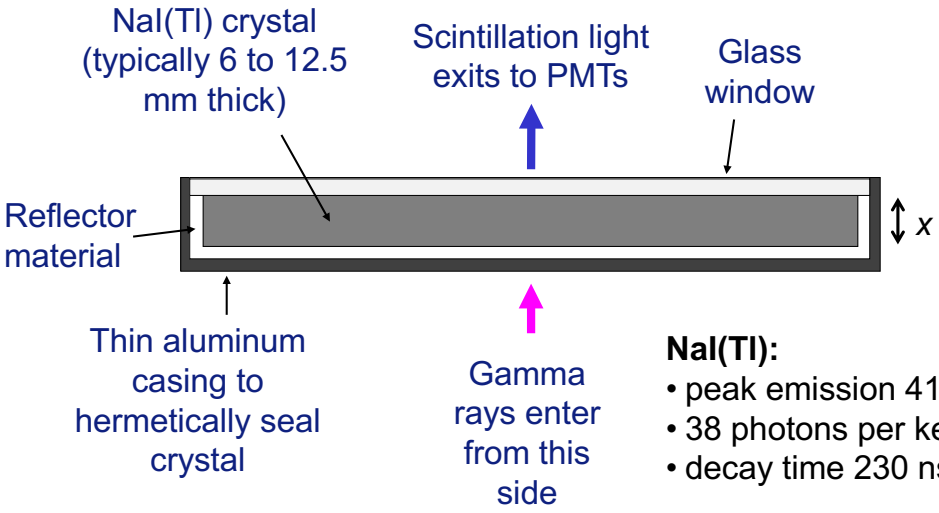

NaI(Tl):

- peak emission 415 nm
- 38 photons per keV
- decay time 230 ns

Head

Area: typically $60 \times 40\,\mathrm{cm}^2$

PMT diameter: typically 50 mm

30–100 PMTs per head

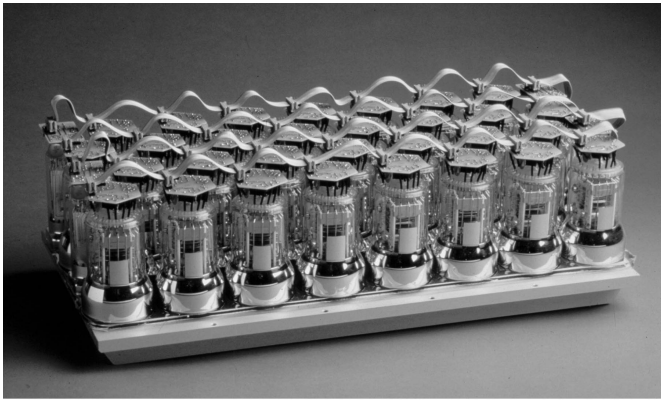

Position reconstruction

In linear approximation:

$$D_1 = \frac{S_2 \times D}{S_1 + S_2}$$

$$D_2 = \frac{S_1 \times D}{S_1 + S_2}$$

where $D = D_1 + D_2$

Event position is calculated as the centroid ("centre of mass") of the PMT signals

More complex algorithms that account for distortions are also employed

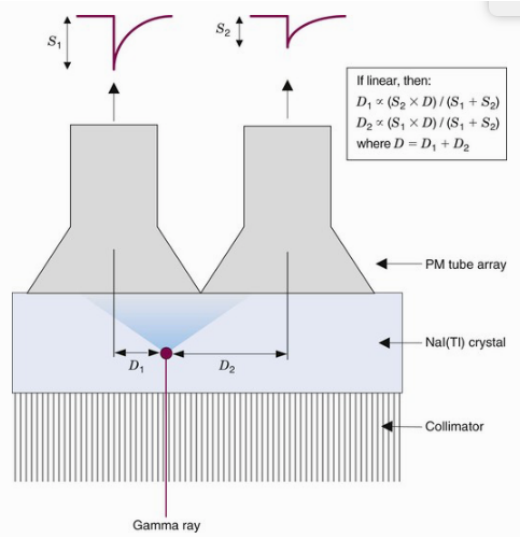

Detection efficiency

Can now define detection efficiency of the system:, $\mathcal{E}$:

$$\mathcal{E} = g\epsilon F_{\text{elec}}$$

where:

- g is the geometrical efficiency
- ϵ is the ratio of the number of γs recorded divided by the the number of γs incident:

$$\epsilon = 1 - \exp\left(-\mu_{\text{scint}} t_{\text{scint}}\right)$$

  where μ_{scint} is the linear attenuation coefficient of the scintillator and t_{scint} its thickness
- F_{elec} is the fraction of the γs accepted by the discriminators (front-end of the electronics)

Spatial resolution

Three major contributions to the spatial resolution:

- **Collimator resolution**, δr_{col}, defined above, usually dominates
- Intrinsic resolution, δr_{int} – ability of PMTs to localise event
- Residual impact of Compton scattering, $\delta r_{\mathrm{Compt}}$ in tissue resulting in non-colinearity of deetected γ with the γ that which left the decay site

System resolution is given by:

$$\delta r_{\mathrm{sys}} = \left[\delta r_{\mathrm{col}}^2 + \delta r_{\mathrm{int}}^2 + \delta r_{\mathrm{Compt}}^2\right]^{\frac{1}{2}}$$

Gamma cameras

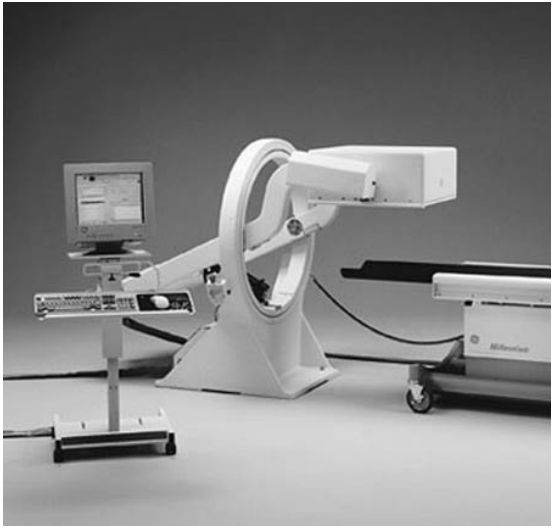

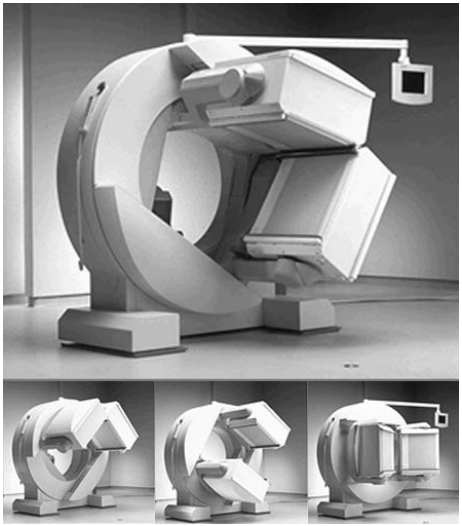

Dynamic imaging study

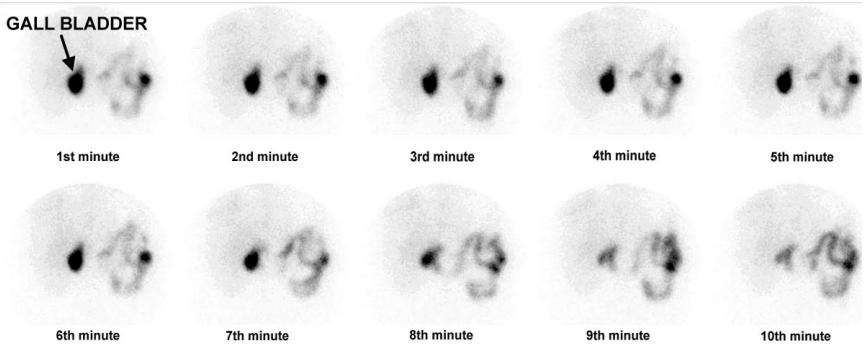

- ^{99m}Tc-HIDA
- At $t - 7$ mins, cholecystkinin was administered to simulate emptying of the gallbladder
- Rate of emptying can be measured from the sequence

Introduction

Gamma camera gives single projected image of object; cf conventional x-ray image

SPECT: Single Photon Emission Computed Tomography; cf X-ray CR

SPECT image of mouse with bone tracer

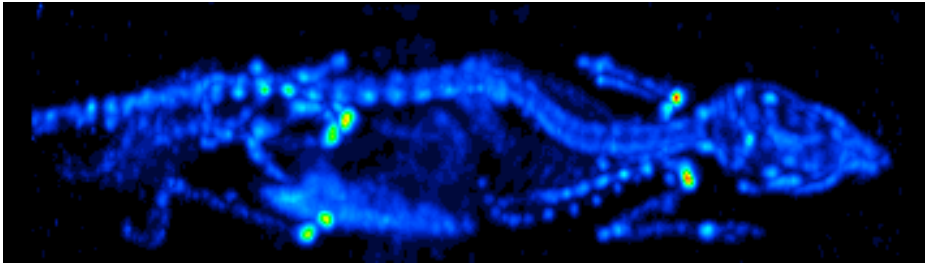

Click here for C. Lackas' animated gif on wikipedia

Image prepared by C. Lackas

Typical SPECT systems

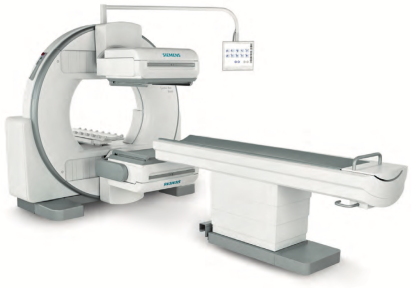

Two (or more) gantry-mounted gamma cameras:

- Gamma cameras rotate around patient; 2D cross section
- Images taken from multiple angles
- Bed moves in longitudinal direction

Allows 3D images to be reconstructed

Ring of planar or pinhole gamma cameras

- 2D images obtained without rotation of detectors
- Images taken from multiple angles at the same time
- Bed moves in longitudinal direction

Allows 3D images to be reconstructed

Circular and contoured orbits

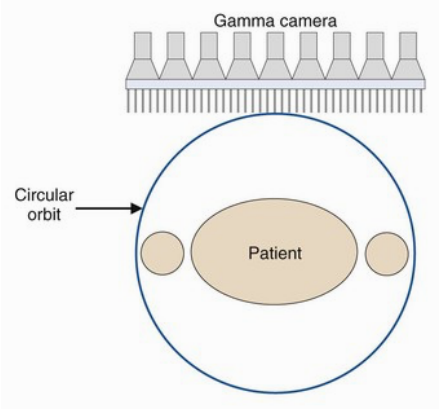

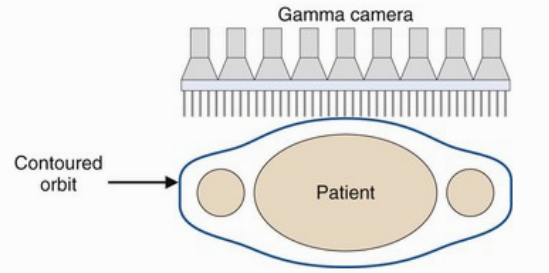

"Elliptical" orbit is more complicated but has the advantage of increased precision

Alternative configurations, in this case for brain scans

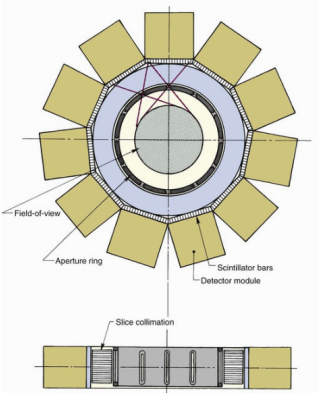

Aperture ring (12 slits) rotates

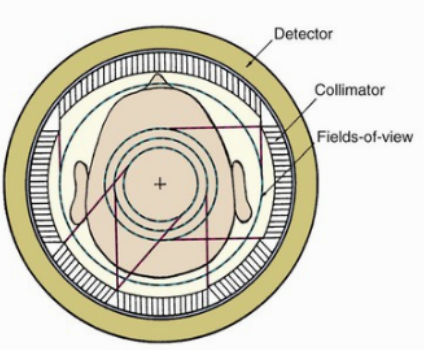

Each collimator section has its own field-of-view diameter

Typical parameters

- 64 to 128 angular views
- 2-3 mm linear sampling along longitudinal axis
- 360° data collection
- Reconstructed on 64×64 or 128×128 matrix
- Field of view $\sim$ 40–60 cm transaxially
- Stack of images covering $\sim$ 30–40 cm longitudinally

Projection on image plane

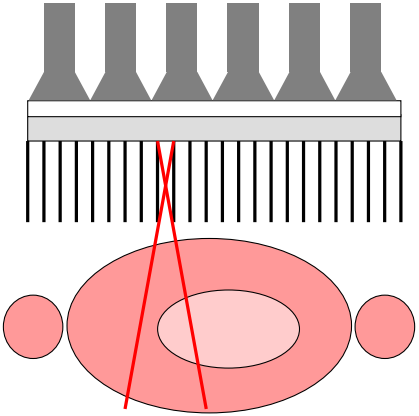

Absorptive collimator means that each hole views a pencil-like area of the object

Repeat for a wide range of angles:

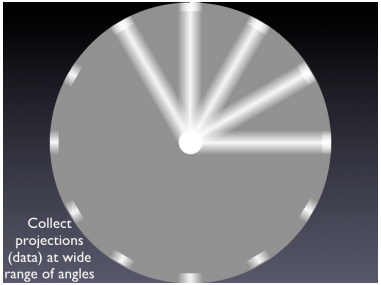

Geometric response; conjugate counting

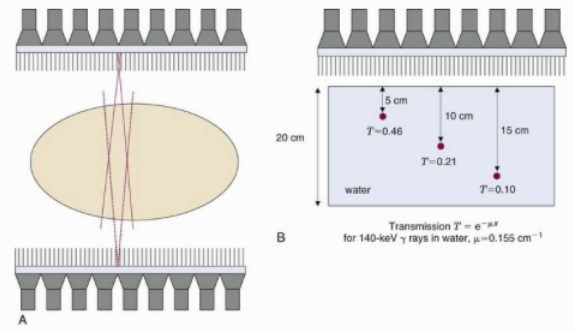

$I(r, \phi) \neq I(r, \phi + \pi)$

- Attenuation of γ intensity
- Divergence of image cone
- Measurements at ϕ and $\phi + \pi$ "conjugate"

Example of attenuation of γs from ^{99m}Tc:

- Exploit conjugate measurements to correct for lost attenuation

Back projection

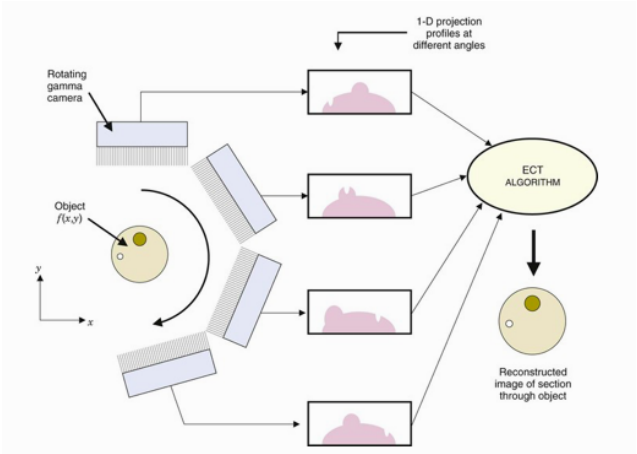

ECT: Emission computed tomography

TCT: Transmission computed tomography

Back projection: local coordinate system

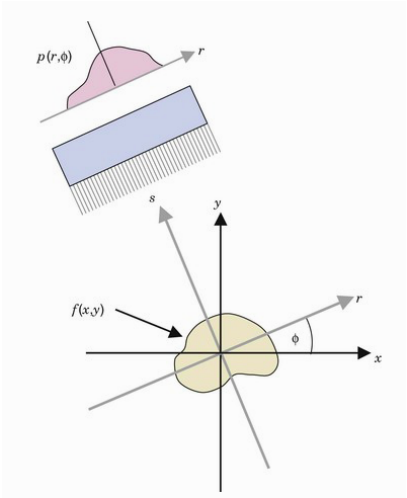

Local coordinate system r, s:

- r: coordinate along gamma camera
- s: distance camera to source

r, s coordinates related to x, y by:

$$\begin{aligned} r &= x\cos\phi + y\sin\phi \\ s &= -x\sin\phi + y\cos\phi \end{aligned}$$

x, y may be reconstructed using:

$$\begin{aligned} x &= r\cos\phi - s\sin\phi \\ y &= r\sin\phi + s\cos\phi \end{aligned}$$

Back projection: sinogram

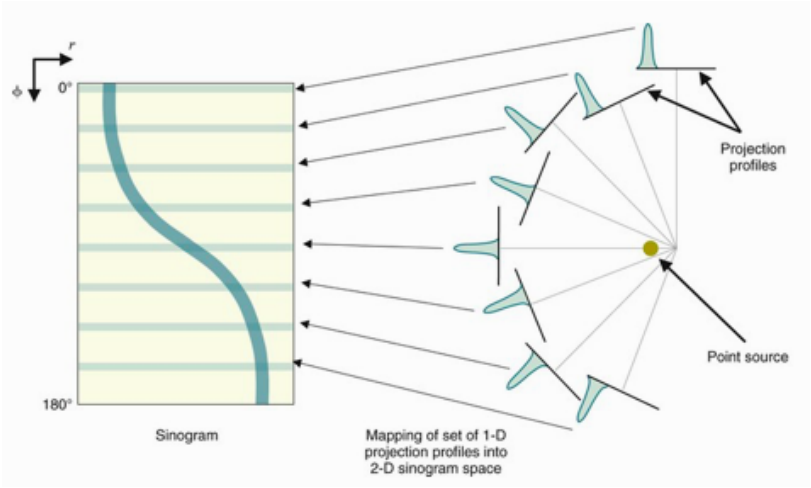

Back projection: profile construction

Measurement at each projection measures a response "profile", $p(r, \phi)$

Want to reconstruct the activity in a particular slice, $f(r, s)$ or $f(x, y)$

In "simple" back projection, the total response measured at a particular r_i, ϕ_i is divided between the pixels along the projected coordinate s

The total (uncorrected) activity, $f'(x, y)$ within a pixel at coordinate x, y is then given by:

$$f'(x, y) = \frac{1}{N} \sum_{i=1}^{N} p(r_i, \phi_i)$$

where the sum runs over the N projections that illuminate the pixel at x, y

Back projection: illustration

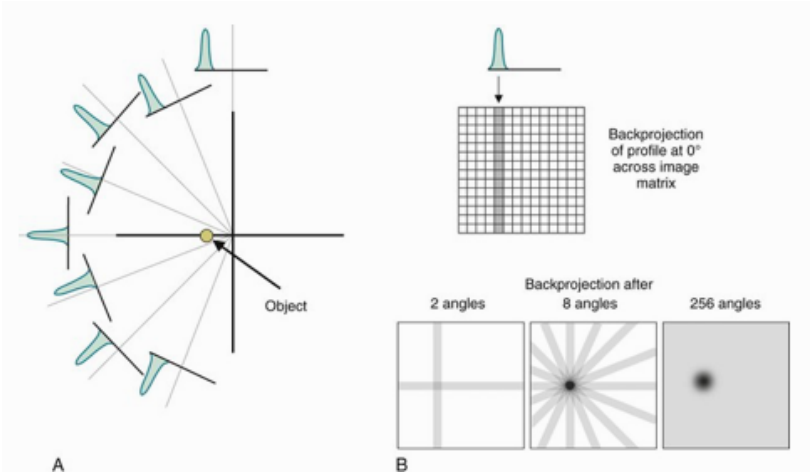

Back projection: illustration using a simple phantom

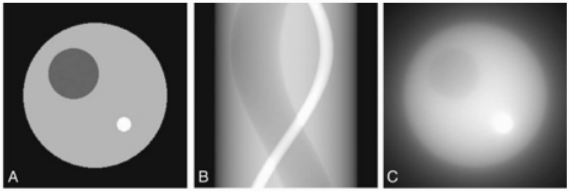

Main features of phantom appear in the image . . . but . . .

The attribution of activity to pixels along the projected coordinate s causes "spoke-like" image with few projections

More projections improve image, but, attribution of activity leads to apparent activity outside the object and blurring of the image

More sophisticated reconstruction algorithms (e.g. filtered back projection, see later) have been developed to overcome this defect

Attenuation depends on γ energy and depth

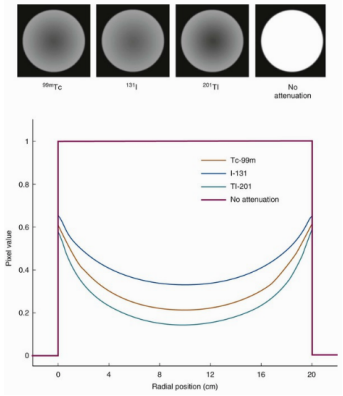

$$E_\gamma^{^{99m}\mathrm{Tc}} = 140\,\mathrm{keV};\ E_\gamma^{^{131}\mathrm{I}} = 364\,\mathrm{keV};$$
$$E_\gamma^{^{201}\mathrm{Tl}} = 70\,\mathrm{keV}$$

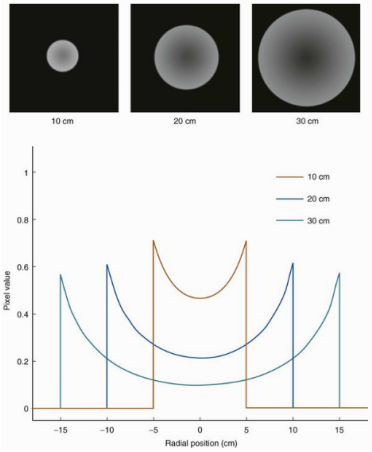

Attenuation

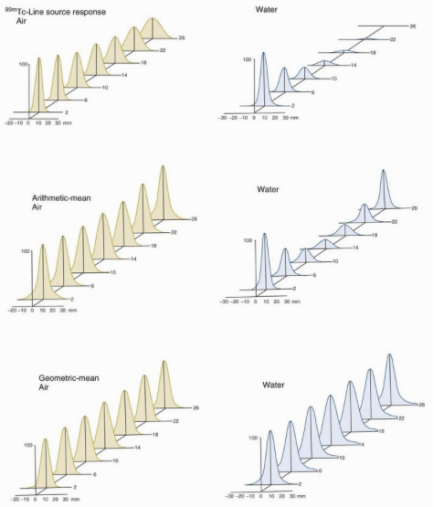

Example:

- High-resolution pin-hole collimator
- Resolution for line source diameter 2.5 mm:
  - As a function of distance source→detector
  - In air (left) and in water (right)
- Corrections applied:
  - Top: no correction
  - Middle: arithmetic mean:
    $$I_A = \frac{1}{2}(I_1 + I_2)$$
  - Bottom: geometric mean:
    $$I_G = (I_1 \times I_2)^{\frac{1}{2}}$$

Arithmetic mean gives most uniform response

Geometric mean

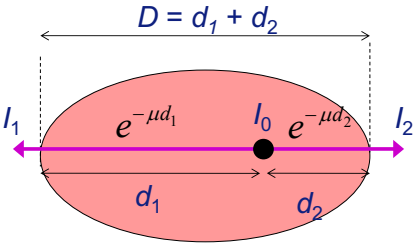

Intensity measured in two conjugate PMTs, numbered 1 and 2:

$$\begin{aligned} I_1 &= I_{01}\exp(-\mu d_1) \\ I_2 &= I_{02}\exp(-\mu d_2) \end{aligned}$$

Geometric mean; I_G:

$$\begin{aligned} I_G^2 &= I_{01} \times I_{02} \\ &= I_{01} \times I_{02}\exp\left(-\mu(d_1+d_2)\right) \end{aligned}$$

If $I_0 = I_{01} + I_{02}$:

$$I_G = I_0 \exp\left(-\mu\frac{D}{2}\right)$$

I.e. I_G depends on total depth D rather than d_1 or d_2.
The result is exact only for homogeneous media and point sources. Corrections can be derived to accommodate these effects.

Attenuation correction

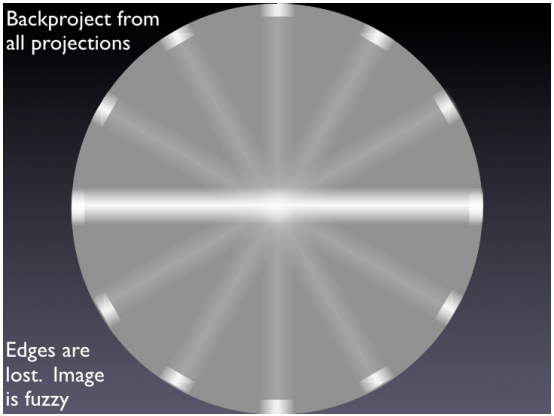

Define, attenuation correction factor, ACF:

$$\mathrm{ACF} = \exp\left(\mu \frac{D}{2}\right)$$

The corrected intensity I_{corr} is then calculated by evaluating:

$$I_{\mathrm{corr}} = \mathrm{ACF} \times I_G$$

Combination of projections

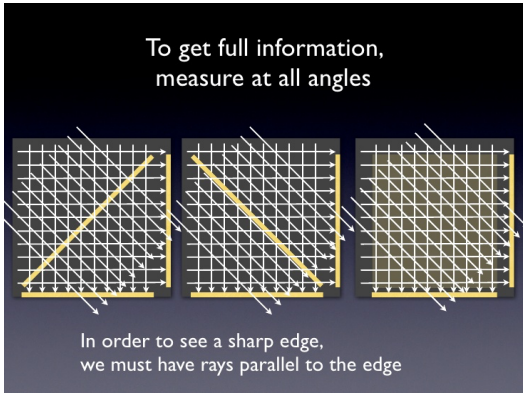

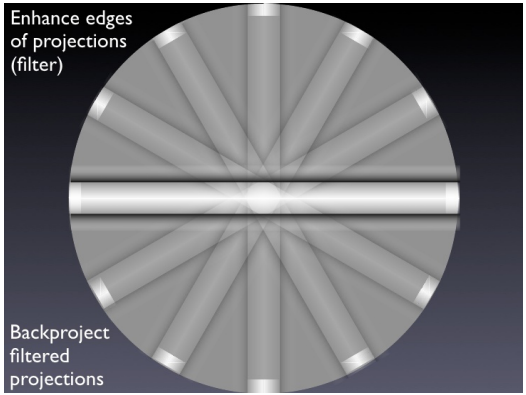

Filtered back projection

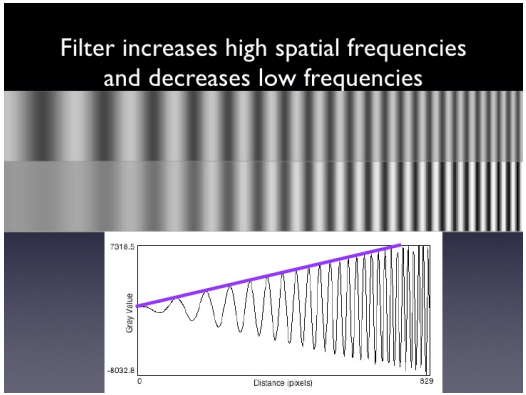

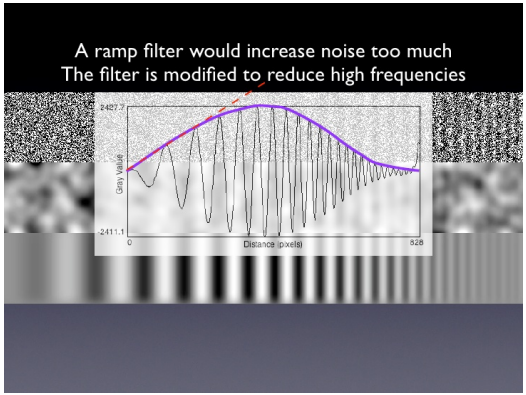

Filtered back projection

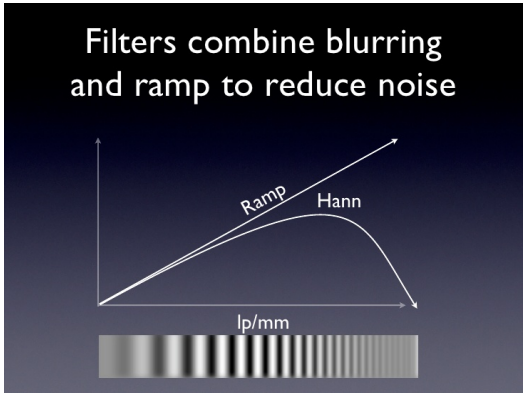

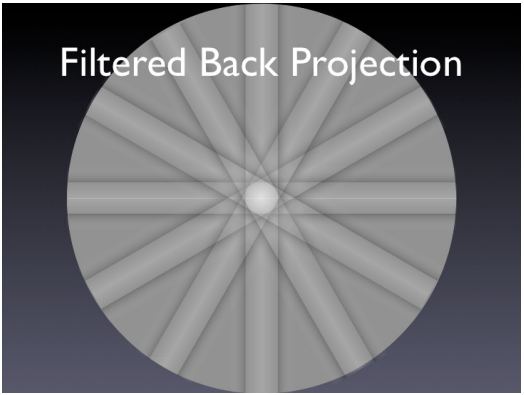

Attenuation correction strategies

1. Exploit ACF in "Chang's multiplicative method"
2. Generate a transmission map using "attenuation scans"
3. Use mean patient shape
   - Disadvantage "there is no mean (or average) patient"
4. Exploit CT image:
   - X-ray image processed to give transmission map that can be used to calculate ACF as a function of position

Will consider 1 and 2 below

Chang's multiplicative method

Steps:

1. Reconstruct image without any attenuation correction
2. Use reconstructed image to identify contour of patient
3. Assume uniform linear attenuation coefficient, μ, and calculate ACF pixel by pixel
4. ...

Calculation of ACF pixel by pixel

For pixel i at position x_i, y_i, a distance d_i from the surface in the direction of the camera, the pixel's attenuation factor, η_i, is given by:

$$\eta_i = \exp(-\mu d_i)$$

For a pixel at x, y, can now sum attenuation over all pixels between x, y and the surface to obtain the total attenuation factor for the path:

$$\eta = \sum_{1}^{N} \exp(-\mu d_i)$$

As before, N is the number of projections. The attenuation correction coefficient, now a function of x and y is given by:

$$\mathrm{ACF}(x, y) = \frac{1}{\sum_1^N \exp(-\mu d_i)}$$

Chang's multiplicative method

Steps:

1. Reconstruct image without any attenuation correction
2. Use reconstructed image to identify contour of patient
3. Assume uniform linear attenuation coefficient, μ, calculate ACF(x, y)
4. Apply ACF pixel by pixel:

$$f(x, y) = f'(x, y) \times \mathrm{ACF}(x, y)$$

where $f'(x, y)$ is the uncorrected response reconstructed in the pixel at x, y, and $f(x, y)$ is the corrected response.

Example

20 cm diameter cylinder with uniform concentration of ^{99m}Tc.

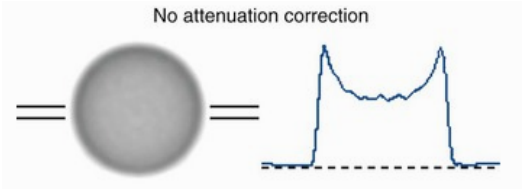

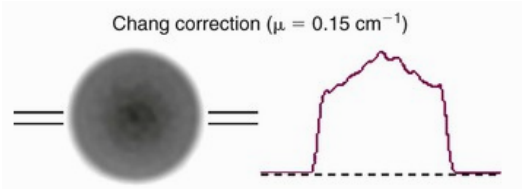

Apparent "over correction" attributed to scattered events.

In this example Chang's method has been applied, followed by a further correction by "forward projecting". The corrected image is projected to the gamma camera. The predicted response of the camera is then compared to the measured response and a further correction is made based on the difference of the forward projection and the measurement.

Transmission scans

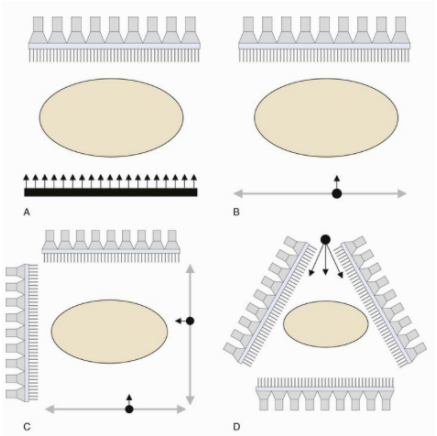

A: Flood source
B: Single source
C: 2 orthogonal sources
D: Stationary line source

Reference scan: I_{ref}; transmission scan: I_{trans}
For a particular projection element:

$$I_{\mathrm{trans}} = I_{\mathrm{ref}} \exp(-\mu d)$$

Taking the logarithm of the ratio:

$$\ln\left(\frac{I_{\mathrm{ref}}}{I_{\mathrm{trans}}}\right) = \mu d$$

Back-projection technique yields

$$\mu d = \sum_i \mu_i d_i$$

where the i^{th} pixel is of size d_i and is characterised by μ_i

Transmission scan: example

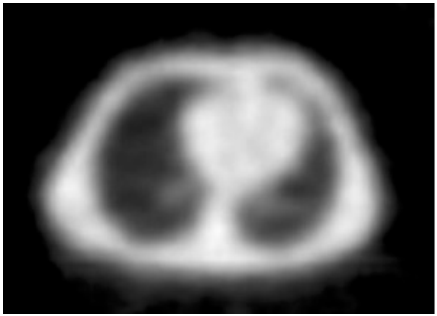

Transmission map of thorax using moving line source.

Radionuclides for transmission scans:

- ^{99m}Tc ($E_\gamma = 140\,\text{keV}$)
- ^{153}Gd ($E_\gamma = 97\,\text{keV}$ and $103\,\text{keV}$)
- ^{123}Te ($E_\gamma = 159\,\text{keV}$)

Long half-life convenient as then source does not need to be replaced frequently

Scatter correction

Primarily due to Compton scattering

Effect is smaller in magnitude than attenuation

Ratio of scattered to non-scattered photons may be as high as 40%, even when using a narrow energy window

Scatter reduces image contrast as events are put in the "wrong place" and leads to an overestimation of radioactivity in a pixel

Loss of contrast may obscure clinically relevant details

Scatter correction

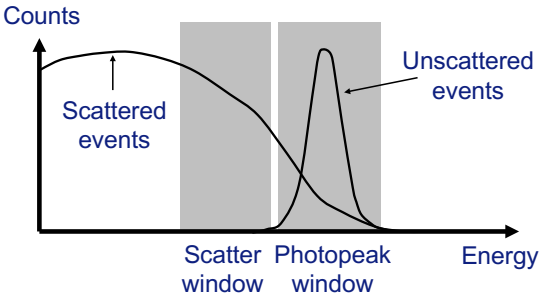

Weighting factor must be determined experimentally, it depends on:

- Choice of energy detection window (photopeak window)
- Size of object being scanned
- Energy resolution of gamma camera

Estimate contribution of scattering events in "photopeak window" by calculating a weighting factor, w_f

Number of events subtracted from photopeak is w_f times number of events in scatter window

Scatter-correction method limited by differences in spatial distribution of scatter and photopeak

Example of impact of scatter correction

20 cm diameter cylinder with uniform concentration of ^{99m}Tc.

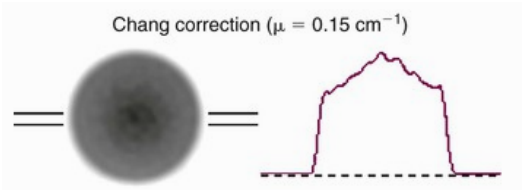

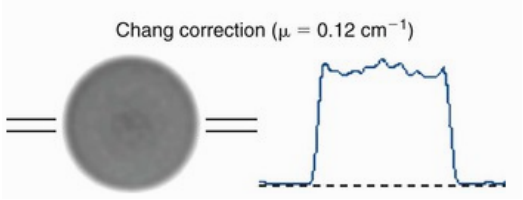

"Over correction" noted above removed by scatter correction

SPECT images of cardiac perfusion

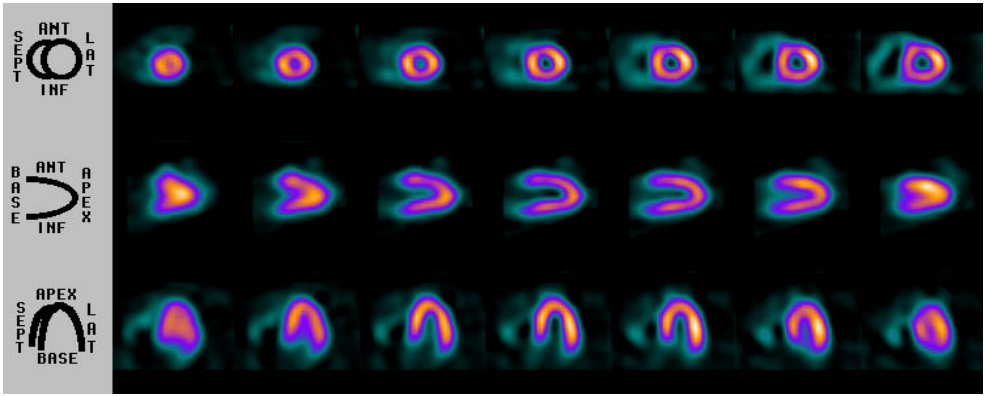

Cardiac perfusion scan using ^{99m}Tc-sestamibi. Images are shown in three slices, as indicated on the LHS. The time sequence (left to right) is in steps of 20 s.

SPECT images of brain perfusion

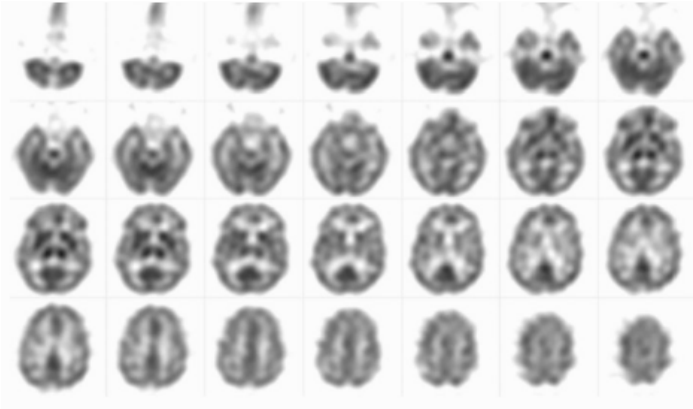

Brain perfusion scan using ^{99m}Tc-HMPAO. Images were acquired with an exposure of 40 s per view.

Positron Emission Tomography; the process

PET exploits photons generated in annihilation: $e^+ + e^- \rightarrow \gamma_1 + \gamma_2$

β^+ from decay scatters elastically off atomic electrons, loosing energy, until it annihilates

Annihilation assumed to be at rest. To conserve energy and momentum:

- Photons produced back-to-back
- Photon energies equal: $E_{\gamma_1} = E_{\gamma_2} = E_\gamma = mc^2 = 511\,\mathrm{keV}$

Back-to-back topology localises annihilation signal to a line in 3D space

PET detectors use inorganic scintillators with large Z:

- E_γ large compared to photons used in SPECT
- So require dense scintillator with greater "stopping power" than NaI

Beta($^+$) decay, reprise by example

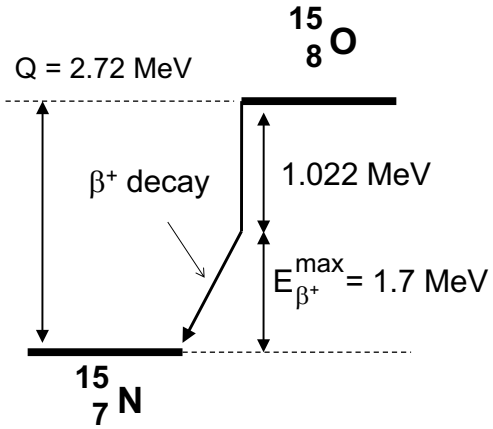

$$^{15}_{8}\mathrm{O} \rightarrow ^{15}_{7}\mathrm{N} + e^- + e^+ + \nu_e$$

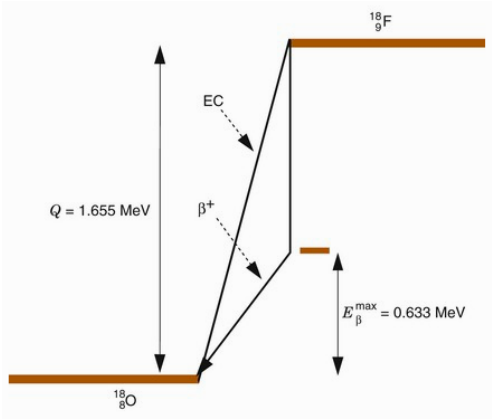

$$^{18}_{9}\mathrm{F} \rightarrow ^{18}_{8}\mathrm{O} + e^- + e^+ + \nu_e$$

Positron emitting radionuclides

Isotope	Half-life	β^+ fraction	Max. kinetic energy	Average positron range in water (mm)
C–11	20.3 mins	0.99	0.96 MeV	1.0 mm
N–13	9.96 mins	1.00	1.19 MeV	1.3 mm
O–15	123 secs	1.00	1.72 MeV	2.0 mm
F–18	110 mins	0.97	0.64 MeV	0.6 mm
Ga–68	68.3 mins	0.88	1.90 MeV	1.2 mm
Rb–82	78 secs	0.95	3.35 MeV	2.8 mm

Principle

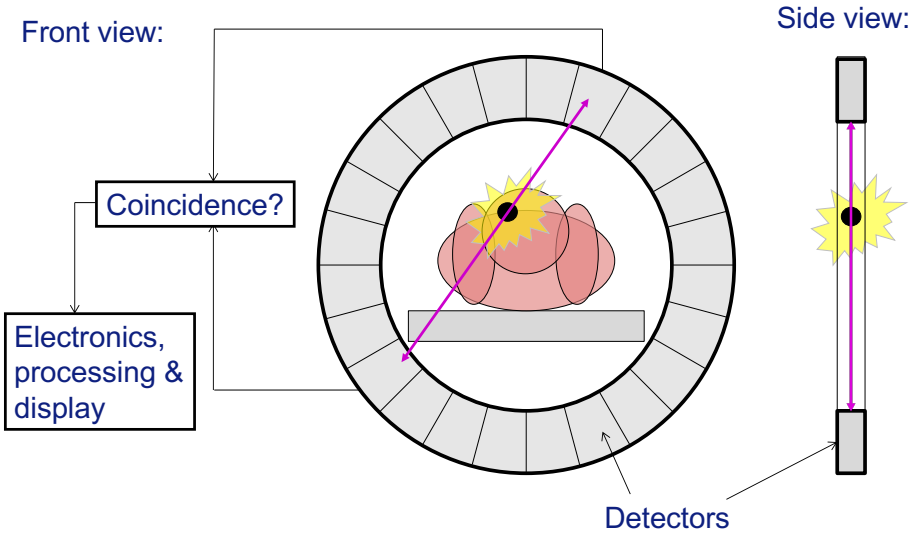
Front view:
Side view:
Coincidence?
Electronics, processing & display
Detectors

Taking views in parallel

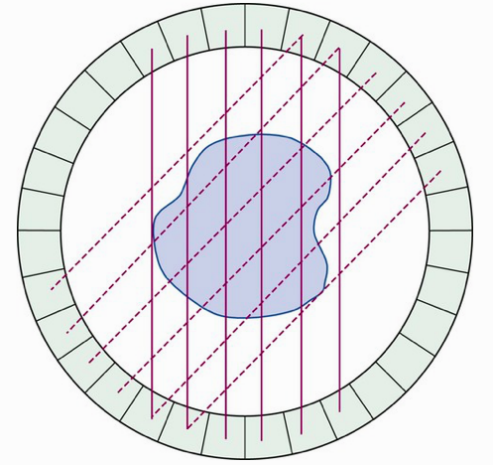

Multiple projections taken at the same time:

- Schematic shows two projections
- Ring of detectors can take all projections simultaneously

$\rightarrow$ An advantage over SPECT

"Annihilation Coincidence Detection" (ACD)

- ACD localises events to a line; "electronic collimation"

Eliminates need for absorptive septa

- Enhances geometrical efficiency substantially

$\rightarrow$ Another advantage over SPECT

"Block detector" for PET

Cuts in scintillator:

- Do not extend to full depth
- Reflective material fills gaps

Light yield function of position

Example of "multiplexing";
Reduces cost of optical readout

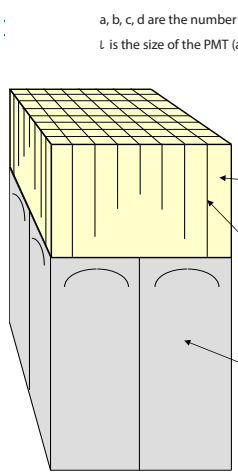

a, b, c, d are the number of counts in the 4 scintillators

ι is the size of the PMT (approximated as the side of a square)

$$X = \iota(a + b - c - d) / (a + b + c + d)$$

$$Y = \iota(a - b + c - d) / (a + b + c + d)$$

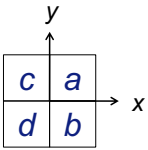

Segmented block of BGO or LSO scintillator

Reflector material between segments

Four single channel photomultiplier tubes

N.B. in the formula on this slide, X and Y are measured relative to the *centre* of block of 4 PMTs

Example:
64 crystals, 4 pmts:
multiplexing factor of 16

"Block detector" for PET

Flood irradiation of block detector with 511 keV γs:

- Spatial localisation of energy deposits
- Non-linear response corrected with "look-up table"

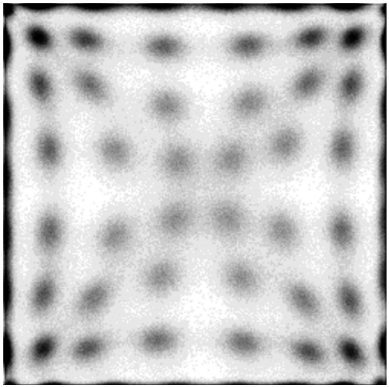

Forming the coincidence

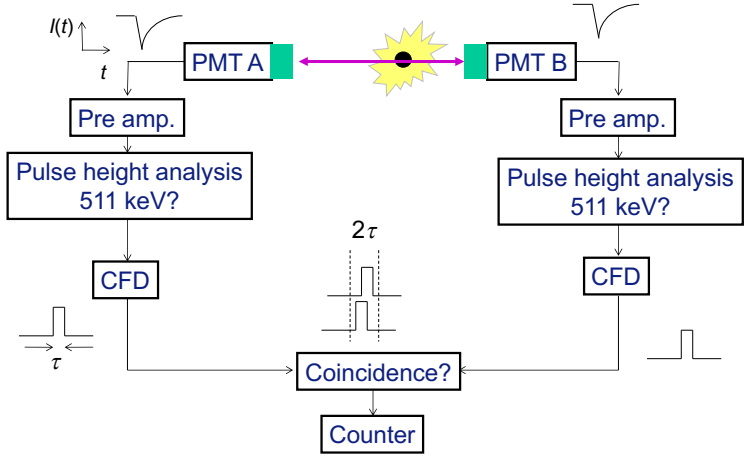

CFD: constant fraction discriminator

Constant fraction discriminator (CFD)

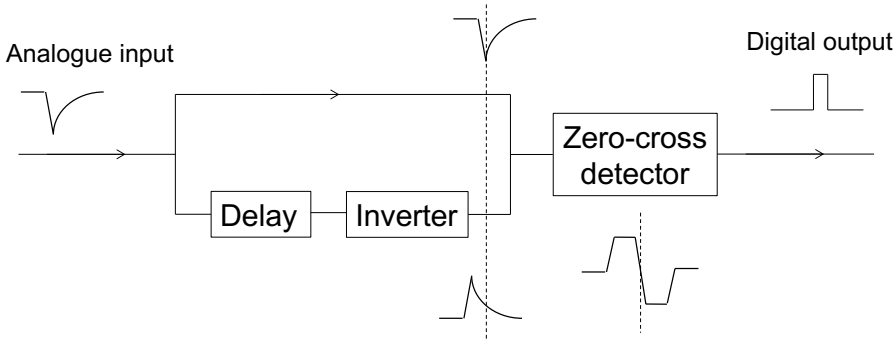

Objective: determine arrival time of pulse that is largely independent of pulse height

- Time at which signal reaches a fraction (e.g. 25%) of its peak amplitude

Time-of-flight measurement

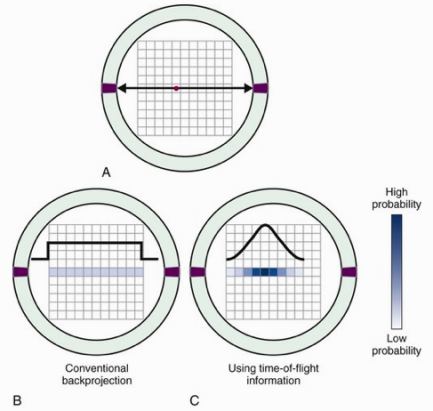

A: ACD configuration
B: No ToF: back-projection with equal probability
C: ToF: back-projection localised at Δd

If time-of-arrival difference is Δt, then:

$$\Delta d = \frac{c\Delta t}{2}$$

where Δd is measured w.r.t. the midpoint

Localises back projection to $\Delta d \pm \sigma_{\Delta d}$

Requires fast scintillator, fast electronics to yield $\Delta t \sim 100 - 200\,\text{ps}$

Leads to $\sigma_{\Delta d} \sim 2 - 3\,\text{cm}$

Of benefit in removal of ambiguities in reconstruction

Intrinsic spatial resolution

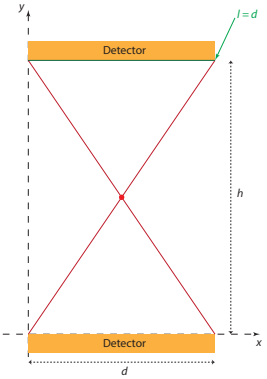

Source at $\left(x = \frac{d}{2}, y = \frac{d}{2}\right)$;
all events in cone accepted

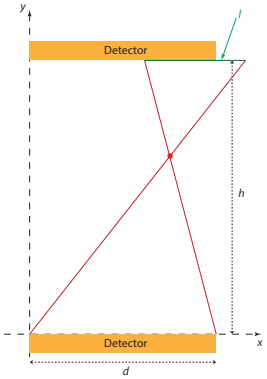

Source at (x, y);
accept only events striking both detectors

Intrinsic spatial resolution

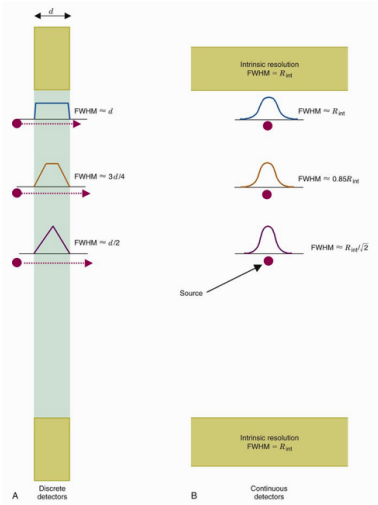

With coordinates defined above, projected length l is given by:

$$l = d\frac{h-y}{y}$$

Observations:

- At fixed y, l is independent of x
- Intensity recorded is a function of x
- At fixed y:
  - PDF rises from 0 at $x = 0$ and $x = d$
  - Plateau in PDF reached when $x_{\mathrm{P}} = \frac{d}{h}y$
- For $y = \frac{h}{2}$ no plateau because $x_{\mathrm{P}} = \frac{d}{2}$

Shown in LH column of figure

Intrinsic spatial resolution

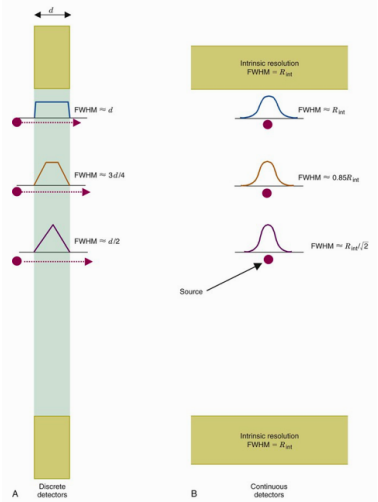

Referring now to RH column of figure ...

Define FWHM at $y = h$: $\mathrm{FWHM} = R_{\mathrm{int}}$

Intrinsic resolution:

- $y = h$: rectangular distribution
  $\sigma_{\mathrm{int}} = \frac{R_{\mathrm{int}}}{2} = \frac{d}{\sqrt{12}}$
- $y = \frac{h}{2}$: triangular distribution
  $\sigma_{\mathrm{int}} = \frac{R_{\mathrm{int}}}{2\sqrt{2}} = \frac{d}{\sqrt{2}\sqrt{12}}$
- Intermediate y: "truncated triangle"
  $\frac{d}{\sqrt{2}\sqrt{12}} \leq \sigma_{\mathrm{int}} \leq \frac{d}{\sqrt{12}}$

Measured intrinsic resolution

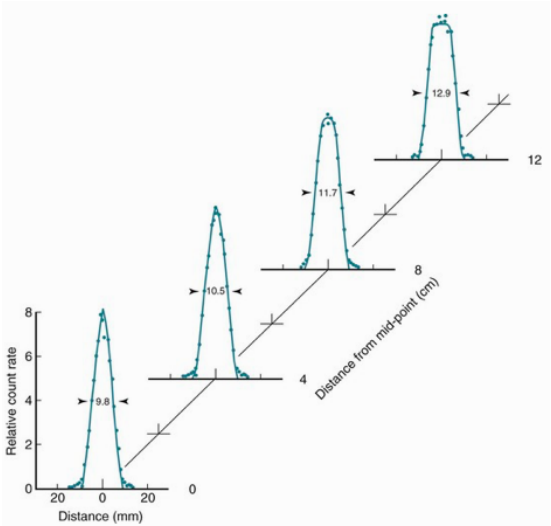

Measured "residuals" for:

- 2 detectors each with $d = 17\,\text{mm}$
- $\sigma_{\text{int}} = 4.91\,\text{mm}$
  $\Rightarrow \text{FWHM} = R_{\text{int}} = 9.81\,\text{mm}$

Resolution favourable cf SPECT with:

- Conjugate sampling
- Arithmetic mean position estimation

For equivalent position resolution PET is:

- More efficient that SPECT (collimator)
- Faster; all images taken at once

Factors that determine system resolution

Intrinsic resolution of PET system degraded by:

- Fundamental physics:
  - Non-zero range of positron as it slows down prior to annihilation
  - Residual momentum of positron at annihilation results in non-colinear photons
- Reconstruction:
  - Depth-of-interaction effect
  - Sampling effect
  - Filter effect

Fundamental physics: positron range

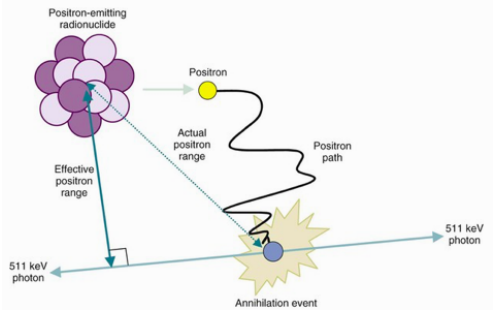

		Extrapolated Range (cm) in			Average Range (cm) in
Radionuclide	E_β^{max} (MeV)	Air	Water	Aluminum	Water
^{3}H	0.0186	4.5	0.00059	0.00022	—
^{11}C	0.961	302	0.39	0.145	0.103
^{14}C†	0.156	21.9	0.028	0.011	0.013
^{13}N	1.19	395	0.51	0.189	0.132
^{15}O	1.723	617	0.80	0.295	0.201
^{18}F	0.635	176	0.23	0.084	0.064
^{32}P	1.70	607	0.785	0.290	0.198
^{82}Rb	3.35	1280	1.65	0.612	0.429

Effective range depends on:

- $E_{\max}$
- Material, i.e. tissue

For relevant PET isotopes:

- $E_{\max}$ in range 0.5–1.8 MeV
- Results in e^+ range in range 2–8 mm

Fundamental physics: positron range

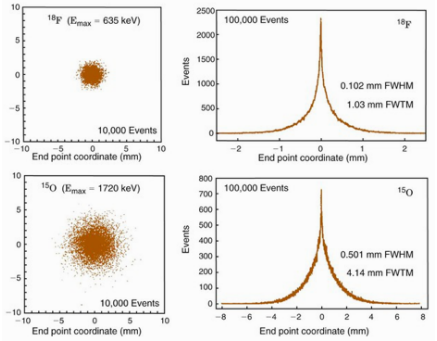

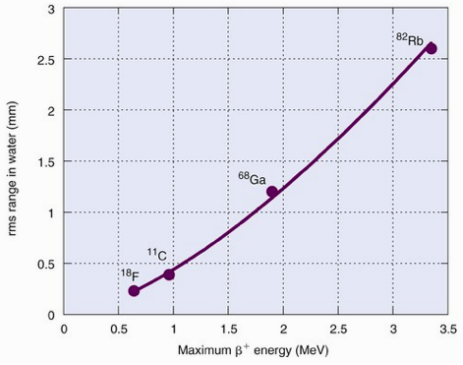

End-point coordinate distribution falls exponentially; certainly not Gaussian!

RMS of the effective range distribution used: FWHM: R_{range}; resolution: σ_{range}

Resolution improves as E_{max} falls

- ^{18}F gives improved resolution over other commonly used isotopes

Fundamental physics: non-colinearity

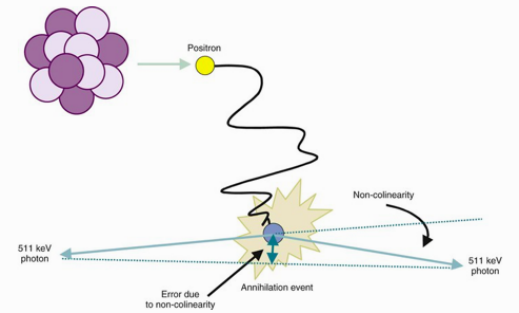

Non-colinearity angular distribution:

- Sufficiently Gaussian, use FWHM
- FWHM approximately 0.5°

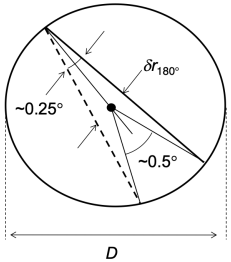

Geometrically:

$$R_{180} = \frac{D}{2} \times 0.25 \frac{\pi}{180} = 0.0022 \times D$$

and so resolution is $\sigma_{180} = \frac{R_{180}}{2}$

System resolution

System resolution, taken to be the resolution of the hardware, may now be evaluated:

- In terms of FWHM:

$$R_{\text{sys}} = \sqrt{R_{\text{int}}^2 + R_{\text{range}}^2 + R_{180}^2}$$

- In terms of resolution:

$$\sigma_{\text{sys}} = \sqrt{\sigma_{\text{int}}^2 + \sigma_{\text{range}}^2 + \sigma_{180}^2}$$

Example: clinical PET scanner:

- 5 mm scintillator: $R_{\text{int}} = 2.5\,\text{mm}$
- ^{18}F-labelled tracer: $R_{\text{range}} = 0.6\,\text{mm}$
- 800 mm diameter scanner: $R_{180} = 1.8\,\text{mm}$

Yields:

- $R_{\text{sys}} = 3.1\,\text{mm}$

Reconstruction: depth-of-interaction (DOI) effect

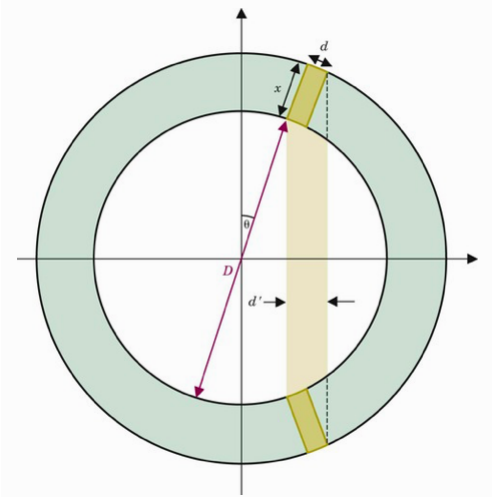

Thickness of scintillator used to stop 511 keV γ introduces a reconstruction uncertainty

For the case sketched, the apparent width of the detector, d', is given by:

$$d' = d\cos\theta + x\sin\theta$$

Can now use d' in the formulæ for, e.g., R_{int}

In a typical system, the DOI effect causes a degradation of $\sim 40\%$ in the resolution at a distance of 100 mm from the centre

Reconstruction: sampling effect

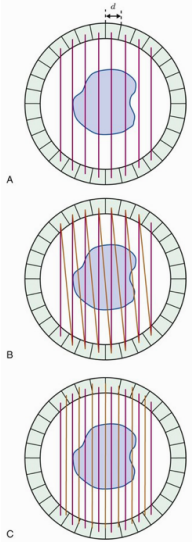

The intrinsic resolution is determined by the detector size, d

A) Sampling "frequency" determined by spacing, also d
Limits minimum feature size that can be resolved

B) Record neighbouring coincidences
Improved sampling; can reduce minimum feature size

c) Treat "neighbouring coincidences" (B) as additional samples
Implementation leads to improvement in detail in image

Reconstruction: filter effect

Image reconstruction exploits techniques such as filtered back projection

Filters are used to suppress noise, but, removing frequencies from the Fourier transform of the image can also remove detail from the image

Image-processing strategies need to be tailored to the situation, e.g. brain scans may require different strategies to abdominal scans

Sensitivity

Sensitivity is determined primarily by detector efficiency and solid angle coverage

True coincidence count rate $\mathcal{R}_{\mathrm{True}}$ for a positron-emitting source in air near midpoint between a pair of detectors is:

$$\mathcal{R}_{\mathrm{True}} = (\mathcal{R}_{\mathrm{e}^+})\,\epsilon^2 G \exp(-\mu T)$$

where:

- $\mathcal{R}_{\mathrm{e}^+}$ is the rate of positron emission (positrons/sec)
- ϵ is the intrinsic detector efficiency
  (no of γ-rays recorded by detector)/(no of γ-rays 'hitting' detector)
- G is the geometric efficiency of an individual detector
  $G = \frac{A_{\mathrm{det}}}{\pi D^2}$
- μ is the linear attenuation coefficient, T the total thickness

Sensitivity

Intrinsic detector efficiency for a variety of scintillators

Scintillator	$\mu_{scintillator}$ (cm^{-1})	$\mathcal{E}$(2 cm)	$\mathcal{E}^2$ (2 cm)	Photon yield (per keV)
NaI (Tl)	0.34	0.49	0.24	38
BGO	0.95	0.85	0.72	8
LSO	0.88	0.83	0.69	20-30
GSO	0.70	0.75	0.57	12-15

Types of coincidence event

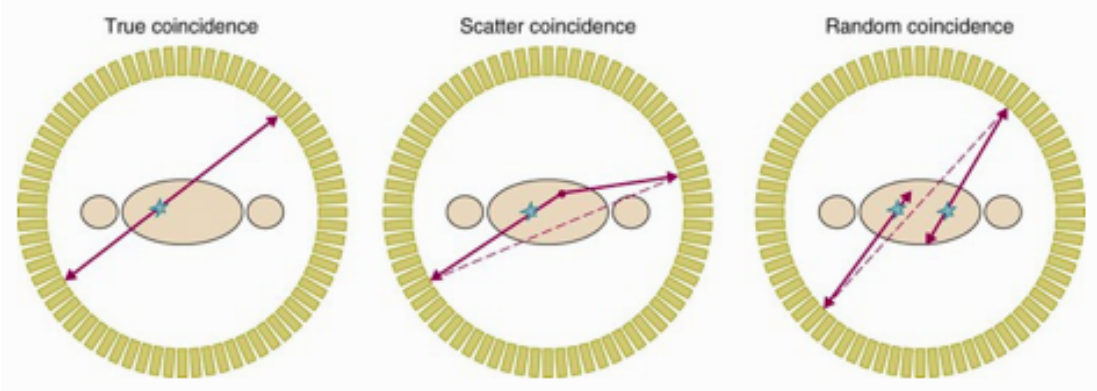

Random coincidence

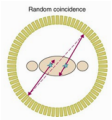

A random coincidence arises when two PMTs each receive a signal within the coincidence time window $\Delta t = 2\tau$

"Singles rate" in detectors i and j are $\mathcal{R}_{si}$ and $\mathcal{R}_{sj}$, random-coincidence rate:

$$\mathcal{R}_{\text{random}} = \Delta t \mathcal{R}_{si} \mathcal{R}_{sj}$$

Ratio of random to true coincidences $\propto \Delta t$; small Δt of benefit

$\mathcal{R}_{\text{random}}$ is proportional to the square of the activity in the body; true-coincidence rate rises linearly

Singles rates, and therefore $\mathcal{R}_{\text{random}}$, can be reduced with absorptive septa at the price of efficiency

Source of random coincidences not localised. Typical rates: $\sim 0.1\,\text{Hz}$ (brain) to $\sim 1\,\text{Hz}$ (abdomen). Reduces contrast & increases error in estimation of total dose

Scatter coincidence

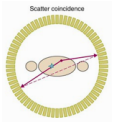

Scatter of one (or both) photons from single annihilation event in tissue or scanner

Pernicious since:

- Energy of scattered photon often differs little from decay photon
  $\rightarrow$ falls within the energy detection window
- Scattered photon is in coincidence with unscattered photon
  tiny ($<< \Delta t$) additional delay from the increased path length

$\mathcal{R}_{\text{scatter}}$ proportional to activity in body; same dependence as true-coincidence rate

$\mathcal{R}_{\text{scatter}}$ can be reduced with absorptive septa at the price of efficiency

Typical rates: $0.2 - 0.5\,\text{Hz}$ (brain) to $0.4 - 2\,\text{Hz}$ (abdomen); scatter-event fraction can be as high as $60 - 70\%$ for abdominal scans. Reduces contrast.

Sample PET scanner geometries

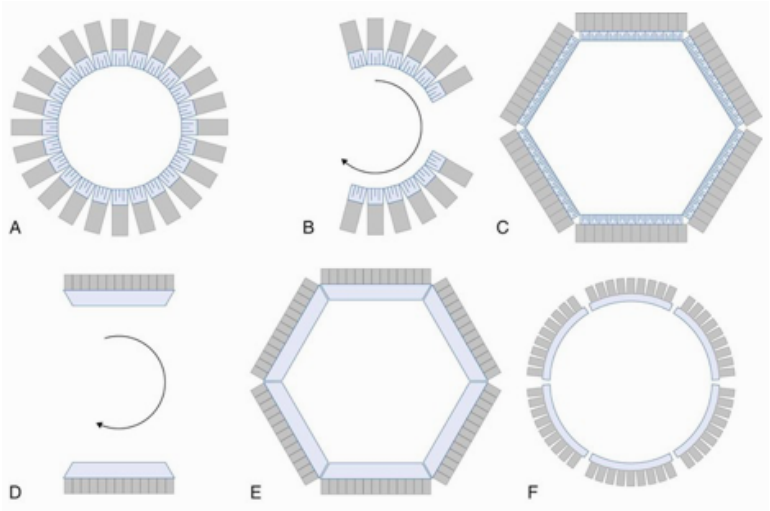

A) Full ring of block detectors
B) Partial ring of block detectors
C) Hexagonal "ring" of quadrant-sharing panel detectors
D) Dual-headed gamma camera
E) Hexagonal array of gamma cameras
F) Ring of curved plates of NaI(T)

With and without septa

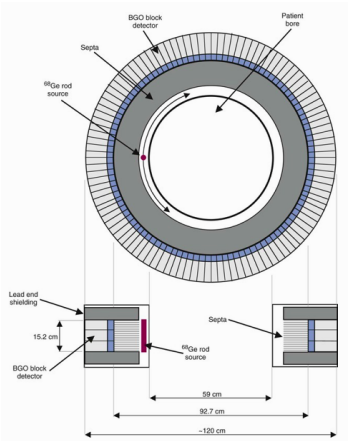

^{68}Ge rod for transmission scans to allow absorption correction

Retracted into Pb shield when not in use

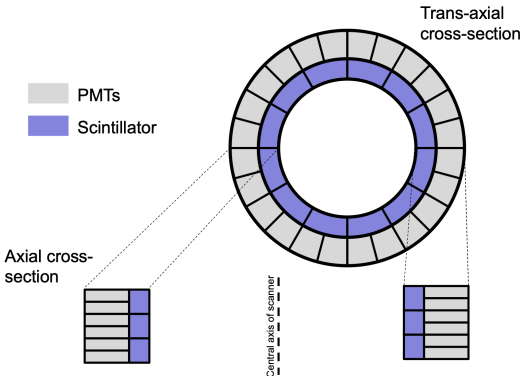

Large increase in sensitivity

Increase in ratio of

- scatter to true coincidences
- random to true coincidences

Event recording topologies

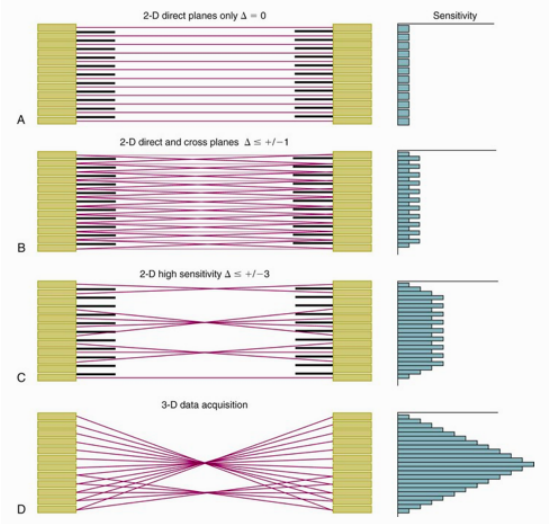

A) 2D data acquisition: septa such that:

- Accept only 'in line' γ pairs
- Reduced rate of scatters & randoms
- Recons: e.g. filtered back projection
- Least efficient

B) Cross planes: septa such that $\Delta = \pm 1$:

- Accept coincidences in neighbouring cells
- Increased rate of scatters & randoms
- Scanner centre, effective separation $= \frac{d}{2}$
- Recons: as in A using effective separation
- For n rings $\Rightarrow 2n - 1$ image planes
- Efficiency enhanced

Event recording topologies

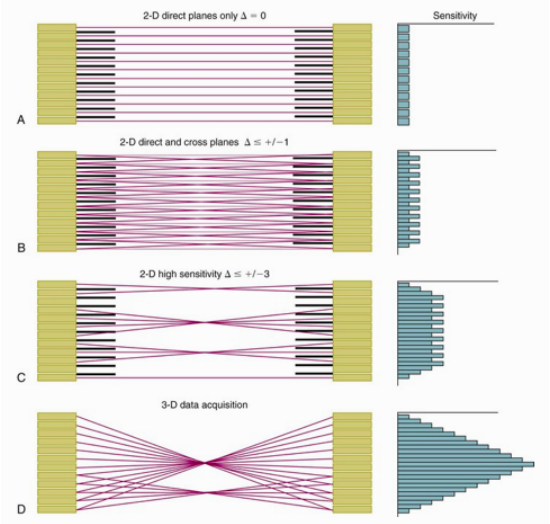

C) Cross planes: septa such that $\Delta = \pm 2; \pm 3$:

- Accept coincs for cells with $|\Delta| = 1, 2, 3$
- Increased rate of scatters & randoms
- Recons: for large $|\Delta|$ resolution decreases
- Efficiency enhanced

D) 3D acquisition mode: no septa

- Accept all coincidences
- Sensitivity increases $\times 4 - \times 8$
- Recons: require 3D algorithm
- Increased rate of scatters & randoms
- Most efficient

Numerical comparison of sensitivities

Histograms in figures A–D indicate spacial dependence of relative efficiency;
$\rightarrow$ indicates, for example, object of interest should be in the centre of a 3D scanner

For some 'typical' systems:

- PET scanner in 2D mode (1 slice per detector ring): 0.002–0.005 counts/s/Bq
- PET scanner in 3D mode (coincidences between all rings): 0.02–0.1 counts/s/Bq
- SPECT (for comparison): 0.0001–0.0003 counts/s/Bq

Corrections; normalisation

Want response to be proportional to activity in a given pixel

PET systems have many (10,000–20,000) PMTs. Various factors determine the signal recorded for a given number of incident photons, including:

- Precise dimensions of crystal in neighbourhood of PMT;
- Coupling of crystal to PMT;
- γ's angle of incidence and crystal uniformity;
- PMT gain and gain in electronics;
- Response of CFD;

So, require to "normalise" signal

Corrections; normalisation

Exploit rod source; take data while performing 360° rotation of rod

Normalisation factor, $\mathcal{N}_{ij}$ for pair of PMTs i, j is given by:

$$\mathcal{N}_{ij} = \frac{N_{ij}}{\bar{N}}$$

where N_{ij} is the number of coincidences recorded between PMTs i and j and $\bar{N}$ is the mean number of coincidences for all PMT pairs

Normalised number of coincidences, $\mathcal{C}_{ij}$ for PMT pair i, j is given by:

$$\mathcal{C}_{ij} = \frac{C_{ij}}{\mathcal{N}_{ij}}$$

where C_{ij} is the number of coincidences recorded between PMTs i, j recorded in a patient scan

Corrections; random coincidences; delayed window method

Coincidence time window Δt usually set to 2τ, where τ is the width associated with the PMT timing signal

Take $t_{\text{delay}} >> \Delta t$, then the number of coincidences between:

- Hit in PMT i at t_i and
- Hit in PMT j at $t_j = t_i + t_{\text{delay}} \pm \Delta t$

will give an estimate of the random coincidence rate

The delayed-window estimate of the random coincidence rate between PMTs i and j can be subtracted from the measured coincidence rate

Subtraction of the random coincidence rate leads to an increase in the statistical (counting) uncertainty:

$$\sigma\left(N_{\text{true}} + N_{\text{scat}}\right) = \sqrt{N_{\text{true}} + N_{\text{scat}} + 2N_{\text{random}}}$$

Corrections; random coincidences; singles method

Random coincidence rate between PMTs i and j determined above:

$$\mathcal{R}_{\text{random}}(i,j) = \Delta t \mathcal{R}_{si} \mathcal{R}_{sj}$$

$\mathcal{R}_{\text{random}}(i,j)$ can now be subtracted PMT pair by PMT pair

Singles rate is large, so, correction for random coincidences based on singles has much greater statistical weight than delayed-window method

For the singles method the increase in the statistical (counting) uncertainty is:

$$\sigma\left(N_{\text{true}} + N_{\text{scat}}\right) = \sqrt{N_{\text{true}} + N_{\text{scat}} + N_{\text{random}}}$$

To use this method requires that the singles rate is monitored continuously

Corrections; scatter coincidences

Energy resolution of BGO/LGO used in PET is inferior to that of NaI making the "dual window" approach used in SPECT is inappropriate for PET

Common approaches to the calculation of the scatter correction:

1. Use the "unscatter-corrected image" and transmission image as input to estimate the rate of scatters
   $\rightarrow$ the image is then re-derived from the scatter-corrected image
2. Use a CT image taken in parallel with the PET image to derive the scatter correction
   $\rightarrow$ the image is then re-derived from the scatter-corrected image
3. Use events reconstructed outside the object. Such events can only arise due to scatter
   $\rightarrow$ the image is then re-derived from the scatter-corrected image

Corrections; attenuation

Attenuation correction derived for two colinear photons derived for SPECT . . . applies here too, so:

$$\mathcal{P}_{\text{coinc}} \propto \exp(-\mu D) \tag{2}$$

where $\mathcal{P}$ is the probability a coincidence will be formed, μ is the attenuation coefficient, and D is the total thickness of the subject

Equation 2 does not depend on the position of the source between the two PMTs

Attenuation correction can be obtained by taking a "blank" transmission scan with the rod source and a transmission scan with the patient in position. The correction factor for PMTs i and j, A_{ij} is given by:

$$A_{ij} = \frac{\text{Blnk}_{ij}}{\text{Trns}_{ij}}$$

where Blnk_{ij} is the result of the blank scan and Trns_{ij} is the result of the patient scan

Corrections; dead time

When the scanner is recording a valid coincidence event it is not able to record a second one

This leads to a period during which the scanner is "dead" and is referred to as "dead time"

Dead time is measured empirically using sources of varying activity to determine the fall-off in efficiency as a function of the activity of the source, the size of the object, and the detection threshold

The dead-time correction is then calculated using a computer model based on the measured dead time

^{18}F: fluorodeoxyglucose (FDG)

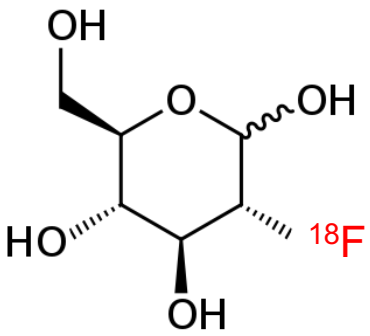

Analogue of glucose

Uptake depends on rate of glucose metabolism

Marker for many disease states and of therapeutic effect

FDG brain scans

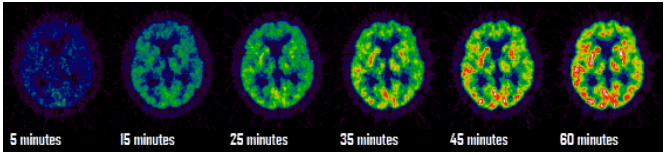

Healthy patient
- normal brain metabolism

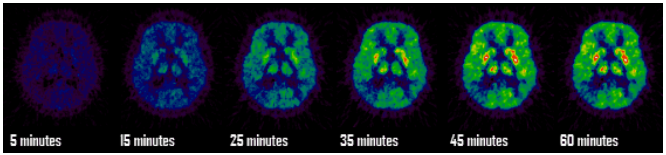

Alzheimers

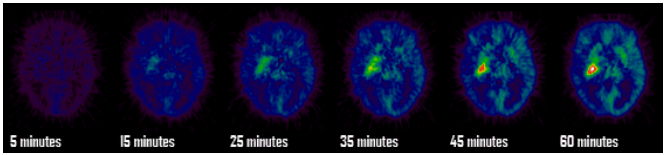

Brain tumour

http://www.insidestory.iop.org

FDG whole-body imaging

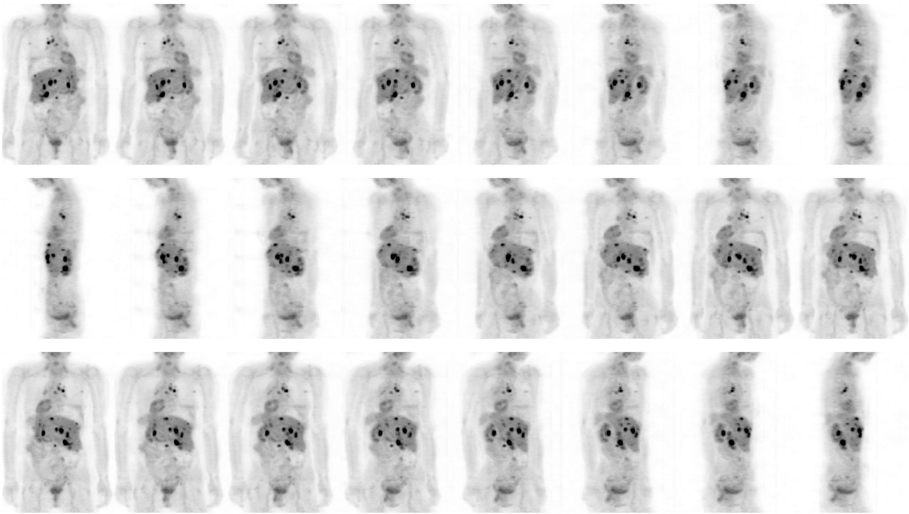

Cardiac imaging with PET

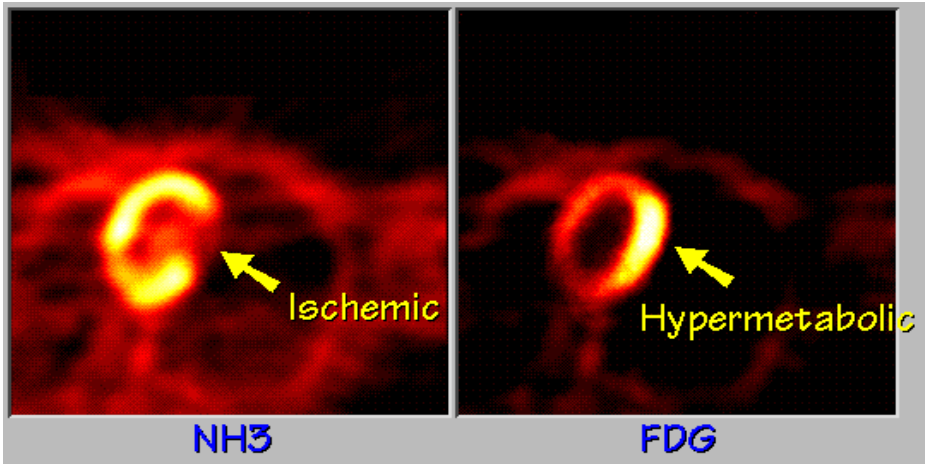

Section 3

Magnetic resonance imaging; MRI

‘Guilt-free’ imaging

Whole-body imager, Star Trek style

Nuclear diagnostics and X-ray imaging:

- Image constructed using ionising radiation
- Necessarily delivers dose to patient
- Dose implies risk of initiating disease

Magnetic resonance imaging (MRI):

- Image generated by exploiting magnetic moment of H nuclei
- Patient immersed in magnetic field
- No permanent harmful effects reported

Nuclear magnetic moment

Proton (and neutron) magnetic moment:

- Nucleons each have spin of $\frac{1}{2}$
- Magnetic moment generated by nuclear charge

  Contributions to nuclear spin arise from quarks and gluons. Quantitative explanation of nuclear magnetic moment is an active area of research
- For NMR and MRI critical point is that the magnetic moment, $\boldsymbol{\mu}$, is related to the nuclear spin, $\mathbf{s}$ by:

$$\boldsymbol{\mu} = \gamma \mathbf{s}$$

  where γ is the "gyromagnetic" ratio

Nuclear magnetic resonance

Effect of uniform magnetic field **B**:

- **B** provides "quantisation axis":
  $\Rightarrow$ nuclear dipoles align with magnetic field
- For proton spin is $\frac{1}{2}$, so only two states:
  Spin "up" and spin "down"
- Energy splitting; 2 energy levels:
  - Lower energy level has magnetic moment parallel to magnetic field
  - Higher energy level has magnetic moment anti-parallel to magnetic field
- Resonance:
  - Call energy splitting ΔE
  - Transitions between the two energy levels cause absorption or emission of electromagnetic (em) radiation for which $\Delta E = h\nu$
  - Resonance occurs when em radiation of frequency ν is injected

Magnetic resonance imaging

Magnetic resonance imaging (MRI) exploits this resonance

Steps:

- Apply uniform magnetic field, align proton (^{1}H) spins
- Apply radiation, at exactly ν, to cause transitions between "spin up" & "spin down" states
- Turn off the radiation . . . and . . .
- "Listen" for radiation at exactly ν as the spins realign

Brilliant! Simple principle and elegant technique. Now exploited in exquisitely sophisticated imaging systems.

The physical principles

1938: I. Rabi: Discovered nuclear magnetic resonance
Nobel Prize 1944

1946: F. Bloch & E. Purcell: Developed methods that allow precision methods using NMR
Nobel Prize 1952

1955/56: E. Odeblad & G. Lindström: Applied NMR to living cells from animal tissue

1968: J.A. Jackson and W.H. Langham: First NMR measurements from living animals

Cancerous and normal cells differ

Raymond Damadian

Relaxation times that characterise recovery of ground-state magnetisation shown to differ between normal and tumour cells

Early proposals for MRI scanners

Alexander Ganssen; patent 1967

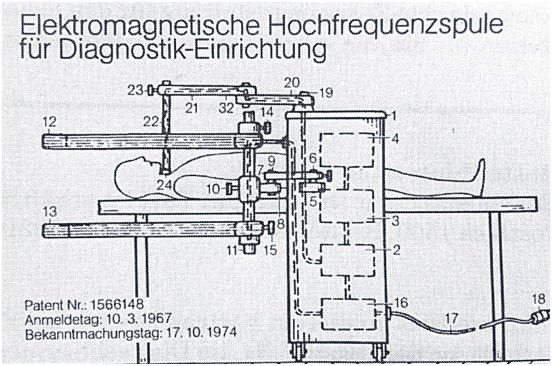

Raymond Damadian; patent 1972

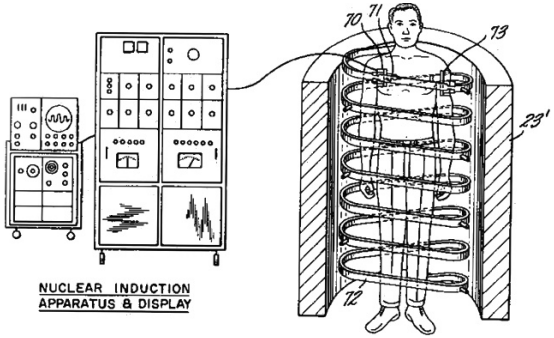

Spatial localisation using magnetic-field gradients

Paul Lauterbur

Superimpose field gradient on main uniform magnetic field. Incident em radiation at frequency ν only resident in a particular location in subject

Nature Vol. 242 16 March 1973

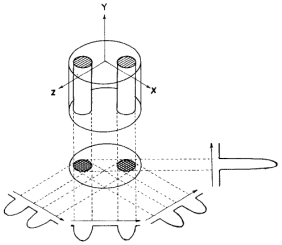

Fig. 1 Relationship between a three-dimensional object, its two-dimensional projection along the Y-axis, and four one-dimensional projections at 45° intervals in the XZ-plane. The arrows indicate the gradient directions.

Fig. 2 Proton nuclear magnetic resonance zeugmatogram of the object described in the text, using four relative orientations of object and gradients as diagrammed in Fig. 1.

Rapid, "snap-shot" MRI

Peter Mansfield

Use of "echo planar imaging" to allow fast "snap-shot" imaging required active screening of fields created by currents induced in cryostat walls

P. Mansfield, Nobel Lecture 2003

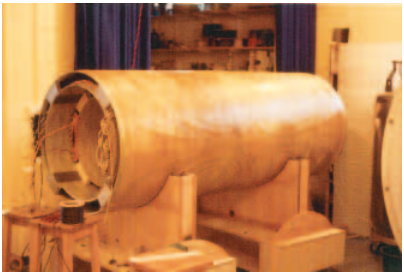

Figure 2. Photograph of a doubly screened active magnetic shielded gradient coil set for insertion in the super-conductive magnet of Figure 1.

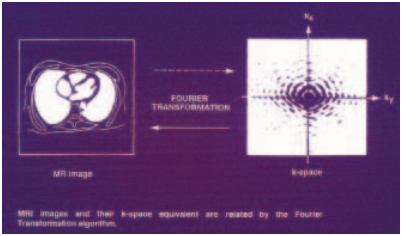

Figure 3. Diagram of a slice through the mediastinum showing the two lung fields and heart mass, also shown is the Fourier transform of this real-space image to the k-space map. (Reproduced with permission from M K Stehling, R Turner and P Mansfield, SCIENCE 253, 43–50 (1991).)

NMR zeugmatography

1975: A. Kumar, D. Welti, R. Ernst

Application of Fourier techniques to the reconstruction of images

Journal of Magnetic Resonance, Vol 18, P 69–83(1975)

zeug·ma·tog·ra·phy (zūg'mă-tog'ră-fē),
Term coined by Lauterbur in 1972 for the joining of a magnetic field and spatially defined radiofrequency field gradients to generate a two-dimensional display of proton density and relaxation times in tissues, the first nuclear magnetic resonance image.

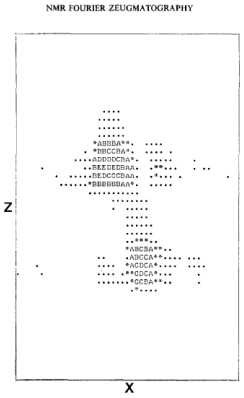

State of the art

Theoretical description; a hybrid of quantum and classical

Nuclear magnetic resonance & MRI are both inherently quantum mechanical effects:

- Signal is generated by manipulating the *spins* of hydrogen nuclei:
  - Spin is postulated to explain hyperfine structure, Stern-Gerlach experiment, ...
  - Understood theoretically through the symmetries of space and time
- Magnetic moment of proton, $\boldsymbol{\mu}$, is related to the proton spin, $\mathbf{s}$, by:

$$\boldsymbol{\mu} = \gamma \mathbf{s}$$

where γ is the "gyromagnetic ratio"

Hybrid, quantum/classical treatment:

- Quantum mechanics: energy splitting and population in ground and excited state
- Classical: magnetisation vector, its precession, and the manipulation of the magnetisation vector to generate the signals used for imaging

Interaction of nuclear magnetic dipole with uniform magnetic field

The contribution, $\delta\mathcal{U}$, to the potential energy of a proton immersed in a magnetic field, $\mathbf{B}$, is given by:

$$\delta\mathcal{U} = -\mathbf{B} \cdot \boldsymbol{\mu}$$

Lets consider a proton which, in the absence of a magnetic field has energy E. Applying the magnetic field introduces $\delta\mathcal{U}$ into the Schrödinger equation resulting in a splitting of the proton energy level such that $E \rightarrow E'$ given by:

$$E' = E \pm E_{m_s}$$

where

$$E_{m_s} = -m\gamma\hbar B_0$$

where m is the quantum number associated with the component of the proton spin parallel to $\mathbf{B}$, $\hbar$ is Planck's constant divided by 2π, and B_0 is the magnitude of $\mathbf{B}$
For the proton:

$$m_s = \pm\frac{1}{2}$$

Larmor equation

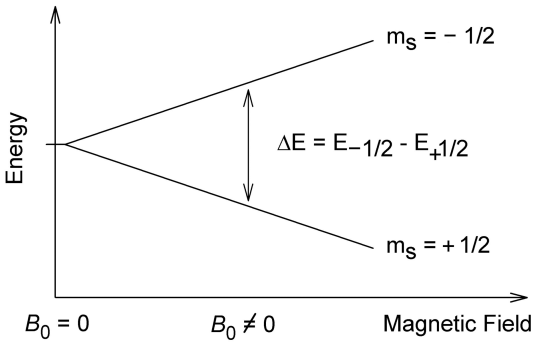

ΔE, splitting between two levels with $m_s = \pm\frac{1}{2}$:

$$\Delta E = \gamma \hbar B_0$$

Planck's law relates energy splitting to the angular frequency, ω, of the radiation required to excite the transition, therefore:

$$\Delta E = \hbar \omega$$

Writing ω in terms of γ and B_0 yields the Larmor equation:

$$\omega = \gamma B_0$$

Gyromagnetic ratios of some nuclei

Definition of gyromagnetic ration, γ:

> *The gyromagnetic ratio, γ, of a particle or system is the ratio of its magnetic dipole moment to its angular momentum*

For charged body of charge q, mass m rotating about an axis of symmetry:

$$\gamma = \frac{qe}{2m}$$

where e is the magnitude of the charge on the electron

For proton, $q = 1$, $m = m_p$, the proton mass.

$\eth$ is sometimes used instead of γ:

$$\eth = \frac{\gamma}{2\pi}$$

nucleus	γ (rad MHz T^{-1})	ð = γ / 2 π
^{1}H	267.513	42.576
^{2}H	41.065	6.536
^{3}He	203.789	32.434
^{7}Li	103.962	16.546
^{13}C	67.262	10.705
^{14}N	19.331	3.077
^{15}N	27.116	-4.316
^{17}O	36.264	5.772
^{19}F	251.662	40.053
^{23}Na	70.761	11.262
^{27}Al	69.763	11.103
^{31}P	108.291	17.235
^{57}Fe	8.681	1.382
^{63}Cu	71.118	11.319
^{67}Zn	16.767	2.669
^{129}Xe	73.997	11.777

Examples

Larmor equation: $\omega = \gamma B_0 \quad \Rightarrow \quad \nu = \frac{\gamma}{}B_0$
For hydrogen nucleus, ^{1}H, $\frac{\gamma}{} = 42.58\,\text{MHz/T}$

What is the resonance frequency for ^{1}H when:

- $B_0 = 1.5\,\text{T}$?
- $B_0 = 3.0\,\text{T}$?

What are the corresponding values for the energy splittings $\Delta E = h\nu$, where h is Planck's constant?

Populations in the two spin states

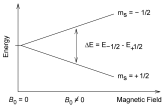

^{1}H in tissue in thermal equilibrium, so, partition between the populations in the two spin states follows the Boltzmann distribution:

$$\frac{N_+}{N_-} = \exp\left(-\frac{\Delta E}{k_\mathrm{B} T}\right)$$

where N_+ and N_- are the number of ^{1}H in $+\Delta E$ and $-\Delta E$ states respectively, k_B is Boltzmann's constant, and T is the temperature
For the human body, $k_\mathrm{B} T \approx 25.7\,\mathrm{meV}$, so:

$$\Delta E << k_\mathrm{B} T$$

Therefore, expanding the exponential and rearranging:

$$N_- - N_+ \approx N_S \frac{\Delta E}{2 k_\mathrm{B} T}$$

Magnetisation

Substituting for ΔE

$$N_- - N_+ \approx N_S \frac{\Delta E}{2k_B T} = N_S \frac{\gamma h B_0}{4\pi k_B T}$$

For $B_0 = 1.5\,\mathrm{T}$:

$$\begin{aligned} \frac{N_- - N_+}{N_S} &\approx \frac{42.58 \times 10^6 \times 6.6 \times 10^{-34} \times 1.5}{2 \times 1.38 \times 10^{-23} \times 300} \\ &\approx 4.5 \times 10^{-6} \end{aligned}$$

i.e. only 4.5 in a million protons in the body are available for activation in MRI at $B_0 = 1.5\,\mathrm{T}$

Bulk magnetisation is measurable

Population-density "mismatch" of ≈ 3 ppm per Tesla arises due to fact that energy splitting is small compared to $k_{\mathrm{B}} T$

Bulk magnetisation still measurable because 1 gram of water contains 10^{22} ^{1}H

Summary

MRI technique is based on manipulation of ^{1}H spins; a quantum-mechanical effect

MRI can be described using a hybrid quantum-mechanical/classical treatment

Application of magnetic field B_0 causes splitting ΔE between the two spin states of an ^{1}H nucleus:

$$\Delta E = \hbar\omega$$

where ω is the Larmor frequency:

$$\omega = \gamma B_0$$

Population of lower energy state of ^{1}H is ≈ 3 ppm per Tesla greater than higher energy state

The Larmor equation and bulk magnetisation; reprise

The quantum mechanical treatment presented in lecture 7 led to the **Larmor equation**:

$$\omega = \gamma B_0$$

ω is the Larmor frequency, B_0 the magnitude of the magnetic field, γ the gyromagnetic ratio

ω is the resonant frequency in an external magnetic field

The **bulk magnetisation** was obtained by considering the partition between the two energy states of the ^{1}H nuclei in the magnetic field:

$$N_- - N_+ \approx N_S \frac{\Delta E}{2k_\mathrm{B}T} = N_S \frac{\gamma \hbar B_0}{2k_\mathrm{B}T}$$

where the notation is that defined in lecture 7

Classical magnetic moment in magnetic field

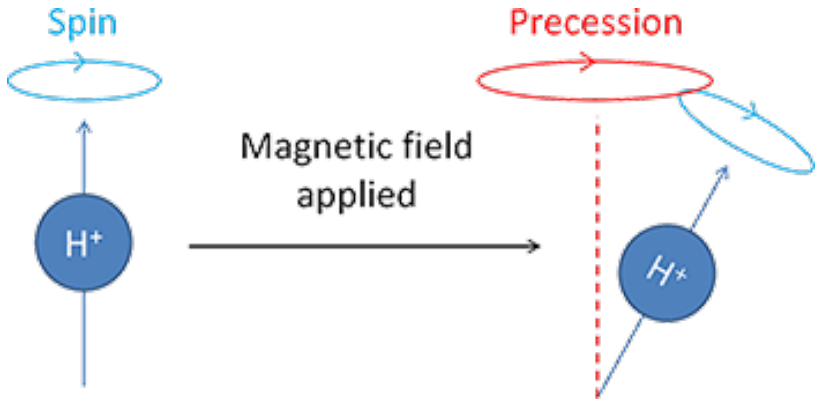

Magnetic moment that makes an angle with a magnetic field will precess around the magnetic-field axis.

Classical derivation of the Larmor equation

Classically, a magnetic moment, **M**, in a magnetic field **B**, experiences a torque given by the Bloch equation:

$$\frac{d\mathbf{M}}{dt} = \gamma\left(\mathbf{M} \times \mathbf{B}\right)$$

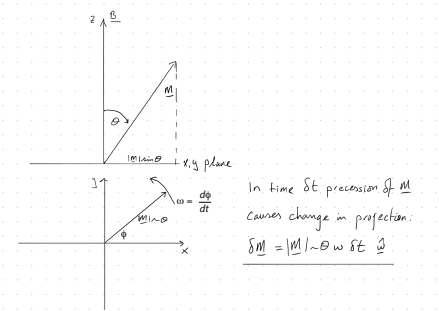

M makes an angle θ w.r.t. **B**. So:

$$\mathbf{M} \times \mathbf{B} = MB_0 \sin\theta\hat{\boldsymbol{\omega}}$$

So:

$$\frac{d\mathbf{M}}{dt} = \gamma MB_0 \sin\theta\hat{\boldsymbol{\omega}} = M\sin\theta\omega\hat{\boldsymbol{\omega}}$$

Which gives the Larmor equation:

$$\omega = \gamma B_0$$

Examples—from lecture 7

Larmor equation: $\omega = \gamma B_0 \quad \Rightarrow \quad \nu = \gamma B_0$

Energy splitting: $\Delta E = \hbar\omega \quad \Rightarrow \quad \Delta E = h\nu$

$h = 4.1357 \times 10^{-15}\,\mathrm{eV\,s}$

For hydrogen nucleus, ^{1}H, $\gamma = 42.58\,\mathrm{MHz/T}$

Calculating the values of ν and ΔE yields:

Magnetic field B_0 (T)	Larmor frequency (MHz)	ΔE (eV)
1.5	63.87	2.64E-07
3.0	127.74	5.28E-07

For comparison:

- FM radio waveband runs from 88.1 MHz to 108.1 MHz;
- $k_\mathrm{B}\,T = 2.59 \times 10^{-2}\,\mathrm{eV}$

Larmor precession

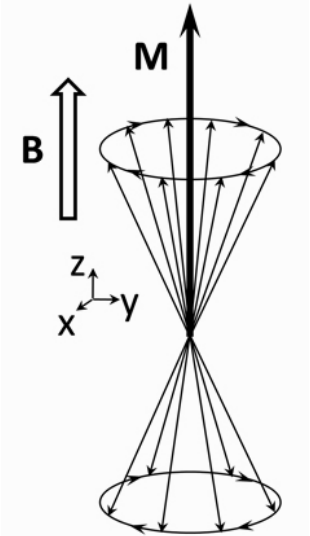

Ensemble of ^{1}H nuclei, the majority (by $\approx 3\,\mathrm{ppm\,T^{-1}}$) orientated parallel to **B** precess at equilibrium around **B** at the Larmor angular frequency ω

Net magnetisation, **M**, produced is parallel to **B**.

There is no net magnetisation in the transverse (x, y) plane; sum of all contributions cancel

Result is that there is no change in the magnitude or direction of the magnetisation vector so no RF signal is produced

Key feature of MRI: manipulate **M** so as to produce a measurable RF signal

First, a static example

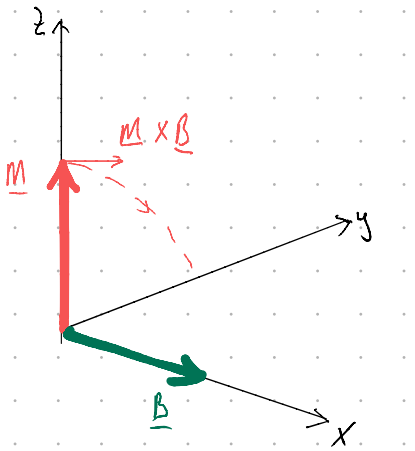

Consider magnetisation **M** parallel to z axis and **B** parallel to the x axis, as shown

Torque, $\mathbf{M} \times \mathbf{B}$, is therefore parallel to the y axis

Net result is that **M** will precess around the x axis towards the y axis

This is what is done in MRI ...

Rotating the magnetisation vector in MRI; principle

Main field, $\mathbf{B}_0$, produced with solenoid

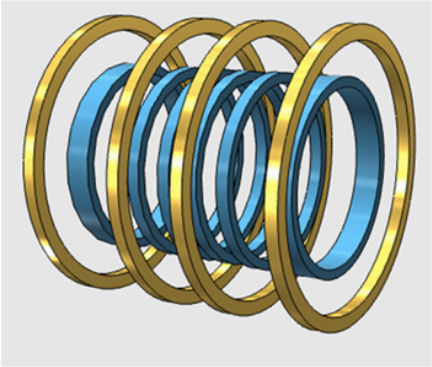

Induces magnetisation $\mathbf{M}$ parallel to $\mathbf{B}_0$

To rotate $\mathbf{M}$ away from $\mathbf{B}_0$ require magnetic field in transverse (x, y) plane

Call the field in the x, y plane $\mathbf{B}_1$; can be produced with a variety of coil arrangements, e.g. dipole or, more efficient, a "bird cage"

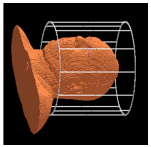

To cause $\mathbf{M}$ to precess require that $\mathbf{M}$ oscillates at the Larmor frequency, ω. I.e. require RF magnetic field $\mathbf{B}_1$

Rotating the magnetisation vector in MRI; mathematics

Take $\mathbf{B}_1$ to be "plane polarised" in x, y such that $B_{1_x} = B_1 \cos(\omega t + \alpha)$ and $B_{1_y} = B_1 \sin(\omega t + \beta)$; α and β are phases

$\mathbf{B}_1$ can be rewritten in terms of two circularly polarised fields:

$\mathbf{B}_{1_{ac}}$; anti-clockwise

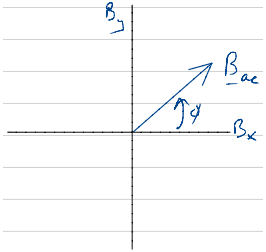

$B_{1_{ac}} = \frac{B_1}{2}$; $\phi_{ac} = \omega t + \alpha'$

$\mathbf{B}_{1_c}$; clockwise

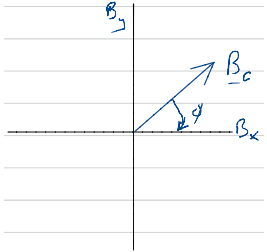

$B_{1_c} = \frac{B_1}{2}$; $\phi_c = \omega t + \beta'$

Rotating the magnetisation vector in MRI

One of the two counter rotating fields will rotate in the same direction as the nuclear precession

In the frame that is co-rotating with the precession of the net magnetisation vector the magnetic field will appear stationary in the transverse (x, y) plane. Call the co-rotating field B_1^+

B_1^+ is equal to either $B_{1_{ac}}$ or B_{1_c} depending on the direction of $\mathbf{B}_0$

The stationary field will therefore cause $\mathbf{M}$ to precess about a rotating axis in the (x, y) plane

The net result is that $\mathbf{M}$ can be rotated into the x, y plane where it will continue to precess

The precession of $\mathbf{M}$ in the x, y plane gives a detectable RF signal

Rotating the magnetisation vector in MRI

M is initially parallel to $\mathbf{B}_0$

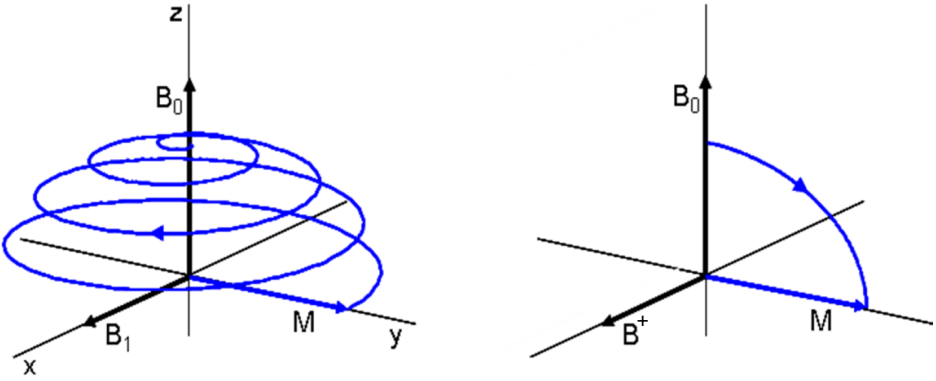

(a) Laboratory Frame of Reference *(b) Rotating Frame of Reference*

The flip angle

The flip angle, α, is proportional to the magnitude and duration of the RF pulse:

$$\alpha = \gamma B_1 t_P$$

where t_P is the duration of the RF pulse

90° pulse rotates magnetisation into transverse plane where it continues to precess

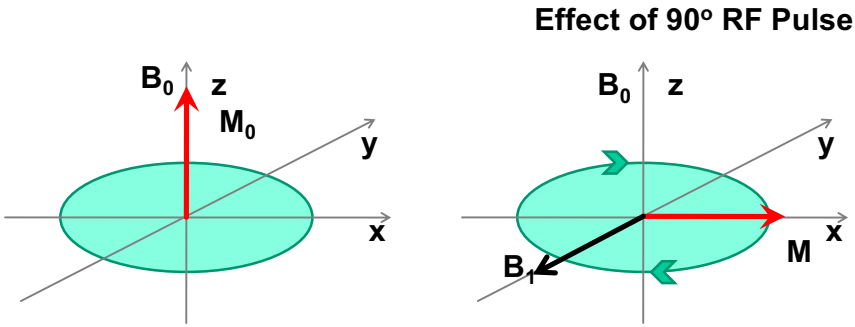

Example: calculating the duration of a 90° pulse

RF transverse magnetic field pulse is applied to rotate **M**

The magnitude of B_1 is $10\,\mu$T (i.e. 10^{-5} T)

At what rate with the **M** rotate away from the $\mathbf{B}_0$ axis?

How long will it take for the flip angle to reach 90°?

Example: calculating the duration of a 90° pulse

Half an answer . . . numerical results next time!

The magnitude of B_1 is $10\,\mu$T (i.e. 10^{-5} T)

At what rate with the **M** rotate away from the $\mathbf{B}_0$ axis?

It will rotate at the Larmor frequency, f_1 arising from the field B_1, i.e. $f_1 = \gamma B_1$

How long will it take for the flip angle to reach 90°?

The angle can be obtained by solving the equation: $\frac{\pi}{2} = \gamma B_1 t_P^{90^\circ}$ for $t_P^{90^\circ}$

Detection of signal precession of magnetisation vector

M rotated using B_1 RF pulse. If flip angle α is not a multiple of 180°, then, result of B_1 pulse is a component of magnetisation in the x, y plane that is precessing

This yields an RF wave that can be detected

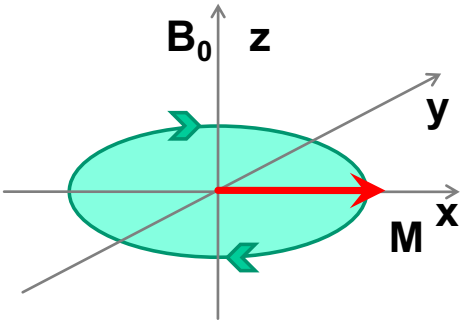

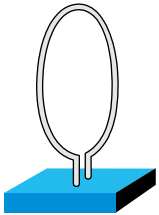

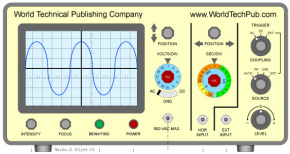

Free induction decay (FID)

Occurs when perturbing field (B_1) is turned off

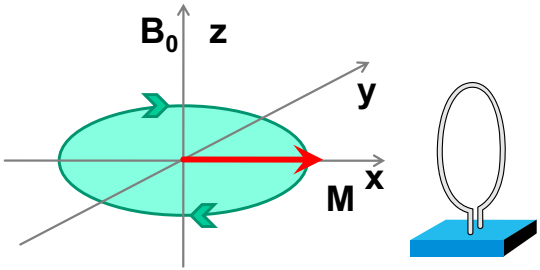

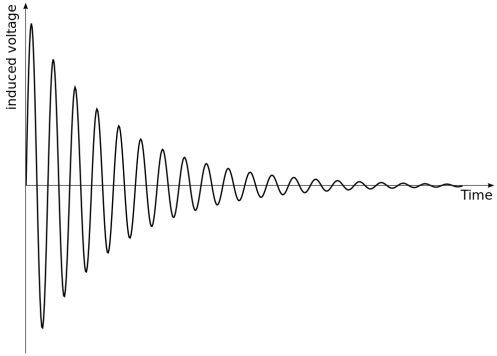

Note; exponential decay of amplitude of transverse magnetisation. Frequency of rotation remains the Larmor frequency corresponding to B_0

Spin-lattice (longitudinal) relaxation

When the B_1 pulse is turned off, the longitudinal magnetisation, M_z, recovers:

$$\frac{dM_z}{dt} = \frac{M_0 - M_z}{T_1} \qquad \Rightarrow M_z(t) = M_0 \left[1 - \exp\left(-\frac{t}{T_1}\right)\right]$$

The process is characterised by a time constant T_1

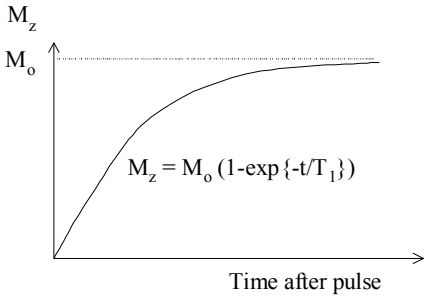

Spin-lattice relaxation:

- ^{1}H spins relax to the low-energy state. Energy released returns to the "lattice" as heat
- Relatively ineffective thermal coupling to ^{1}H nuclei results in T_1 being large, typically $T_1 > 200\,\text{ms}$

Spin-spin (transverse) relaxation

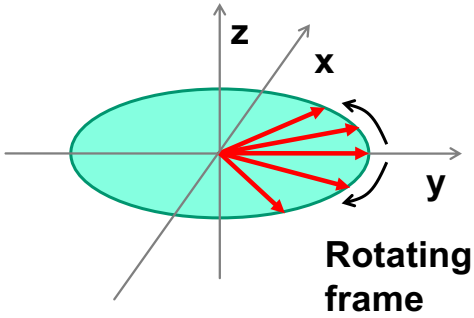

Contributions to M_{xy} smear out (decohere) rapidly

Causes M_{xy} to decay quickly

Some factors that affect the decoherence rate:

- Resonance frequency changes due to local magnetic fields
- Thermal excitations
- Spin "mobility"
- Presence of large molecules o, paramagnetic ions or molecules, outside interference

Spin-spin (transverse) relaxation

When the B_1 pulse is turned off, transverse magnetisation, decays:

$$\frac{dM_{xy}}{dt} = -\frac{M_{xy}}{T_2} \qquad \Rightarrow M_{xy}(t) = M_0 \exp\left(-\frac{t}{T_2}\right)$$

The process is characterised by a time constant T_2

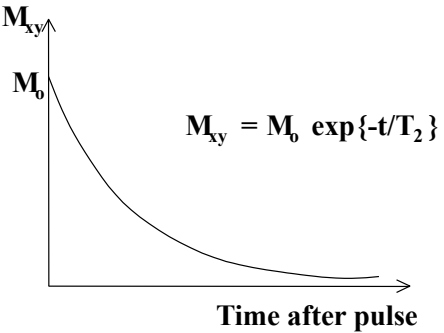

Spin-spin relaxation:

- ^{1}H spins interact magnetically with their neighbours
- Coupling causes a variety of magnetic fields, causing a variety of precessions
- Effective randomisation of precessional modes leads to efficient depolarisation in transverse plane
- Results in T_2 being comparatively small, typically $T_2 \lesssim 100\,\text{ms}$

Relaxation times for a variety of tissues

Tissue Type	T1 (ms)	T2 (ms)
Adipose tissues	240-250	60-80
Whole blood (deoxygenated)	1350	50
Whole blood (oxygenated)	1350	200
Cerebrospinal fluid (similar to pure water)	4200 - 4500	2100-2300
Gray matter of cerebrum	920	100
White matter of cerebrum	780	90
Liver	490	40
Kidneys	650	60-75
Muscles	860-900	50

Relaxation times characteristic of tissue type

For materials important for human imaging $T_1 > T_2$

Bloch equation revisited

Block equation may now be updated to include FID:

$$\frac{d\mathbf{M}}{dt} = \gamma\left(\mathbf{M} \times \mathbf{B}_0\right) - \frac{\mathbf{M}_{xy}}{T_2} + \frac{M_0 - M_z}{T_1}\hat{\mathbf{k}}$$

where:

- The first term describes the torque produced by the main (solenoid) field $\mathbf{B}_0$
- The second term describes the evolution of the transverse magnetisation vector $\mathbf{M}_{xy}$ due to the spin-spin interaction; time constant T_2
- The third term describes the evolution of the longitudinal magnetisation M_z due to the spin-lattice interaction; time constant T_1
- M_0 is the net magnetisation at equilibrium aligned with and proportional to $\mathbf{B}_0$

Complication: additional factors affecting the decay of the transverse magnetisation

T_2, the intrinsic spin-spin relaxation time is determined by non-reversible thermodynamic processes at the nuclear level.

The spin-spin time constant is reduced by a number of factors. A significant contribution comes from inhomogeneities in the main field $\mathbf{B}_0$

Inhomogeneities give rise to reversible thermodynamic processes. The associated relaxation of the transverse magnetisation is characterised by a time constant T_2'

The effective spin-spin time constant, T_2^* is given by:

$$\frac{1}{T_2^*} = \frac{1}{T_2} + \frac{1}{T_2'}$$

$T_2' < T_2$ and so $T_2^* < T_2$. Need to develop techniques to recover T_2 as this carries the clinically-relevant information

Comparison of T_2 and T_2'

T_2

- The individual dipoles that sum up to produce the transverse magnetization are not precessing at precisely the same rate
- As a water molecule tumbles due to thermal motions, each H nucleus feels a small, randomly varying magnetic field in addition to B_0
- When the random field adds to B_0, the dipole precesses a little faster, and when it subtracts from B_0, it precesses a little slower
- For each nucleus the pattern of random fields is different, so as time goes on the dipoles get progressively more out of phase with one another, and as a result no longer add coherently

T_2'

- The source of this T_2' effect is magnetic field inhomogeneity
- Because the precession frequency of the local transverse magnetization is proportional to the local magnetic field, any field inhomogeneity will lead to a range of precession rates
- Over time the precessing magnetization vectors will get out of phase with one another so that they no longer add coherently to form the net magnetization
- As a result, the net signal is reduced because of this destructive interference
- Static field offsets rather than fluctuating fields

Summary

Classically, the Larmor frequency corresponds to the rate of precession of the net magnetisation vector

An RF magnetic field pulse, $\mathbf{B}_1$, oscillating at the Larmor frequency in the x, y plane is applied to rotate the net magnetisation

Free induction decay causes the longitudinal magnetisation to recover with time constant T_1 and the transverse magnetisation to decay with time constant T_2

T_1 and T_2 are characteristic of the tissue, $T_1 > T_2$

An effective spin-spin relaxation time $T_2^* < T_2$ arises due to field inhomogeneities and other effects

What does it take to make an MRI image

NMR can be used to generate signals that depend on the concentration of ^{1}H in tissue; the basis of an imaging technique

The spin-lattice and spin-spin relaxation times, T_1 and T_2 respectively, depend on tissue type—so can be used to distinguish neighbouring tissues

To generate an image need to:

- Extract T_1 and T_2; and
- Spatially localise the signal

This lecture: extraction of T_1 and T_2 using RF pulse sequences
Next lecture: spatial localisation

Relaxation times revisited

Tissue Type	T1 (ms)	T2 (ms)
Adipose tissues	240-250	60-80
Whole blood (deoxygenated)	1350	50
Whole blood (oxygenated)	1350	200
Cerebrospinal fluid (similar to pure water)	4200 - 4500	2100-2300
Gray matter of cerebrum	920	100
White matter of cerebrum	780	90
Liver	490	40
Kidneys	650	60-75
Muscles	860-900	50

Relaxation times characteristic of tissue type

For materials important for human imaging $T_1 > T_2$

T_1 characteristic of recovery of longitudinal magnetisation

T_2 must be extracted from the decay of the transverse magnetisation which is characterised by T_2^* which is related to T_2 by:

$$\frac{1}{T_2^*} = \frac{1}{T_2} + \frac{1}{T_2'}$$

The spin-lattice relaxation time constant, T_1

System set up in equilibrium; net magnetisation, $\mathbf{M}_{\mathrm{eqm}}$, parallel to $\mathbf{B}_0$ and of magnitude M_{eqm}

90° RF magnetic field pulse applied to rotate net magnetisation, $\mathbf{M}_{\mathrm{eqm}}$, into x, y plane

Take $t = 0$ to be time at which 90° degree pulse ends. Magnitude of transverse magnetisation, M_{xy}, at $t = 0$:

$$M_{xy}(t = 0) = M_{xy}(0) = M_{\mathrm{eqm}}$$

M_{xy} decays exponentially, as described in lecture 8

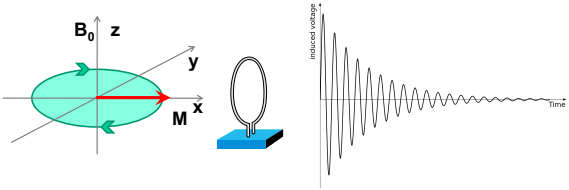

The spin-lattice relaxation time constant, T_1

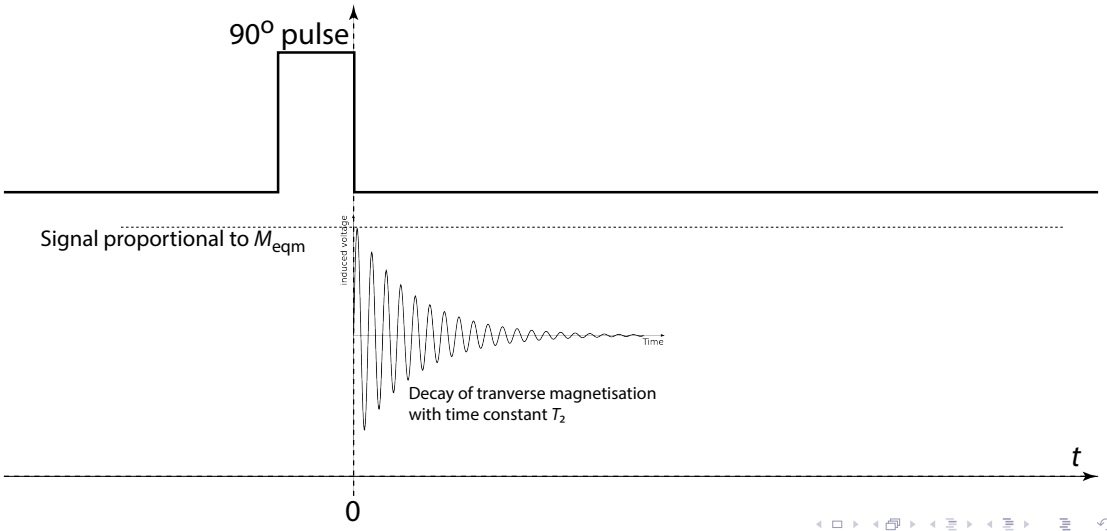

The spin-lattice relaxation time constant, T_1

Longitudinal magnetisation recovers according to:

$$M_z(t) = M_{\text{eqm}} \left[1 - \exp\left(-\frac{t}{T_1} \right) \right]$$

So, for $t \gtrsim 5T_1$, $M_z - M_{\text{eqm}} \lesssim 0.5\%$, i.e. longitudinal magnetisation has recovered

If a second 90° pulse is applied for $t < 5T_1$ then the resulting M_{xy} will be less than M_{eqm}

For example, if the second 90° pulse is applied at $t = T_1$, then $M_{xy}(t = T_1) = 0.63 M_{\text{eqm}}$

The spin-lattice relaxation time constant, T_1

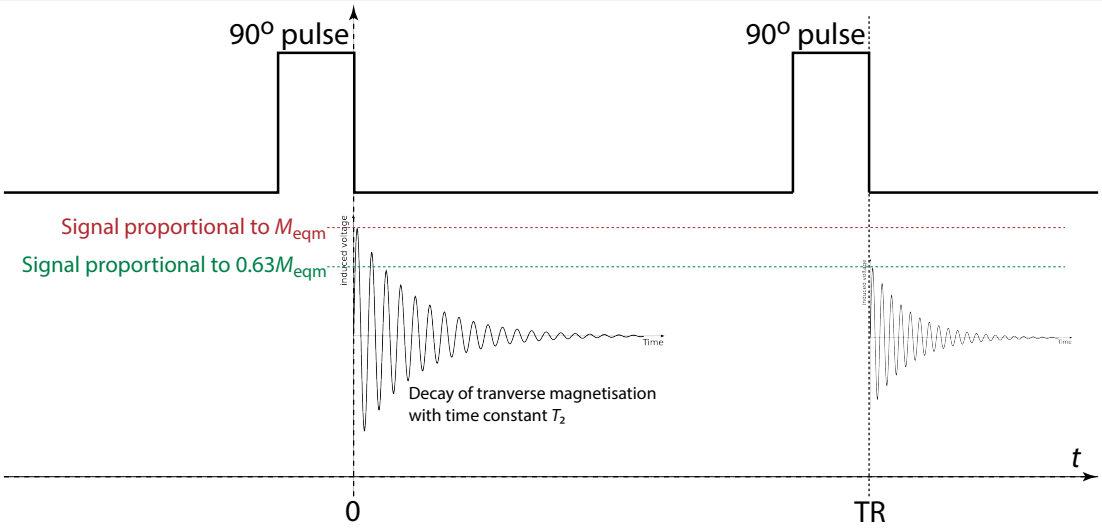

The spin-lattice relaxation time constant, T_1

Longitudinal magnetisation recovers according to:

$$M_z(t) = M_{\text{eqm}} \left[1 - \exp\left(-\frac{t}{T_1} \right) \right]$$

So, for $t \gtrsim 5T_1$, $M_z - M_{\text{eqm}} \lesssim 0.3\%$, i.e. longitudinal magnetisation has recovered

If a second 90° pulse is applied for $t < 5T_1$ then the resulting M_{xy} will be less than M_{eqm}

In general:

$$M_z(\text{TR}) = M_{\text{eqm}} \left[1 - \exp\left(-\frac{\text{TR}}{T_1} \right) \right]$$

So, repetition of 90° pulse at $t = \text{TR}$ gives $M_{xy}(\text{TR}) = M_z(\text{TR})$

Can extract T_1 by measuring $M_{xy}(\text{TR})$ as a function of TR

The spin-lattice relaxation time constant, T_1

"**Partial saturation pulse sequence**", graphical representation of evolution of magnetisation

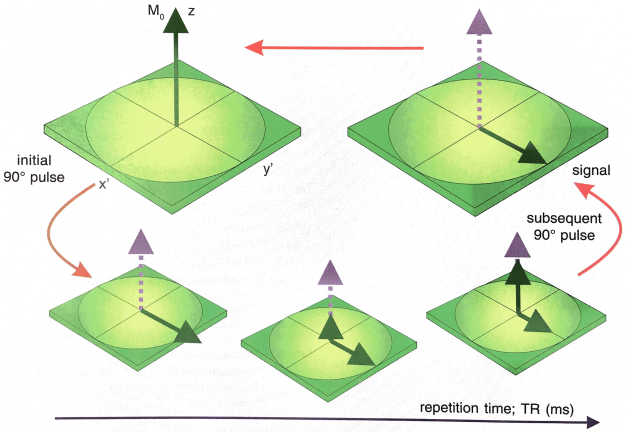

The spin-lattice relaxation time constant, T_1

Comparison of relative signal intensity in partial saturation sequence for two different tissues

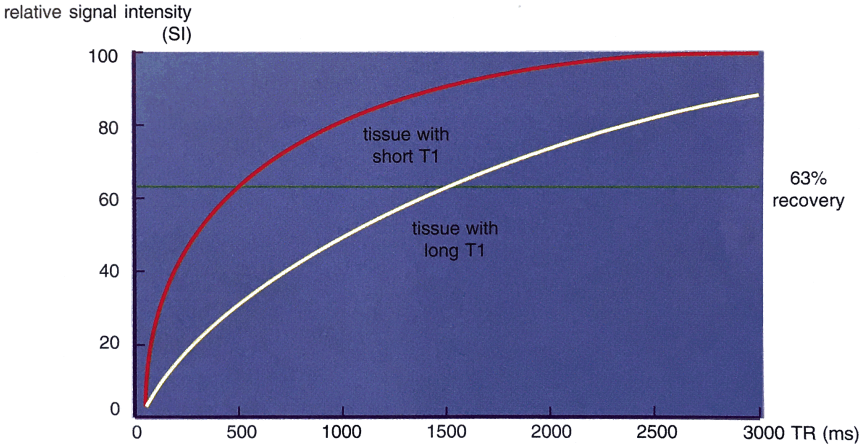

The spin-lattice relaxation time constant, T_1

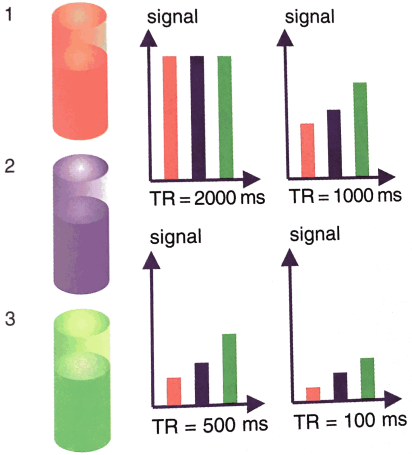

Example three types of tissue:

1. Blood: $T_1 = 1350\,\text{ms}$
2. Muscle: $T_1 = 875\,\text{ms}$
3. Fat: $T_1 = 230\,\text{ms}$

Note how tissues can be distinguished by comparing signal behaviour as a function of TR

Spin-spin relaxation time, T_2

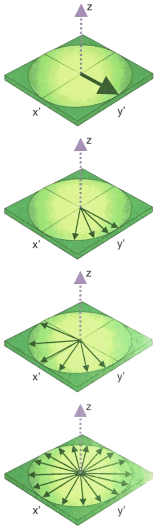

System set up in equilibrium; net magnetisation, $\mathbf{M}_{\mathrm{eqm}}$, parallel to $\mathbf{B}_0$ and of magnitude M_{eqm}

90° RF magnetic field pulse applied to rotate net magnetisation, $\mathbf{M}_{\mathrm{eqm}}$, into x, y plane

Take $t = 0$ to be time at which 90° degree pulse ends. At this instant net magnetisation begins to precess around $\mathbf{B}_0$

Rate of precession of individual ^{1}H nuclei depends on local magnetic environment: some precess faster, some slower. Results in decoherence, time constant T_2^* (see lecture 8)

Spin-spin relaxation time, T_2

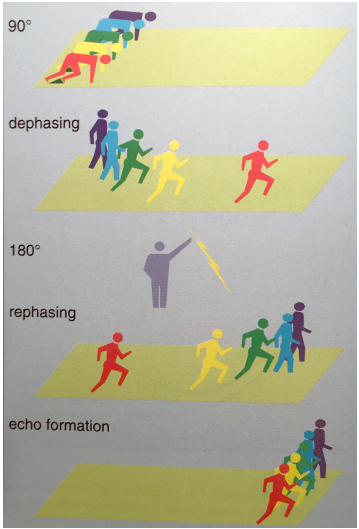

Before "doing the spins", an analogy:

- A set of sprinters have been prepared at the starting line
- The "starting gun" is the end of the 90° pulse
- The sprinters run for a period of time, t_{run}
- At t_{run} the sprinters' phase is rotated by 180°:
  The first becomes the last, etc.
- After a further t_{run} all sprinters are back in line
- The line of sprinters at $t = 2t_{\mathrm{run}}$ is an "echo" of the situation at $t = 0$

Spin-spin relaxation time, T_2

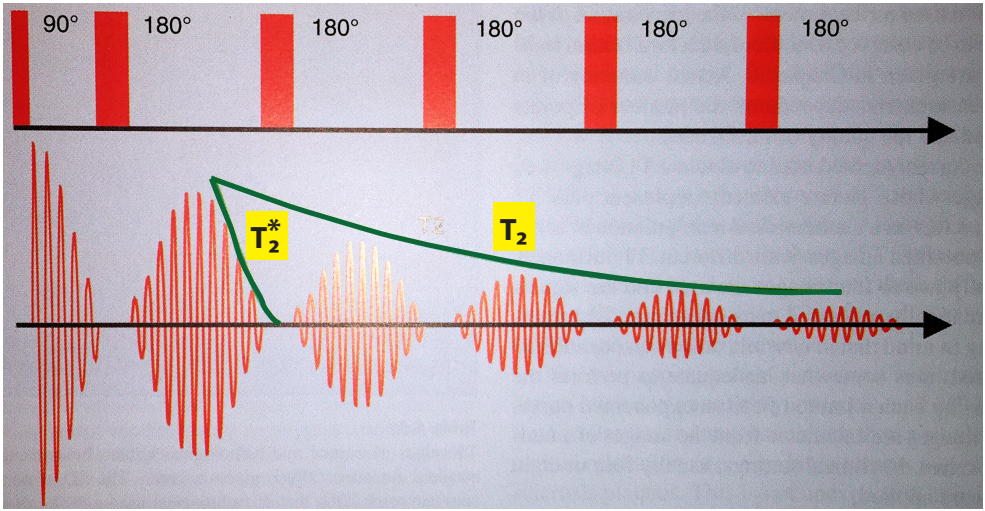

The spin-spin relaxation time constant, T_2

"**Spin echo sequence**", graphical representation of evolution of magnetisation

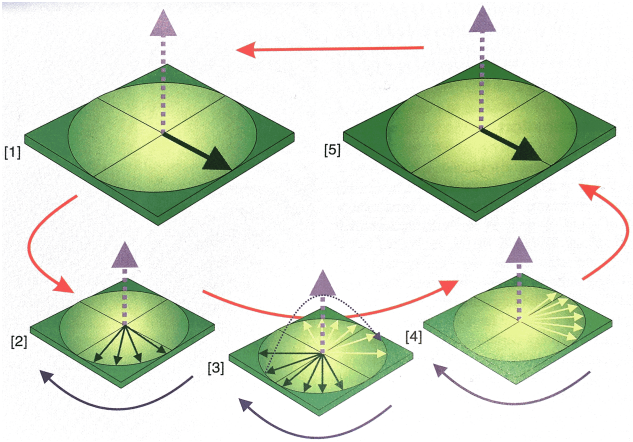

The spin-spin relaxation time constant, T_2

"**Spin echo sequence**", graphical representation of evolution of magnetisation

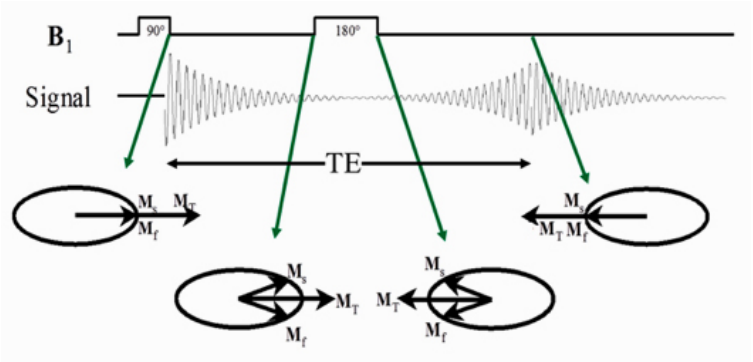

Spin-spin relaxation time, T_2

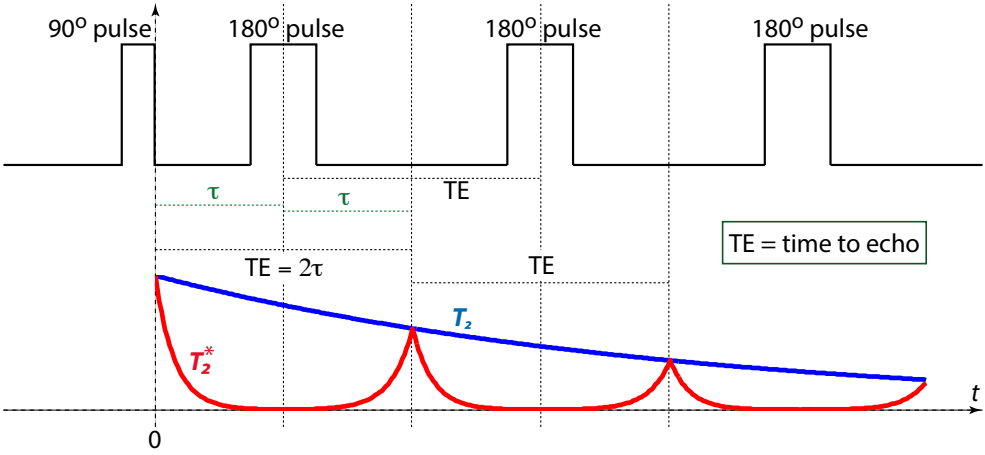

$$M_{xy}(\mathrm{TE}) = M_{\mathrm{eqm}} \exp\left(-\frac{\mathrm{TE}}{T_2}\right)$$

Inversion recovery pulse sequence: T_1

"**Inversion recovery pulse sequence**", graphical representation of evolution of magnetisation

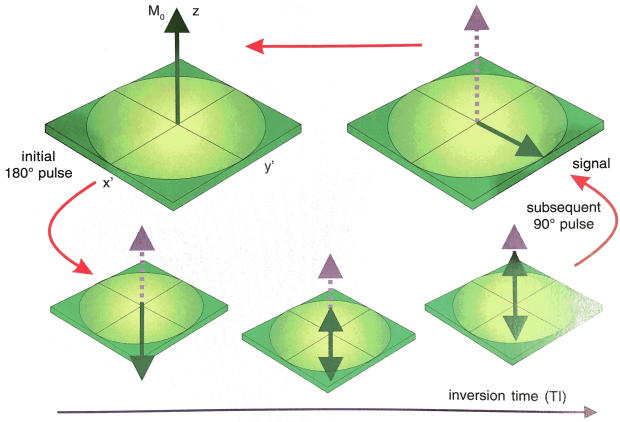

Inversion recovery pulse sequence: T_1

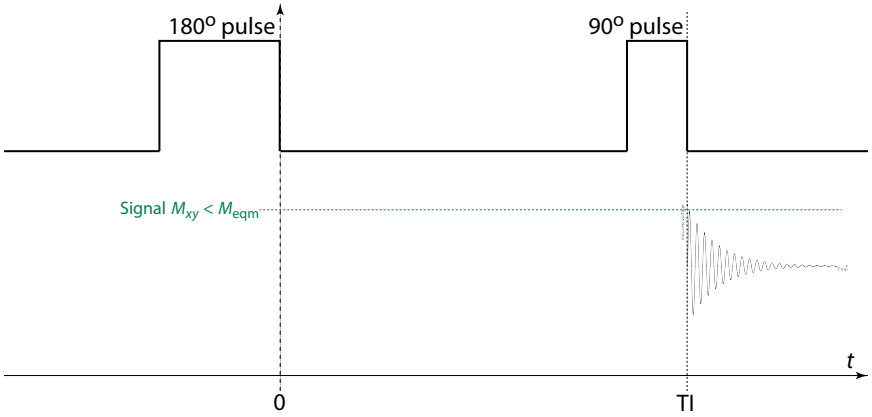

$$M_z(\mathrm{TI}) = M_{\mathrm{eqm}}\left[1 - 2\exp\left(-\frac{\mathrm{TI}}{T_1}\right)\right]$$

Example

You are required to optimise the contrast between CSF and grey matter.

For CSF: $T_1 = 2350\,\text{ms}$ and $T_2 = 180\,\text{ms}$
For grey matter: $T_1 = 900\,\text{ms}$ and $T_2 = 126\,\text{ms}$

Sketch the relaxation curves for the two tissues as a function of TR and TE.

To optimise the contrast find the TR and TE values that maximise the difference between the relaxation curves. This can be done by differentiating and solving for TR or TE when the derivative is 0.

Would you choose "T_1" contrast or "T_2" contrast to maximise the contrast between CSF and grey matter?

Summary

Block equation taking into account effective spin-spin relaxation time, T_2^*:

$$\frac{d\mathbf{M}}{dt} = \gamma\left(\mathbf{M} \times \mathbf{B}_0\right) - \frac{\mathbf{M}_{xy}}{T_2^*} + \frac{M_0 - M_z}{T_1}\hat{\mathbf{k}}$$

Partial saturation pulse sequence: series of 90° pulses separated by TR:

$$M_z(\mathrm{TR}) = M_{\mathrm{eqm}}\left[1 - \exp\left(-\frac{\mathrm{TR}}{T_1}\right)\right]$$

Inversion recovery pulse sequence: 180° pulse followed at $t = \mathrm{TI}$ by a 90° pulse. Sequence repeats after $t > 5T_1$:

$$M_z(\mathrm{TI}) = M_{\mathrm{eqm}}\left[1 - 2\exp\left(-\frac{\mathrm{TI}}{T_1}\right)\right]$$

Summary

Spin-echo pulse sequence: 90° pulse followed by series of 180° pulses separated by TE:

$$M_{xy}(\mathrm{TE}) = M_{\mathrm{eqm}} \exp\left(-\frac{\mathrm{TE}}{T_2}\right)$$

Introduction

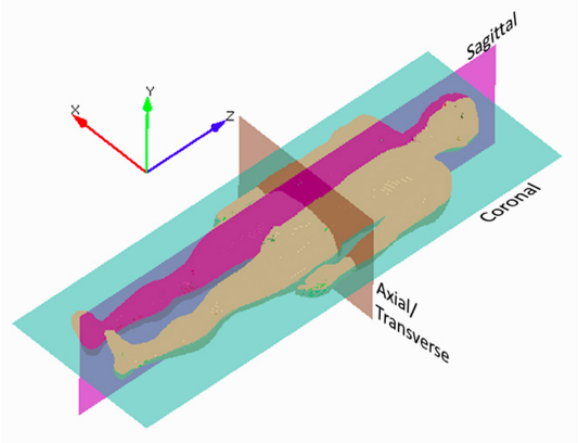

Conventional terminology & orientation of RH coordinate system

Contrast between tissues is afforded by RF B_1 pulse sequences such as those discussed in the preceding lectures

To make an image, need to localise the signals to appropriately small regions of space

To localise signals exploit:

- Resonance, i.e. Larmor frequency $\nu = \gamma B$
- By making B a function of position

i.e. make ν a function of position:

$$\nu(x, y, z) = \gamma B(x, y, z)$$

Slice selective excitation

Goal: excite a slice of tissue of thickness δ

So far a uniform "main field" $\mathbf{B}_0 = B_0\hat{\mathbf{k}}$ has been considered

Require to make B_z a function of position to make Larmor frequency position dependent

Apply "gradient" fields G_i such that B_z becomes:

$$B_z(x, y, z, t) = B_0 + xG_x(t) + yG_y(t) + zG_z(t)$$

Ideally G_i only have one field component directed along the z direction so that:

$$\mathbf{B} = B_z(x, y, z, t)\hat{\mathbf{k}}$$

With appropriate choice of G_i can generate a field gradient in any direction

Transverse slice; i.e. plane at fixed z

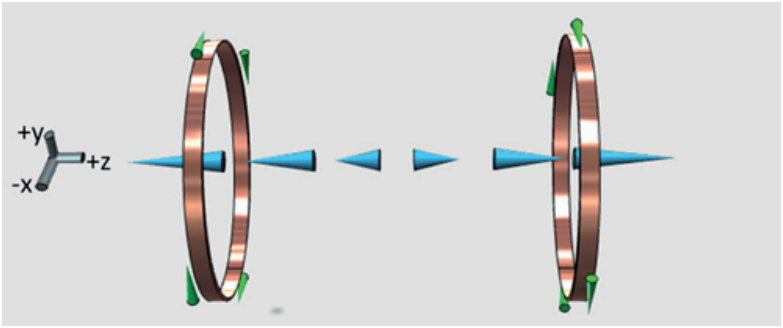

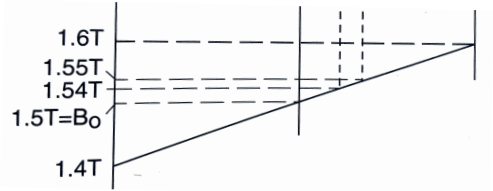

Example:
Helmholtz coils in opposition

Ideal gradient:
G_z = constant

Transverse slice; slice thickness and bandwidth

Lets say that response needs to be isolated to a slice: $\delta z = 5\,\text{mm}$ centred about $z = 0$
Take:

- The magnitude of the main field to be $B_0 = 1.5\,\text{T}$
- The field gradient $G_z = 50\,\text{mT}\,\text{m}^{-1}$
- $\gamma = 42.58\,\text{MHz}\,\text{T}^{-1}$

Take the slice to be $-2.5 < z < 2.5\,\text{mm}$, then the Larmor frequency will run over the following range:

$$\begin{aligned} \nu_{\min} &= (1.5 - 0.125 \times 10^{-3}) \times 42.58 \approx 63.8646\,\text{MHz} \\ \nu &= 1.5 \times 42.58 \approx 63.87\,\text{MHz} \\ \nu_{\max} &= (1.5 + 0.125 \times 10^{-3}) \times 42.58 \approx 63.8753\,\text{MHz} \end{aligned}$$

So, the spread of frequencies, the **bandwidth**, $\Delta\nu$ is:

$$\Delta\nu = 63.8646 - 63.8753 \approx 10.7\,\text{kHz}$$

Transverse slice; excitation of spins in slice

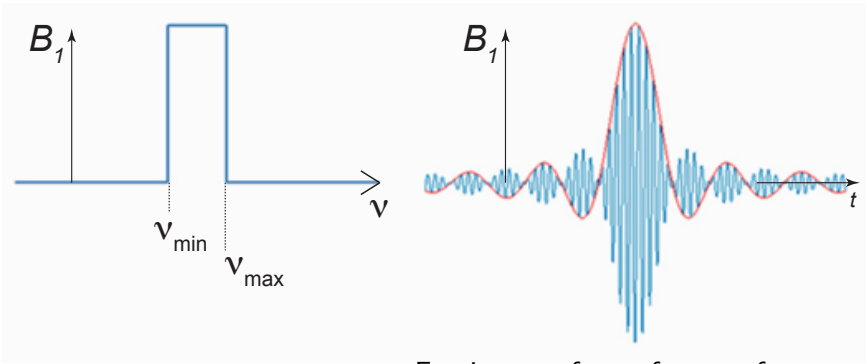

Idealised, square frequency distribution

Fourier transform of square frequency distribution

B_1 oscillates at ν, amplitude is modulated according to "sinc" function (red line)

Transverse slice: excitation pulses

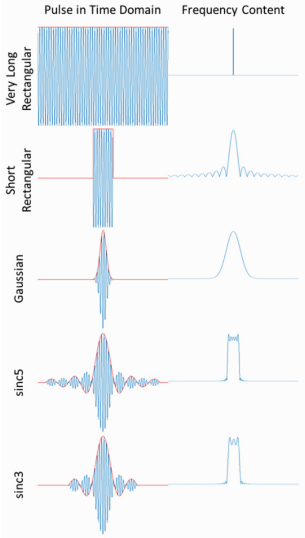

Frequency content of a variety of excitation pulses:

- *Very long rectangular*: narrow band of Larmor frequencies
- *Short rectangular*: frequency distribution follows "sinc" function:

$$A(\nu) \propto \mathrm{sinc}(\nu) = \frac{\sin \nu}{\nu}$$

  where $A(\nu)$ is the amplitude of contribution at frequency ν
- *Gaussian*: Fourier transform of Gaussian in t is a Gaussian in ν
- *sincN*: Since square pulse requires contributions over all ν, the frequency range is often truncated. The "sincN" function represents a sinc function for which the frequency range is truncated after N zero crossings

Transverse slice: determining the slice thickness

Slice thickness is determined by bandwidth ($\Delta\nu$) and field gradient (G_z)

Sorry for the change in notation!

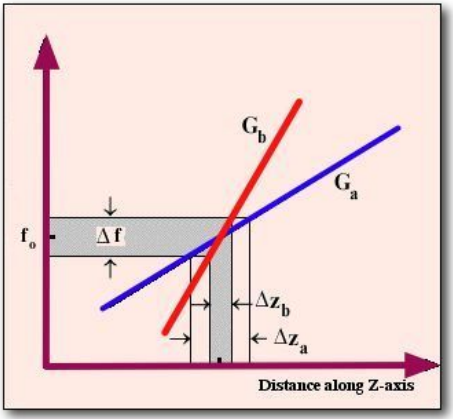

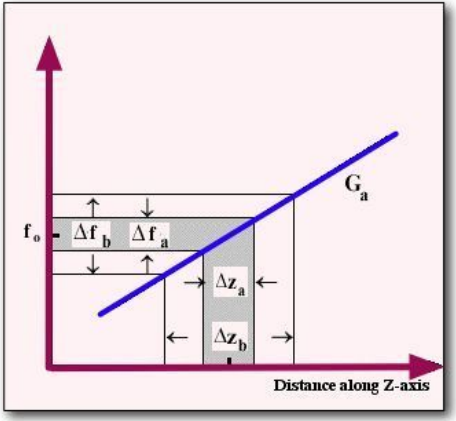

Transverse slice: spin rephasing pulse

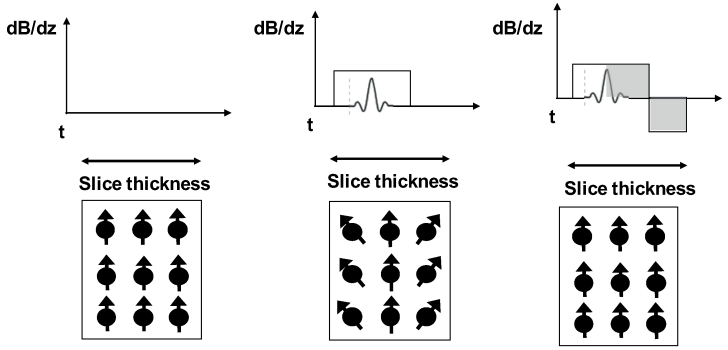

Larmor frequency across slice changes. So, over the time that the gradient pulse is applied, the spins precess at different rates

Therefore, at the end of the pulse the phase of the spins differs as a function of z

A rephasing pulse which reverses the field gradient (i.e. for which $G_z \rightarrow -G_z$) is applied

Transverse slice: spin rephasing pulse

Size of the spin rephasing pulse is determined by considering the rate at which the phase difference accumulates

Rate of precession is given by the Larmor frequency, ω, so change in phase of a spin during the gradient pulse is given by:

$$\Phi = \omega\tau = \gamma\left(B_0 + zG_z\right)\tau$$

where τ is the length of the gradient pulse in time

So, phase difference between edges of the slice and the centre is:

$$\Delta\Phi = \gamma\tau G_z\frac{\delta z}{2}$$

So, rephasing pulse, G_z^{rephase}, and the length over which it is applied, τ^{rephase} must satisfy:

$$G_z^{\text{rephase}}\tau^{\text{rephase}} = G_z\frac{\tau}{2}$$

Transverse slice: partial spin-echo pulse sequence

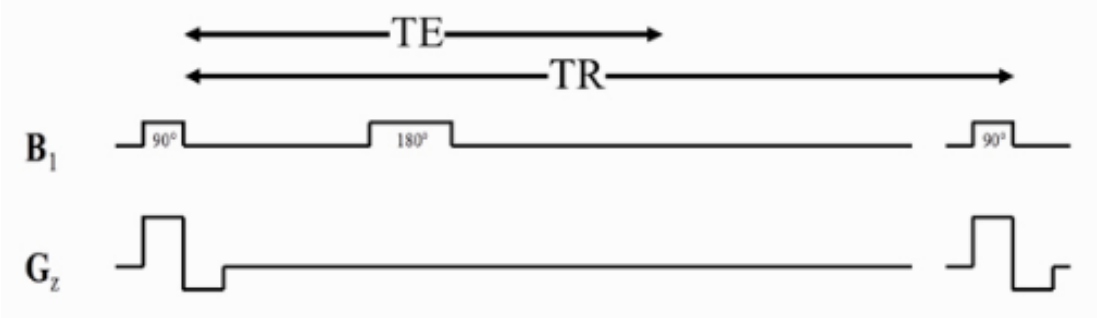

B_1 rotates net magnetisation in the selected slice with gradient pulse applied

Encoding spatial information into the net magnetisation

The basis is a 2D Fourier transform:

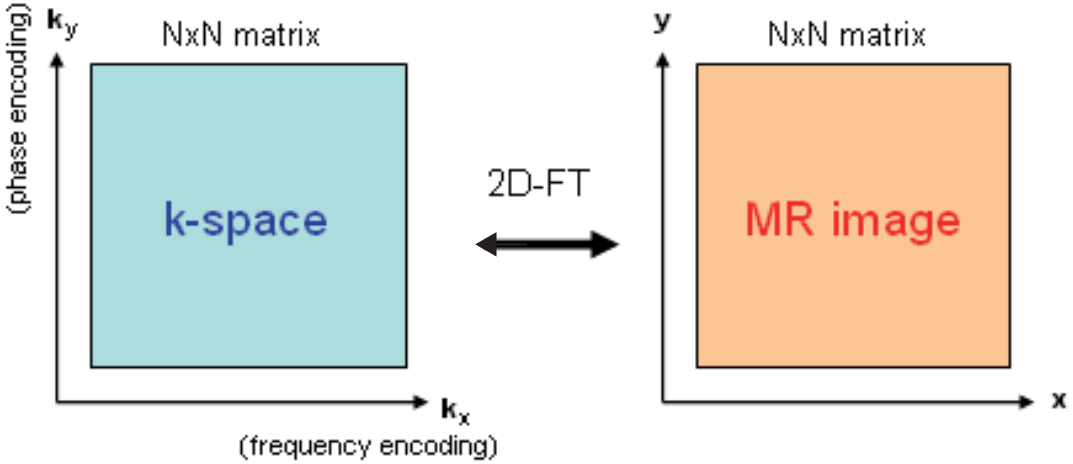

2D Fourier transformation

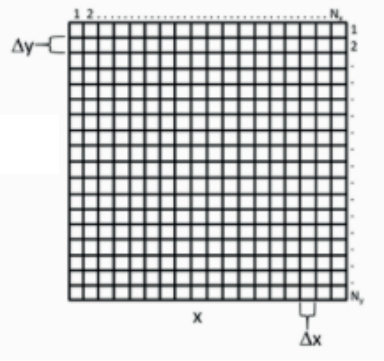

2D image in "coordinate space", x, y, presented in pixel grid

Field of view, FOV, in coordinate space:

$$(x_{\max} - x_{\min}, y_{\max} - y_{\min})$$

Pixel size (resolution):

$$\Delta x = \frac{x_{\max} - x_{\min}}{N_x}$$

$$\Delta y = \frac{y_{\max} - y_{\min}}{N_y}$$

2D Fourier transformation

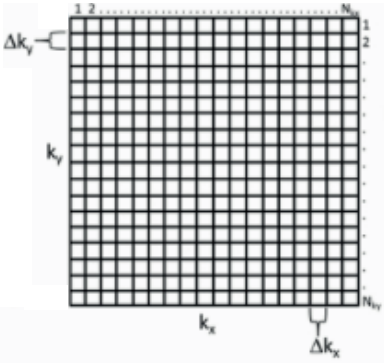

2D image in "k space", k_x, k_y, presented in pixel grid

Field of view, FOV, in k space:

$$(k_{x\,\max} - k_{x\,\min}, k_{y\,\max} - k_{y\,\min})$$

Pixel size (resolution):

$$\Delta k_x = \frac{k_{x\,\max} - k_{x\,\min}}{N_x}$$

$$\Delta k_y = \frac{k_{y\,\max} - k_{y\,\min}}{N_y}$$

2D Fourier transformation

Transformation between resolution in coordinate-space and k-space representations:

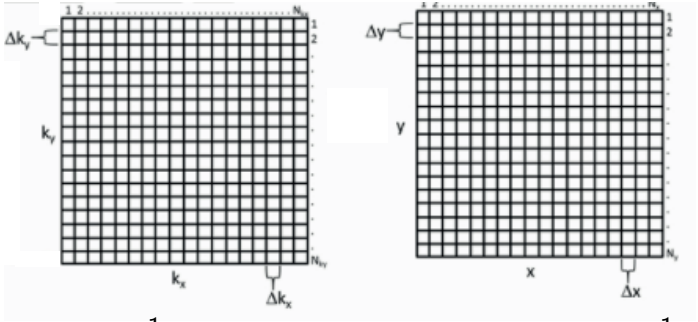

$$\Delta k_x = \frac{1}{(x_{\max} - x_{\min})} \qquad \Delta x = \frac{1}{(k_{x\,\max} - k_{x\,\min})}$$

$$\Delta k_y = \frac{1}{(y_{\max} - y_{\min})} \qquad \Delta y = \frac{1}{(k_{y\,\max} - k_{y\,\min})}$$

2D Fourier transformation

Define $\rho(x, y)$ to be the intensity pixel-by-pixel in coordinate space.

2D Fourier transform from coordinate to k space is then:

$$S(k_x, k_y) = \int_{y_{\min}}^{y_{\max}} \int_{x_{\min}}^{x_{\max}} \rho(x, y) \exp(-i2\pi k_x x) \exp(-i2\pi k_y y)\, dxdy$$

where $S(k_x, k_y)$ is the intensity pixel-by-pixel in k space

Inverse Fourier transform takes k-space intensity map to coordinate-space intensity map:

$$\rho(x, y) = \int_{k_{y\,\min}}^{k_{y\,\max}} \int_{k_{x\,\min}}^{k_{x\,\max}} S(k_x, k_y) \exp(i2\pi k_x x) \exp(i2\pi k_y y)\, dk_x dk_y$$

Example one: a single dot

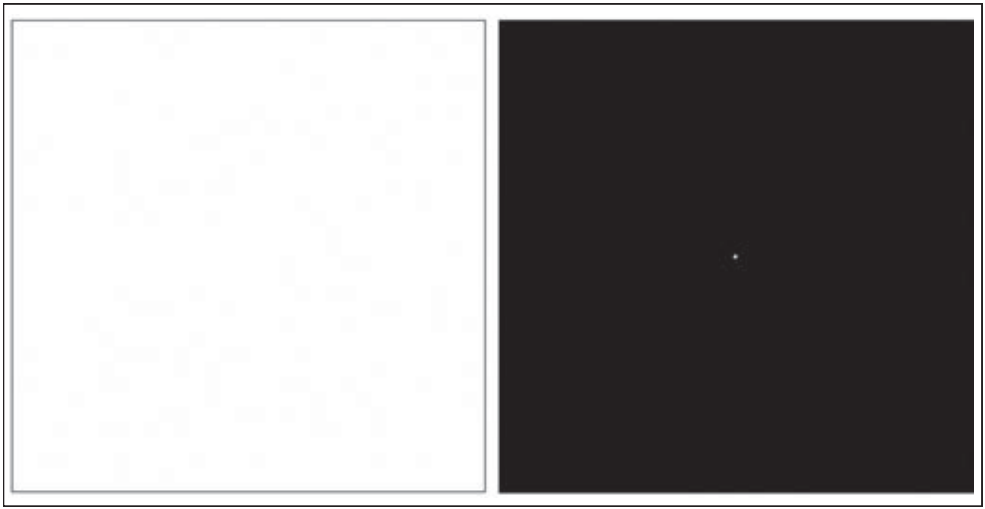

Example two: three dots

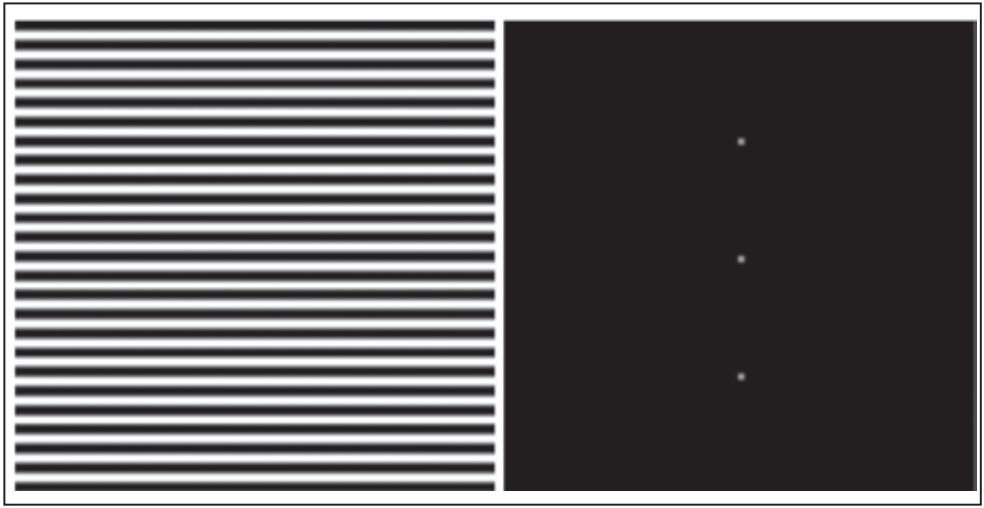

Example three: Square in centre of field of view

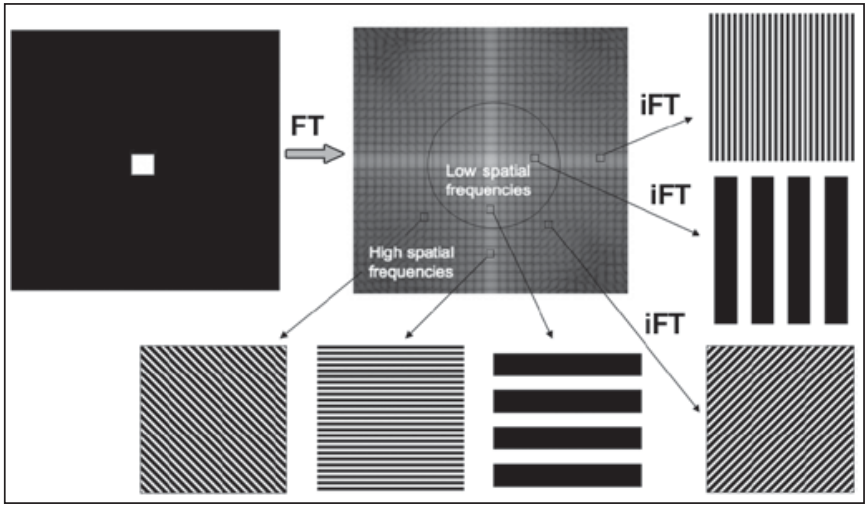

Example three: Abraham Lincoln

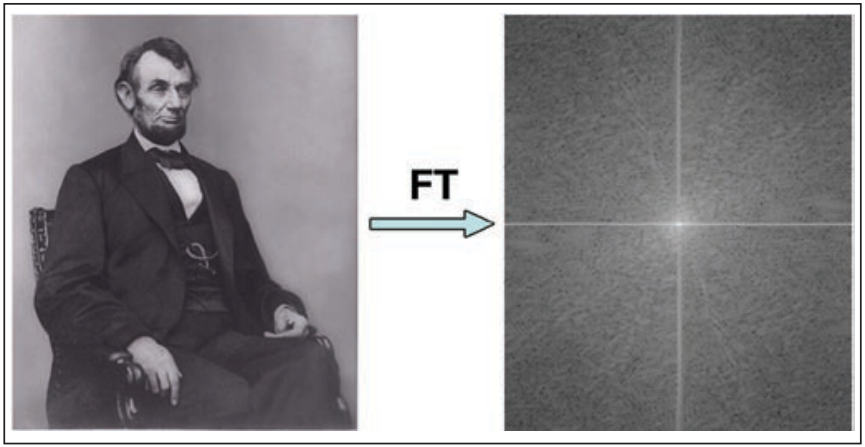

Example three: Abraham Lincoln

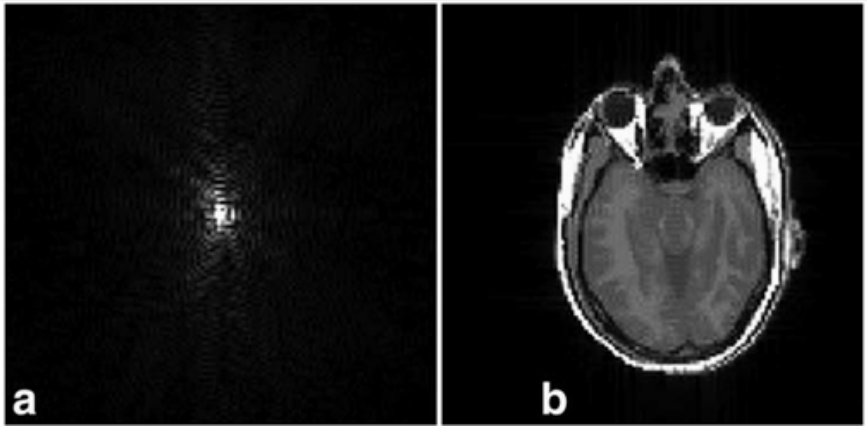

(a) k-space image of head

(b) coordinate-space image of head

Challenge: record k-space image using NMR signals

Spatial encoding and field gradients

Gradient pulse causes Larmor frequency to become a function of position

If a delay is introduced between application of gradient pulse and readout, then the phase of the nuclear precession will become a function of position

Exploit these features to:

- Encode x position into k_x via "frequency encoding"
- Encode y position into k_y via "phase encoding"

Remember, gradient pulses G_i are such that:

$$B_z(x, y, z, t) = B_0 + xG_x(t) + yG_y(t) + zG_z(t)$$

$G_x = \frac{\partial B_z}{\partial x}$; i.e. a magnetic-field gradient in x direction

magnetic field xG_x is in the $\hat{\mathbf{k}}$ direction

$G_y = \frac{\partial B_z}{\partial y}$; i.e. a magnetic-field gradient in y direction

magnetic field yG_y is in the $\hat{\mathbf{k}}$ direction

Conversion of field gradient into k space

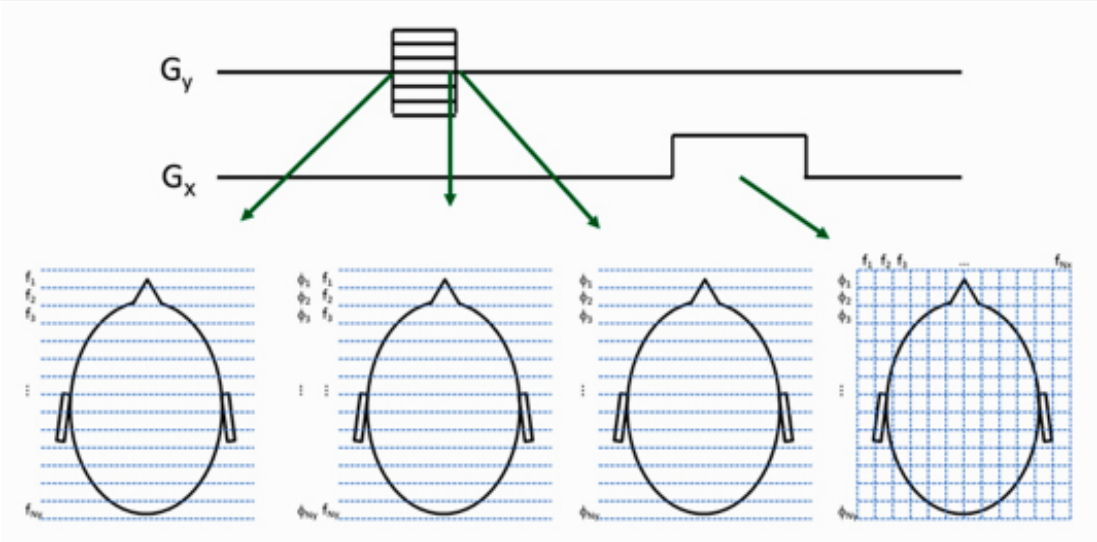

Conversion of field gradient into k space

Example:

phase encode y,

frequency encode x

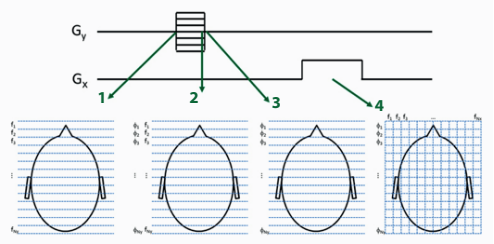

1. At start of phase encoding-pulse, spins are in phase. G_y causes Larmor frequency to be function of y: $\nu = f(y)$
2. At end of phase encoding pulse, phase of precession, ϕ, has become a function of y, i.e. $\phi \rightarrow \phi(y)$
3. As time passes, phase dependence on y is preserved, i.e. $\phi = \phi(y)$
4. Gradient pulse G_x causes Larmor frequency to become a function of x. Result is that y-position information is encoded in $\phi = \phi(y)$ and x-position information is encoded in $\nu = f(x)$

Spatial encoding gradient pulses part of pulse sequence

Example:

phase encode y,
frequency encode x

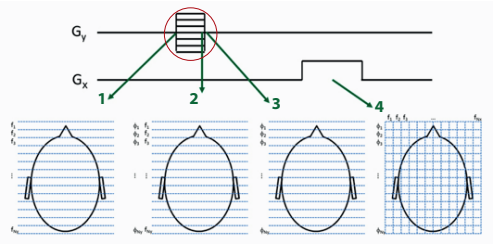

Phase- and frequency-encoding pulses part of a longer pulse sequence that repeats with period TR

At each repeat the amplitude of G_y, the phase-encoding pulse, has a different amplitude (as indicated on the figure)

For example:

- 1^{st} iteration of sequence: $G_y = 0$;
- 2^{nd} iteration of sequence: $G_y = +\eta$;
- 3^{rd} iteration of sequence: $G_y = -\eta$;
- ...

Example pulse sequence

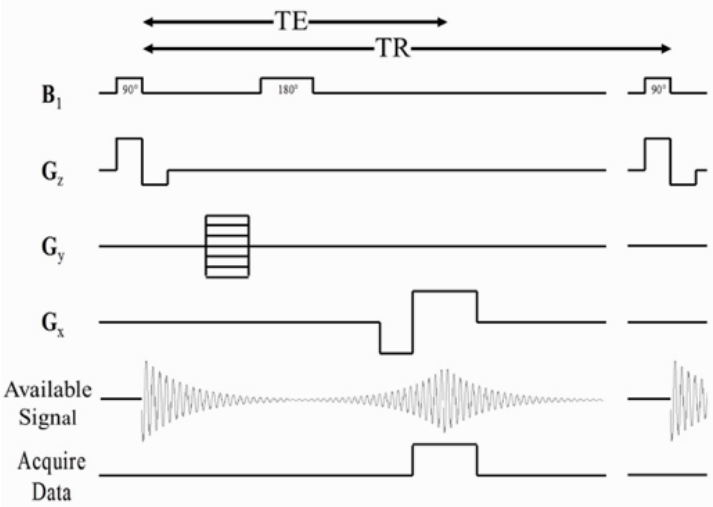

Example of spin-echo pulse sequence

Data is acquired at spin-echo time as shown

Combination of phase and frequency encoding pulses and repetition to obtain N_y data points completes ones transverse slice

Summary

Slice-selective excitation achieved using magnetic field gradient such that Larmor frequency becomes function of position

Spatial information is encoded into net magnetisation in k-space

2D Fourier transform used to transform image in k space to image in coordinate space

k-space image in slice is obtained using frequency and phase encoding

Pulse sequence is repeated to collect data for all $N_x \times N_y$ pixels of image

Generation of an MRI image

Tissue specificity in MRI is generated principally by three physical quantities:

- The net magnetisation at equilibrium, M_{eqm}:
  - This is a measure of "proton density";
  - Often referred to as proton density and M_{eqm} expressed as the fraction its value for water
- T_1: the spin-lattice relaxation time constant; and
- T_2: the spin-spin relaxation time constant

In a spin-echo sequence the time to repetition, TR, and the time to echo, TE, are adjusted to enhance the sensitivity of the signal amplitude to these three basic characteristics

The instantaneous signal intensity is proportional to the instantaneous magnitude of the magnetisation transverse to $\mathbf{B}_0$

This statement is **important** to get to grips with the generation of contrast in MRI

Pulse sequence; reminder

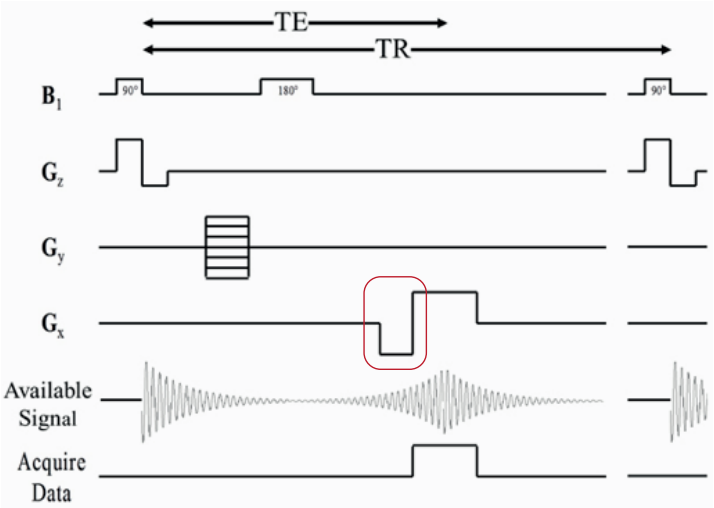

Note presence of "pre-winding pulse" circled in red

- Phase-encoding pulse causes phase to be position dependent
- Incoherence induces causes a loss of signal, so
- "Negative" gradient pulse applied in frequency encoding direction to "pre-wind" spins and cause an echo re-enforcing the signal at readout

Values of the basic parameters for a variety of tissues

Tissue	Proton density	1.5 T		3 T	
		T_1 ms	T_2 ms	T_1 ms	T_2 ms
Cartilage	0.94	1024	42	1168	37
Skeletal muscle	0.95	1084	37	1416	41
Blood	0.97	1441	308	1932	275
Fat	0.94	343	160	380	130
CSF	1.00	4550	60	4550	30
Brain matter (white)	0.99	688	81	833	68
Brain matter (grey)	1.00	1195	97	1436	93

Proton-density weighted image

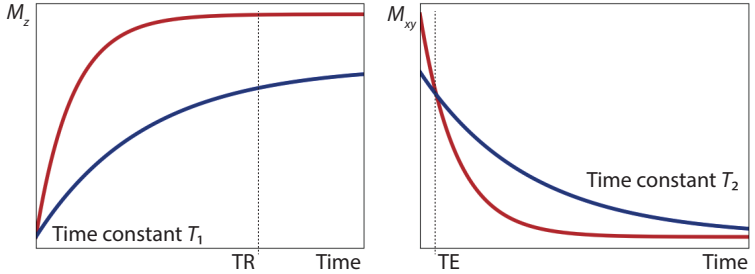

$B_0 = 3\,\mathrm{T}$; set $\mathrm{TR} = 2500\,\mathrm{ms}$ and $\mathrm{TE} = 10\,\mathrm{ms}$

	T_1 (ms)	$\frac{\mathrm{TR}}{T_1}$	T_2 (ms)	$\frac{\mathrm{TE}}{T_2}$	Relative brightness
Blood	1932	1.29	275	0.04	Medium
CSF	4550	0.55	30	0.33	Low
White matter	833	3.00	68	0.15	High
Grey matter	1436	1.74	83	0.12	Medium

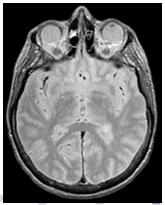

Proton-density weighted image

Tissue	Proton density	1.5 T		3 T	
		T_1 ms	T_2 ms	T_1 ms	T_2 ms
Cartilage	0.94	1024	42	1168	37
Skeletal muscle	0.95	1084	37	1416	41
Blood	0.97	1441	308	1932	275
Fat	0.94	343	160	380	130
CSF	1.00	4550	60	4550	30
Brain matter (white)	0.99	688	81	833	68
Brain matter (grey)	1.00	1195	97	1436	93

Proton-density weighted image:

- TR long: long enough that M_{eqm} is restored between repetitions
- TE short: such that effects of different $T2$ are not allowed to evolve

Such images have strong signal from all tissues, but relatively low contrast between them

T_1 weighted image

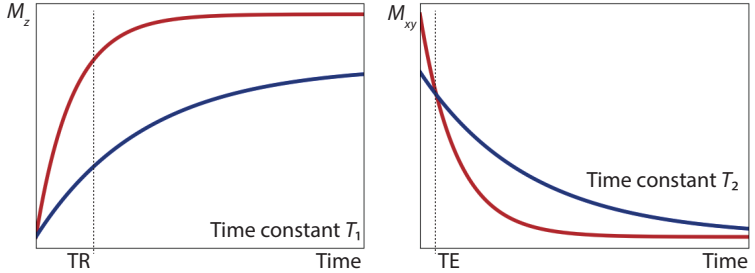

$B_0 = 3\,\mathrm{T}$; set $\mathrm{TR} = 500\,\mathrm{ms}$ and $\mathrm{TE} = 10\,\mathrm{ms}$

	T_1 (ms)	$\frac{\mathrm{TR}}{T_1}$	T_2 (ms)	$\frac{\mathrm{TE}}{T_2}$	Relative brightness
Blood	1932	0.25	275	0.04	Low/Medium
CSF	4550	0.11	30	0.33	Low
White matter	833	0.60	68	0.15	High
Grey matter	1436	0.35	83	0.12	Medium/Low

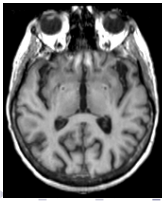

T_1 weighted image

Tissue	Proton density	1.5 T		3 T	
		T_1 ms	T_2 ms	T_1 ms	T_2 ms
Cartilage	0.94	1024	42	1168	37
Skeletal muscle	0.95	1084	37	1416	41
Blood	0.97	1441	308	1932	275
Fat	0.94	343	160	380	130
CSF	1.00	4550	60	4550	30
Brain matter (white)	0.99	688	81	833	68
Brain matter (grey)	1.00	1195	97	1436	93

T_1 weighted image enhancing signal from e.g. fat, white mater:

- TR short: such that M_{eqm} can only recover fully between repetitions in tissues with low T_1
- TE short: enough that the effects of different $T2$ are not allowed to evolve

Tissues such as fat appear bright in such images

T_2-weighted image

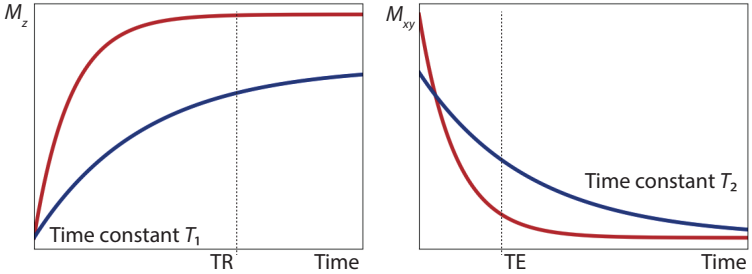

$B_0 = 3\,\mathrm{T}$; set $\mathrm{TR} = 2500\,\mathrm{ms}$ and $\mathrm{TE} = 100\,\mathrm{ms}$

	T_1 (ms)	$\frac{\mathrm{TR}}{T_1}$	T_2 (ms)	$\frac{\mathrm{TE}}{T_2}$	Relative brightness
Blood	1932	1.29	275	0.4	Medium
CSF	4550	0.55	30	3.3	High
White matter	833	3.00	68	1.5	Low
Grey matter	1436	1.74	83	1.2	Medium/Low

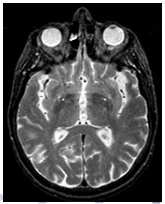

T_2-weighted image

Tissue	Proton density	1.5 T		3 T	
		T_1 ms	T_2 ms	T_1 ms	T_2 ms
Cartilage	0.94	1024	42	1168	37
Skeletal muscle	0.95	1084	37	1416	41
Blood	0.97	1441	308	1932	275
Fat	0.94	343	160	380	130
CSF	1.00	4550	60	4550	30
Brain matter (white)	0.99	688	81	833	68
Brain matter (grey)	1.00	1195	97	1436	93

T_2 weighted image enhancing signal from e.g. blood and CSF:

- TR long: long enough that M_{eqm} is restored between repetitions
- TE long: enough that the decay rates determined by $T2$ **are** allowed to evolve

"Tissues" such as blood & CSF appear bright in such images

Comparison of T_1, T_2, and proton-density weighting

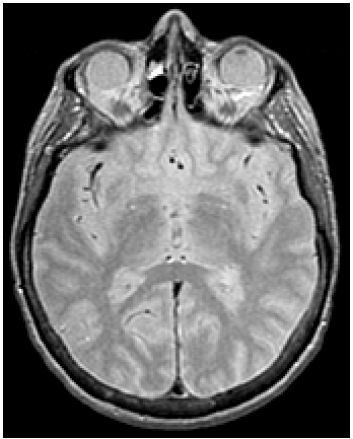

Proton-density weighted

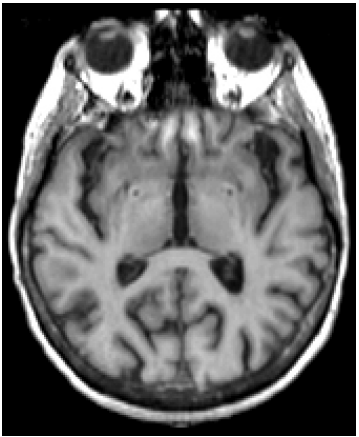

T_1 weighted

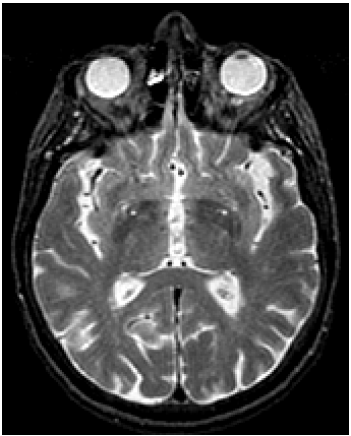

T_2 weighted

Inversion recovery pulse sequence; reminder

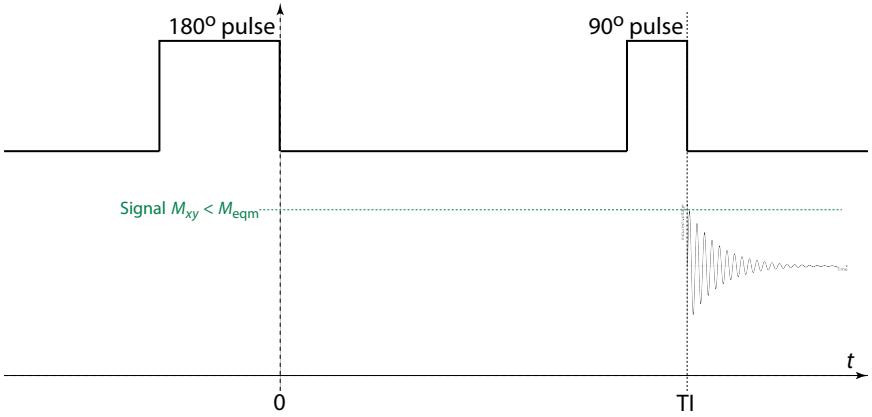

$$M_z(\mathrm{TI}) = M_{\mathrm{eqm}}\left[1 - 2\exp\left(-\frac{\mathrm{TI}}{T_1}\right)\right]$$

Advantages of inversion recovery

Inversion recovery provides contrast in three ways:

1. Suppress ("null") the signal from particular tissues
2. Enhanced T_1 contrast
3. Additive (rather than competitive) T_1 and T_2 effects

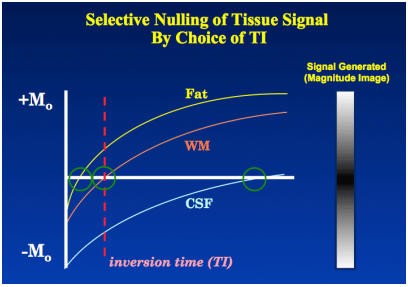

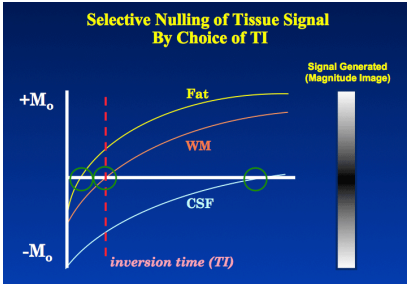

Advantages of inversion recovery

Inversion recovery provides contrast in three ways:

1. Suppress ("null") the signal from particular tissues
2. Enhanced T_1 contrast
3. Additive (rather than competitive) T_1 and T_2 effects

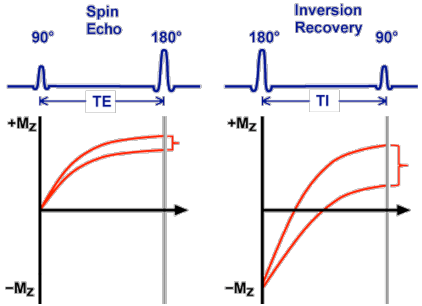

$$M_z(\mathrm{TI}) = M_{\mathrm{eqm}}\left[1 - 2\exp\left(-\frac{\mathrm{TI}}{T_1}\right)\right]$$

Advantages of inversion recovery

Inversion recovery provides contrast in three ways:

1. Suppress ("null") the signal from particular tissues
2. Enhanced T_1 contrast
3. Additive (rather than competitive) T_1 and T_2 effects

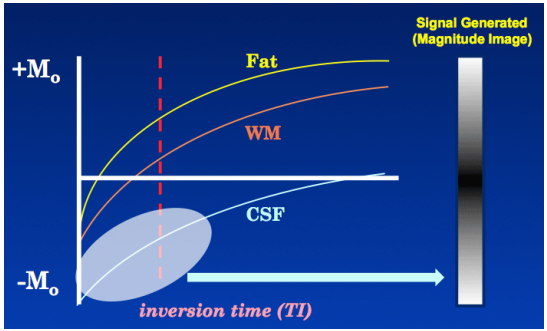

When TI is less than the "null point", the net magnetisation is the magnetisation of the tissues with long T_1 will remain inverted and enhance the transverse magnetisation the decay of which is characterised by T_2

Inversion recovery

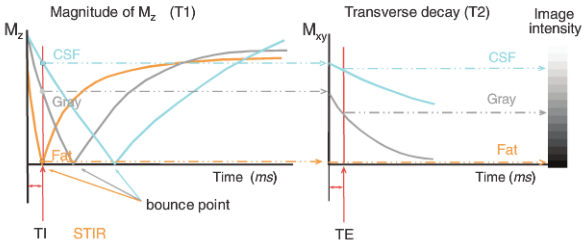

Short TI inversion recovery

Fluid attenuated inversion recovery

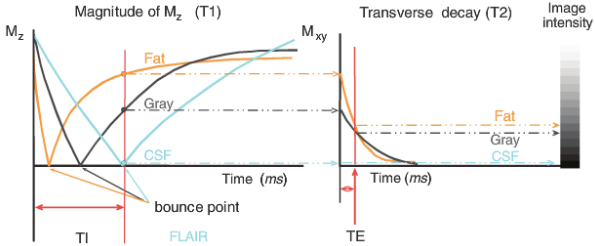

Inversion recovery image of brain

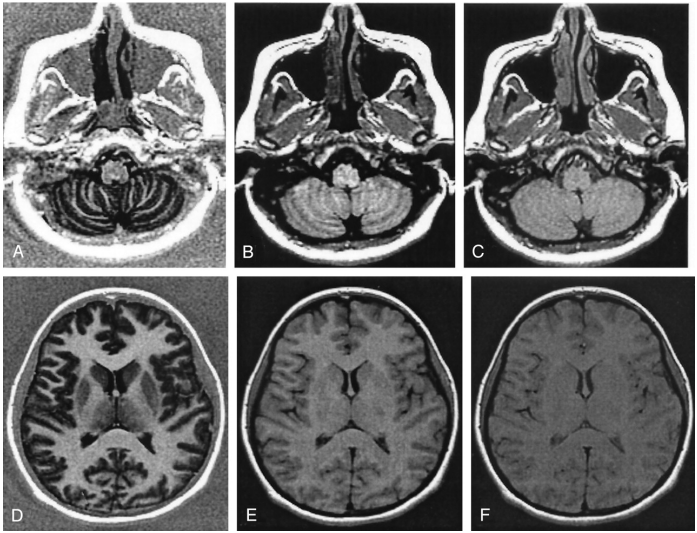

Question 1

What is the optimal TR to get maximum T_1 contrast between two tissues A and B for which the T_2 values are very similar and for which the T_1 values are $T_{1A} = 700\,\text{ms}$ and $T_{1B} = 900\,\text{ms}$?

Answer 1

We know:

$$M_z(\mathrm{TR}) = M_{\mathrm{eqm}}\left[1 - \exp\left(-\frac{\mathrm{TR}}{T_1}\right)\right]$$

and

$$M_{xy}(\mathrm{TE}) = M_{\mathrm{eqm}}\exp\left(-\frac{\mathrm{TE}}{T_2}\right)$$

So, the signal S may therefore be written:

$$S\left(\mathrm{TR}, \mathrm{TE}\right) = S_0\left[1 - \exp\left(-\frac{\mathrm{TR}}{T_1}\right)\right]\exp\left(-\frac{\mathrm{TE}}{T_2}\right)$$

Can now write down the difference between the signals from tissues A and B:

$$\Delta S = S_A - S_B$$

The maximum contrast will be when ΔS is maximised.

Answer 1, continued

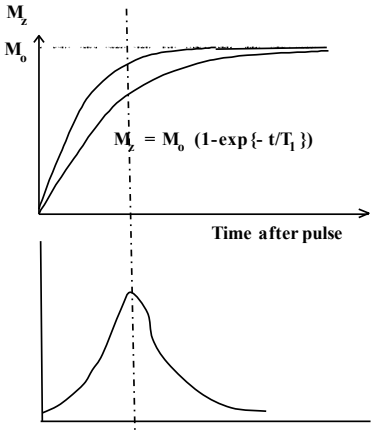

So, evaluate:

$$\frac{\partial \Delta S}{\partial \mathrm{TR}} = 0$$

And solve for $\mathrm{TR}_{\max}$ to show that:

$$\mathrm{TR}_{\max} = \ln\left(\frac{T_{1B}}{T_{1A}}\right)\frac{T_{1A}T_{1B}}{T_{1B} - T_{1A}} = 791.6\,\mathrm{ms}$$

Question 2

What inversion time, TI, should be used to "null" the response of a tissue for which $T_1 = 700\,\text{ms}$?

Answer 2

We know:

$$M_z(\mathrm{TI}) = M_{\mathrm{eqm}}\left[1 - 2\exp\left(-\frac{\mathrm{TI}}{T_1}\right)\right]$$

So, M_{xy} crosses zero when TI is equal to TI_0 given by:

$$\left[1 - 2\exp\left(-\frac{\mathrm{TI}_0}{T_1}\right)\right] = 0$$

This occurs when:

$$\mathrm{TI}_0 = T_1 \ln 2 = 0.69 \times 700 = 483\,\mathrm{ms}$$

Summary

The contrast of an MRI image is flexible, to find optimal settings require:

- Knowledge of tissue properties to determine sequence timings
- The impact of disease on relaxation time constants;

T_1 contrast is introduced through TR setting

T_2 contrast is introduced through TE setting

Inversion recovery sequence has advantages, for example in allowing selective de-excitation of tissue, at the cost of longer patient time in scanner

Artefacts in MRI

Ghosting due to total internal reflection of bright sources in optical photography

Just as in optical photography, artefacts are unwanted image features

Artefacts arise from many causes:

- Field imperfections (not addressed below)
- Movement of patient or organ
- Magnetic material (e.g. from bone repairs)
- Chemical composition uncertainties

My objective is to give examples, there is an extensive literature on the subject

Reconstruction of the MR image; reprise

Gradient pulses G_i are used to allow slice-selective excitation and to allow spatial information to be encoded into the net magnetisation:

$$B_z(x, y, z, t) = B_0 + xG_x(t) + yG_y(t) + zG_z(t)$$

Spatial information is encoded into net magnetisation in k-space, often:

- Frequency encoding is used to encode features in the x direction
- Phase encoding is used to encode features in the y direction

2D Fourier transform used to transform image in k space to image in coordinate space

Pulse sequence is repeated to collect data for all $N_x \times N_y$ pixels of image

Spin-echo sequence; reprise

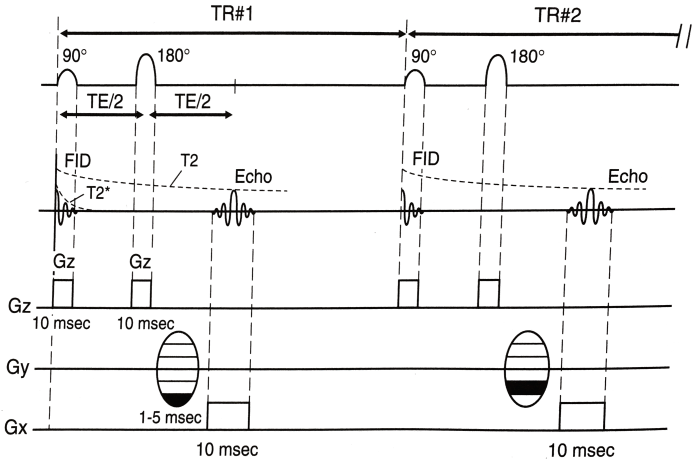

Readout occurs when frequency-encoding pulse (G_x) is on (T_S, the sampling time)

Each repetition corresponds to a new G_y, i.e. a new encoding of phase

Take N_y repetitions to fill N_y rows in the image

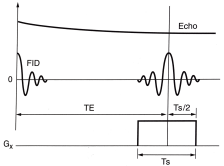

Phase encoding; reprise (1 of 3)

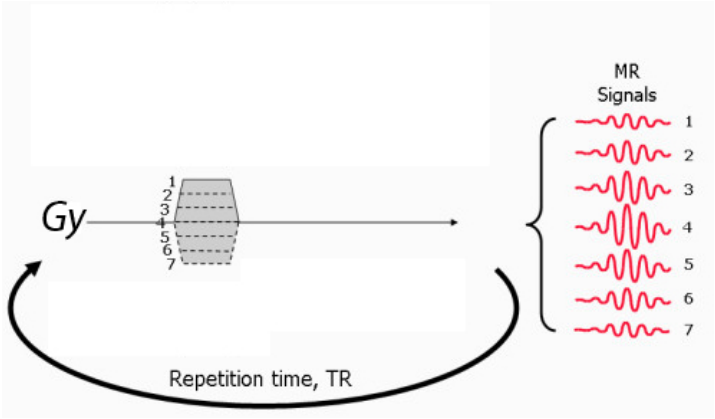

Central line in k-space will contain phase-encoding step with weakest gradient and strongest signal

Periphery of k-space sill contain phase-encoding steps with the strongest gradients and weakest signal

Each slice "has its own k-space because excitation is tuned to G_z

Phase encoding; reprise (2 of 3)

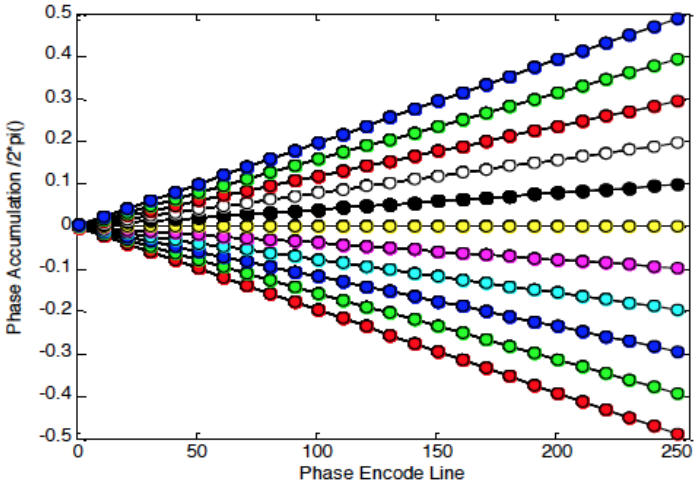

Phase wrt $y = 0$ accumulates with time, t, while phase-encoding gradient, G_y, is on:

$$\Phi(G_y, y, t) = (\gamma G_y)\, yt \qquad (3)$$

The slope of the line in the figure is determined by y

I.e. the rate of change of phase (frequency) is given by:

$$\frac{\Delta\Phi}{\Delta t} = (\gamma G_y)\, y$$

2D Fourier transform revisited

If the phase-encoding pulse is of length τ_{pe}, then the change of phase of the spins relative to $y = 0$ at the end of the pulse will be given by:

$$\frac{\Delta\Phi}{\Delta y} = (\gamma G_y \tau_{pe})$$

Lets take the start of the frequency-encoding pulse, G_x, to be at $t = 0$, then, the phase advance of ^{1}H nuclei at x after time t will be:

$$\phi(G_x, x, t) = (\gamma G_x) xt \qquad \text{i.e.} \qquad \frac{\Delta\phi}{\Delta x} = (\gamma G_x) t$$

As in lecture 10, let $\rho(x, y)$ be the intensity pixel-by-pixel in coordinate space, then the signal S will be given by:

$$S\left(G_y, \tau_{pe}, G_x, t\right) = \int_{y_{\min}}^{y_{\max}} \int_{x_{\min}}^{x_{\max}} \rho\left(x, y\right) \exp\left[-i\left(\gamma G_x t\right) x\right] \exp\left[-i\left(\gamma G_y \tau_{pe}\right) y\right] dxdy$$

2D Fourier transform revisited

In lecture 10, 2D Fourier transform from coordinate to k space was given as:

$$S(k_x, k_y) = \int_{y_{\min}}^{y_{\max}} \int_{x_{\min}}^{x_{\max}} \rho(x, y) \exp(-i2\pi k_x x) \exp(-i2\pi k_y y)\, dxdy$$

where $S(k_x, k_y)$ is the intensity pixel-by-pixel in k space

If we identify:

$$\begin{aligned} k_x &= \frac{\gamma}{2\pi} G_x t \\ k_y &= \frac{\gamma}{2\pi} G_y \tau_{pe} \end{aligned}$$

then:

$$S(k_x, k_y) = S(G_y, \tau_{pe}, G_x, t)$$

And the measured signal, S, is the k-space representation of the coordinate-space intensity ρ

Phase encoding; reprise (3 of 3)

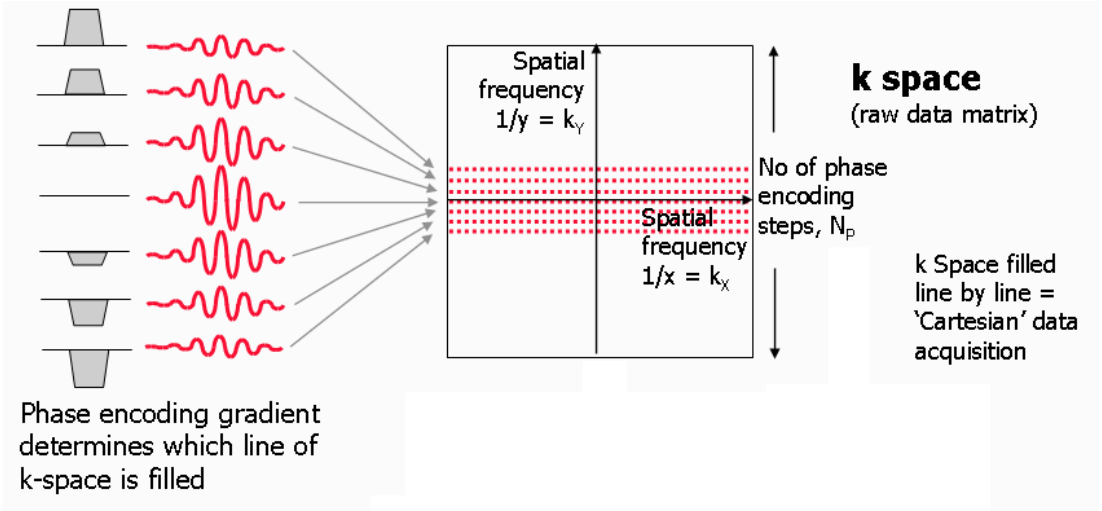

In summary

The slice is selected by tuning the RF frequency and G_z

The k_x coordinate is obtained from frequency encoding **at readout**

The k_y coordinate is obtained from phase encoding **"passively" by manipulating phase during free induction decay (FID)**

Trial: square centred at $(x, y) = (0, 0)$

Consider spatial encoding, x, direction

Coordinate space

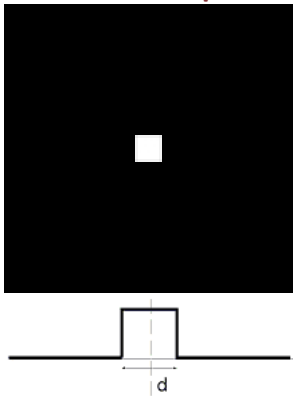

$$S(x) = \begin{cases} S_0 & \text{for } -\frac{d}{2} < x < \frac{d}{2} \\ 0 & \text{otherwise} \end{cases}$$

k space

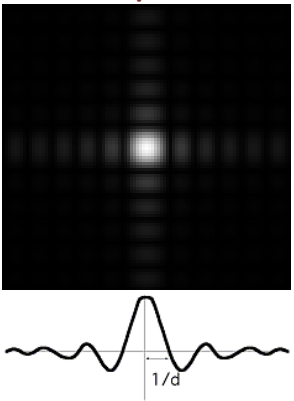

$$S(\Delta k_x) = S_0' \text{sinc}(\Delta k_x)$$

Sampling of the signal recorded along k_x

The Fourier transform of "sinc" function will give "box" function if all Δk_x are sampled

But, sinc function is only sampled at intervals of Δk_x

This means that Fourier transform of the sampled sinc function generates a series of (distorted) images of the box:

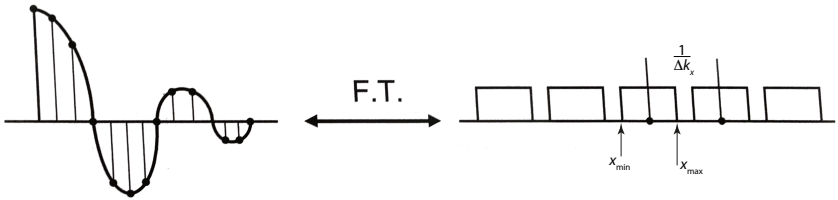

Sequence truncated at field of view

Sampling of the signal recorded along k_x

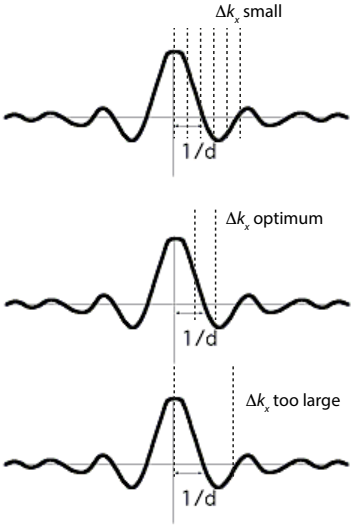

Nyquist theorem:
To reconstruct a bandwidth limited signal, require to sample the highest frequency that the signal contains at least twice

In our case, the bandwidth is limited by the truncation of the sinc function by the field of view in k space

At limit of resolution, box functions are "just separated"

If sampling rate is too low, $\Delta k_x > \frac{2}{2\pi(x_{\max} - x_{min}}$), the boxes overlap and aliasing occurs

Aliasing

Image of head with appropriate sampling rate (field of view)

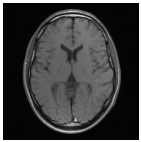

Truncated field of view yields sampling rate that is too low . . .

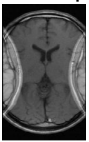

. . . and leads to aliasing

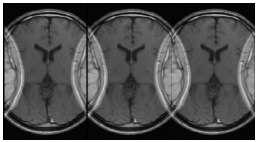

Aliasing (wraparound)

Image of head with appropriate sampling rate (field of view)

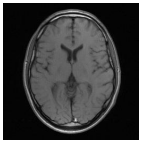

Truncated field of view yields sampling rate that is too low . . .

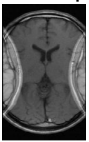

. . . and leads to aliasing

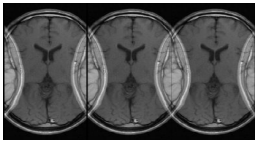

Effect of truncation in k space

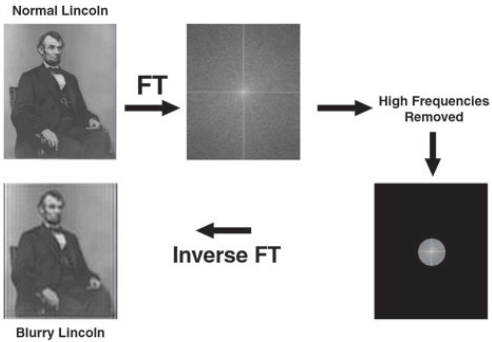

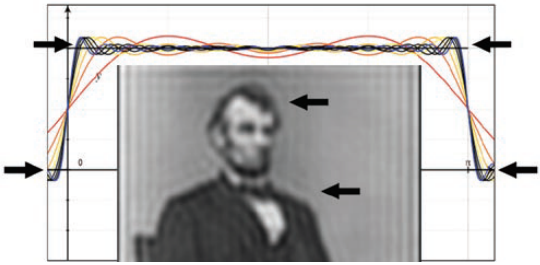

The Gibbs phenomenon

Artefact occurs at interfaces between tissues which have a rapid change in signal . . . "high contrast interfaces"

E.g. skull to brain

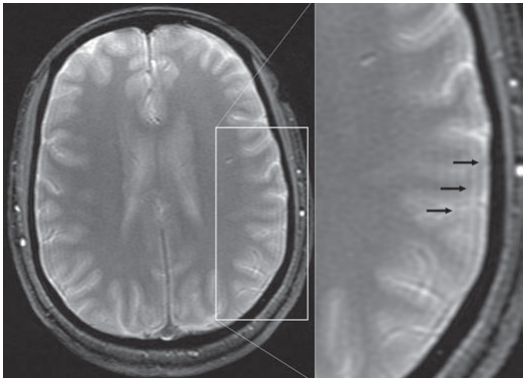

Motion artefacts; general comments

Motion artefacts most commonly observed in the phase-encoding direction

This is because:

- Motion along any field gradient results in the abnormal integration of phase, which is then incorrectly mapped onto the phase-encoding direction
- Frequency encoding is performed while G_x gradient pulse is on; typically for around 10 ms. Only very modest displacements can occur in such a short time. The result is that random displacements in the frequency-encoding direction lead to blur
- By contrast, displacements due to motion can build up between phase-encoding pulses, G_y, as these occur at intervals of TR . . . and TR can range from, e.g. 500 ms to a second or so

Example: displacement along x

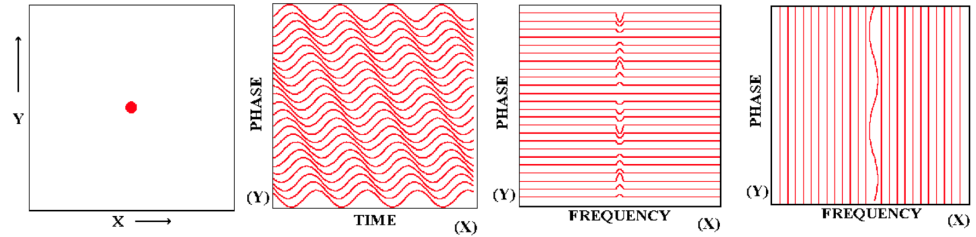

Example: displacement along x – continued

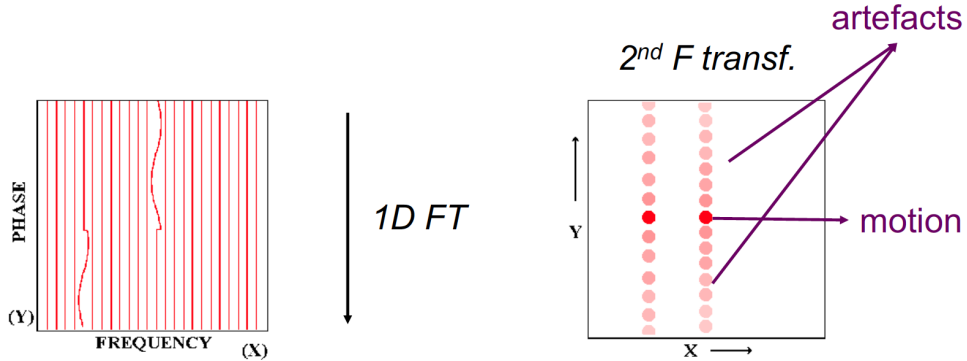

Displacement artefacts: questions 1

What causes the artefacts seen in the following images?

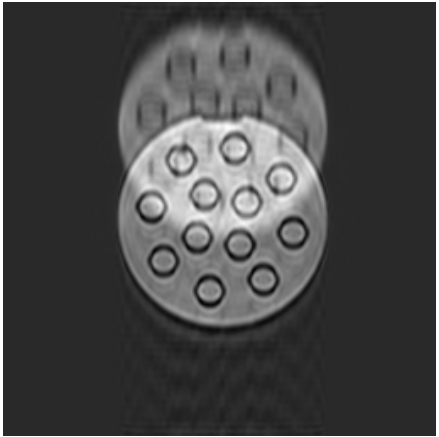

Displacement artefacts: questions 2

What causes the artefacts seen in the following images?

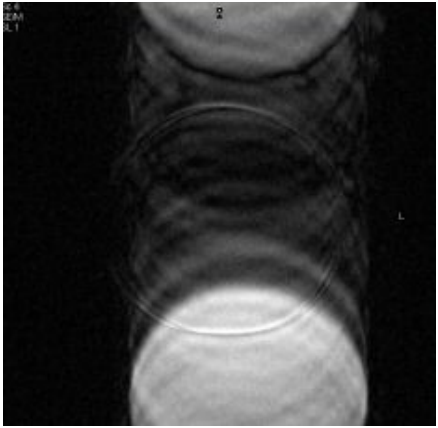

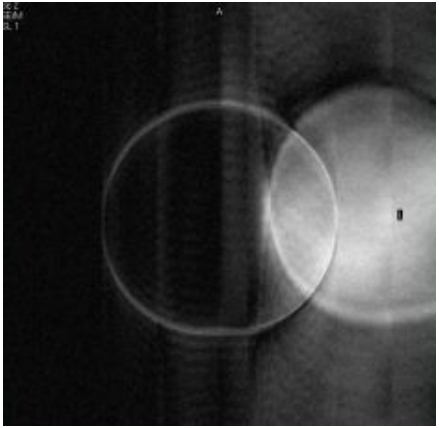

Summary

Spatial encoding, key facts:

- The slice is selected by tuning the RF frequency and G_z
- The k_x coordinate is obtained from frequency encoding **at readout**
- The k_y coordinate is obtained from phase encoding **"passively" by manipulating phase during free induction decay (FID)**

Aliasing (wraparound) artefact:

- Related to limited field of view;
- Spatial frequencies $k_i < k_{i\,\min}$ or $k_i > k_{i\,\max}$ wraparound and appear at $k_{i\,\max} - k_i$ or $k_{i\,\min} + k_i$ respectively

Summary

Gibbs artefact (truncation artefact): removal of high k_i leading to:

- Loss of definition at edges of features;
- Striations in the neighbourhood of edges at which there is a large step in brightness

Random motion artefacts:

- Most often occur in the phase-encoding direction;
- Often associated with ghosting in the phase-encoding direction

Spatial encoding, reprise

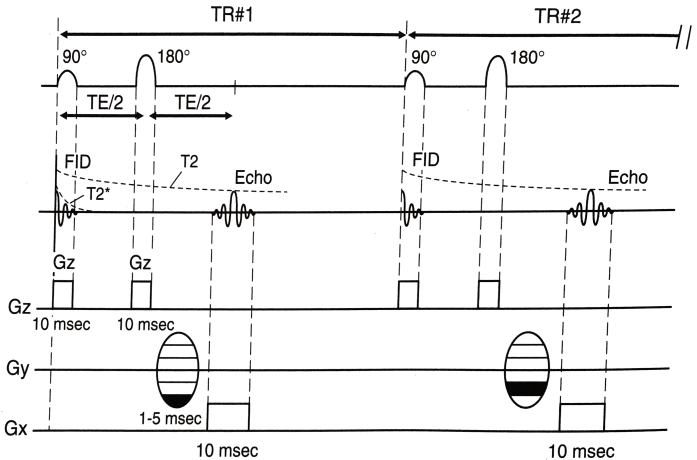

Signal, S: $S = S(G_x, t, G_y, \tau_{pe})$

Frequency encoding in x direction:

$$\phi(G_x, x, t) = (\gamma G_x x)\, t$$

Phase encoding in y direction:

$$\Phi(G_y, y, \tau_{pe}) = (\gamma G_y y)\, \tau_{pe}$$

Transformation to k space:

$$k_x = \frac{\gamma}{2\pi} G_x t$$
$$k_y = \frac{\gamma}{2\pi} G_y \tau_{pe}$$

$$S(G_y, \tau_{pe}, G_x, t) = S(k_x, k_y) = \int_{y_{\min}}^{y_{\max}} \int_{x_{\min}}^{x_{\max}} \rho(x, y) \exp[-i(\gamma G_x t)\, x] \exp[-i(\gamma G_y \tau_{pe})\, y]\, dxdy$$

Periodic motion; overview

Organs that undergo periodic motion include the heart, aorta, ...

Frequency encoding takes place over a period of $\sim 10\,\text{ms}$ when the G_x pulse is on. This corresponds to a frequency of 100 Hz; i.e. 100 cycles *per second*. Such rapid oscillations are not present in the body. Oscillations at the frequency of the heart beat, for example, lead to only small excursions while G_x is on and so lead to minor loss of detail in the image

The process of phase encoding requires multiple (N_y) repetitions to complete. While the G_y pulse itself is short, it is repeated at time intervals equal to TR

The time period relevant for phase encoding, therefore, is TR. A typical value for TR is 500 ms, corresponding to a frequency of 2 Hz. Many structures in the body, for example the heart, execute periodic motion with period comparable to TR

Periodic-motion artefacts, therefore, occur in the phase-encoding direction

Periodic motion artefact

The phase, Φ, used for spacial encoding in the phase-encoding direction is given by:

$$\Phi(G_y, y, \tau_{pe}) = (\gamma G_y y)\, \tau_{pe}$$

If the position, y of a feature undergoes periodic motion, then:

$$y \rightarrow y' = y + d_0 \sin \omega_{pma} t$$

And so the phase that enters the phase-encoding equation becomes a function of the "periodic motion artefact" frequency ω_{pma}:

$$\Phi(G_y, y, \tau_{pe}) \rightarrow \Phi'(G_y, y, \tau_{pe}, \omega_{pma}) = \left(\gamma G_y y'\right) \tau_{pe} = 2\pi k_y y' = 2\pi k_y \left(y + d_0 \sin \omega_{pma} t\right)$$

Addition of phase, leads to displacement in k space

Periodic motion artefact

In considering the impact of the additional phase added by periodic motion, we must remember that coordinate space is represented across the k space

Consider again the square at the centre of coordinate space

Coordinate space

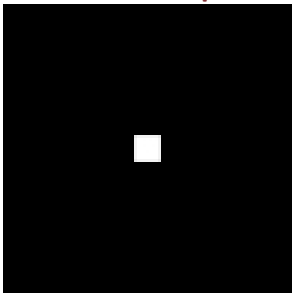

k space

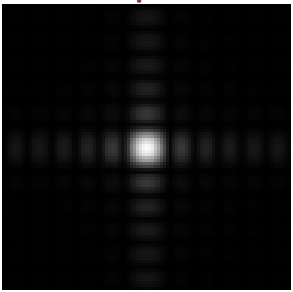

The result of the additional phase is to shift the whole pattern in k space

Periodic motion artefact

For a complete treatment, we need to look at the impact of Φ' on the encoding equation ...

Instead, lets consider the modulation of the phase-encoding pattern that results from the periodic motion

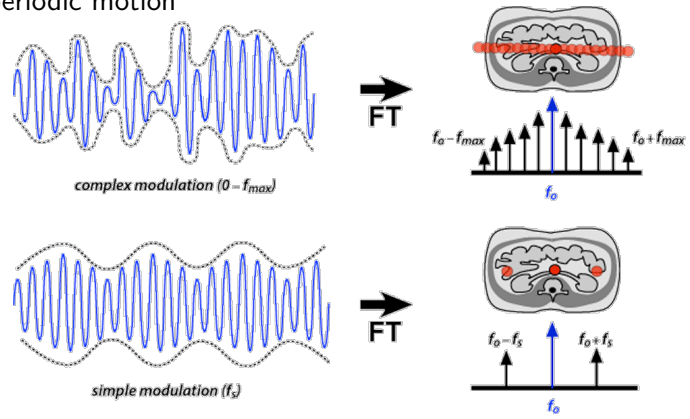

The amplitude of the periodic shift in the y direction generated by the periodic motion is given by:

$$\delta y = \frac{\mathrm{TR}}{\tau_{pma}} \left[y_{\max} - y_{\min} \right]$$

Periodic motion: breathing and heart beat

Image of chest showing ghosting arising from breathing and heart beat

Respiratory motion causes a number of distinct images of the chest wall

Cardiac motion, more complex and multi-facetted, results in the column of overlaping images to the right of centre

In general, the more rapid the motion, the more widely spread will be the ghosts:

$$\delta y \propto \frac{1}{\tau_{pma}}$$

Periodic motion: problem

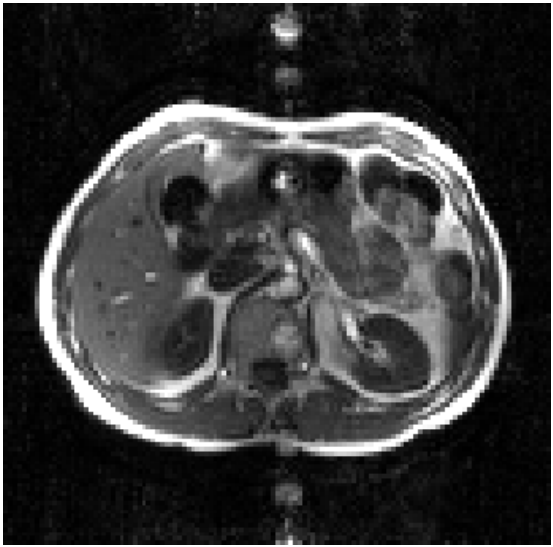

The periodic motion artefact in the image facing is caused by the periodic motion of a small region of the scan plane The imaging

parameters that were used were TE= 40 ms and TR= 100 ms

1. Estimate the period of the movement from the separation of the ghosts (assume that the field of view is 40 cm).
2. What structure in the body might give rise to this repeating feature?
3. Identify the position of the primary source of the artefact in the image.

Answer will be given in the answers to the second problem sheet.

Origin of the chemical shift artefact

The chemical shift artefact occurs when the chemical environment causes the precessional frequency for ^{1}H nuclei in different molecules to differ

The artefact can arise at tissue boundaries or can be due to a particular tissue being composed of a variety of molecules each of which contribute significantly to the signal

Consider for example, the precessional rates of ^{1}H in water and in fat in a magnetic field of 1.5 T:

- The gyromagnetic ratio for ^{1}H in water differs from that in fat by 3.5 ppm
- For water, at 1.5 T, the Larmor frequency is given by $\nu_w = \gamma B_0 = 42.6 \times 1.5 = 64\,\text{MHz}$
- 3.5 ppm of ν implies a "chemical shift" in the Larmor frequency of fat of $3.5 \times 10^{-}6 \times 64 \times 10^6 = 220\,\text{Hz}$
- ν_{fat} is larger than ν_w by 220 Hz at 1.5 T

Magnitude of the chemical-shift artefact

Consider an image that has $N_x = 256$ pixels in the x direction and for which the sampling time over which the frequency-encoding pulse G_x is on is 8 ms

Under these conditions, the bandwidth, BW, corresponding to the full x-coordinate range is:

$$\mathrm{BW} = \frac{N_x}{T_S} = \frac{256}{8 \times 10^{-3}} = 32\,\mathrm{kHz}$$

This meams that the frequency step per pixel, Δf is given by:

$$\Delta f = \frac{\mathrm{BW}}{N_x} = \frac{32 \times 10^3}{256} = 125\,\mathrm{Hz}$$

We see that Δf is smaller than the chemical shift between the Larmor frequency for fat and water at 1.5 T

Chemical shift example 1: vertebrae

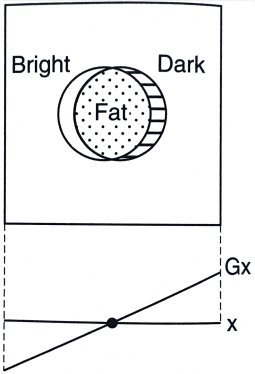

Circle of fat in water volume. Chemical shift causes fat contribution to be displaced towards lower x. Result: a bright band on one side of the fat body (signals from the water and fat overlap), dark band on the other side

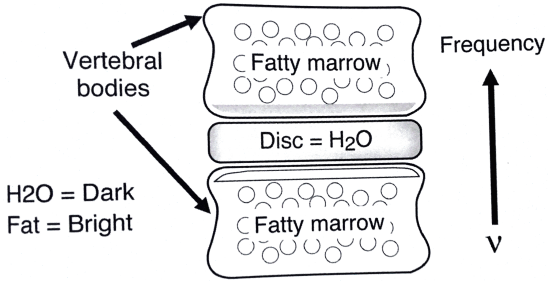

Dark band observed at bottom of "upper" fatty marrow

Bright band observed at top of "bottom" fatty marrow

Chemical shift example 2: voxel sharing water and fat

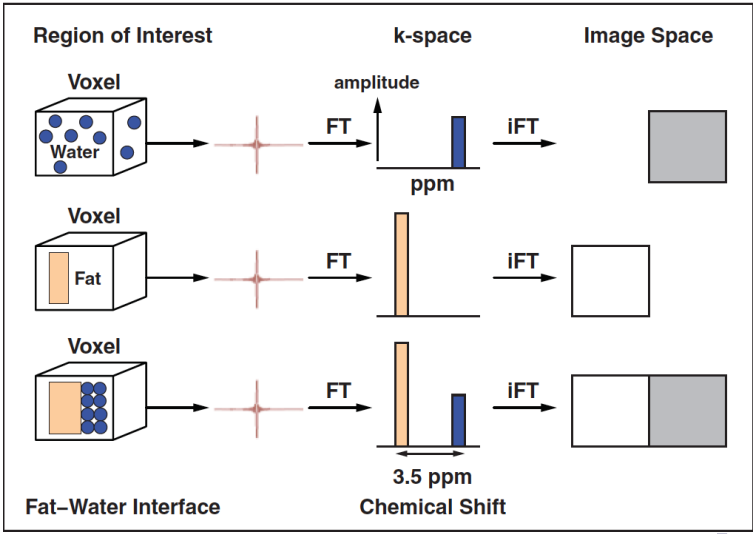

Chemical shift example 2: voxel sharing water and fat

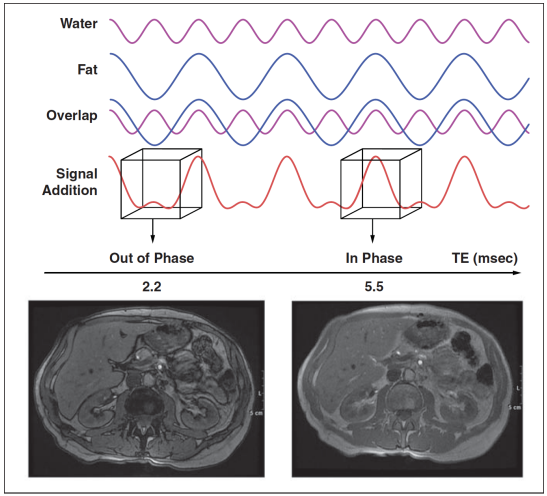

Signal from fat and water is out of phase when TE= 2.236 ms. Signals from fat and water in single voxel therefore interfere destructively. Result is a dark band surrounding fat-water interfaces

At TE= 5.516 ms, signals are back in phase and constructive interference occurs restoring normal contrast

The exam

Imperial College London

BSc/MSci EXAMINATION May 2020

This paper is also taken for the relevant Examination for the Associateship

MEDICAL IMAGING : ND & MRI

For Third and Fourth-Year Physics Students

13 May 2020: 10:00 to 11:15

The paper consists of two sections A & B.
Section A contains two questions [20 marks each]
Section B contains four questions [5 marks each]

*Candidates are required to answer **ALL** parts of Section A and **TWO** questions from Section B.*

Marks shown on this paper are indicative of those the Examiners anticipate assigning.

General Instructions

At the top of each page of your answers, write your CID number, module code, question number and page number. Scan and upload your answers to the Turnitin dropboxes as described in the guidance documents in the Blackboard module for this exam. Upload each answer to the dropbox provided for that specific question.

Your uploaded file name should be of the form CID_ModuleCode_QuestionNumber(s).pdf

For each answer you should prepare a coversheet which should be the first page of your scanned answer. The coversheet should contain the following:

- your CID
- module name and code
- the question number
- the number of pages in your answer

You should not write your name anywhere on your answers.

You are reminded that Examiners attach great importance to legibility, accuracy and clarity of expression.

[Examination instructions continue on next page. . .]

2020 ND&MRI exam—rubric same as in previous years

Section A — compulsory

- 1 question on nuclear diagnostics – from lectures 1 to 6
- 1 question on MRI – from lectures 7 to 13

Section B — also compulsory

- 2 questions on nuclear diagnostics – from lectures 1 to 6
- 2 questions on MRI – from lectures 7 to 13

Summary

Periodic motion artefact:

- Occur in phase-encoding direction
- Shifts observed result from periodic displacement of response in k space
- Magnitude of periodic shift in y coordinate $\propto \frac{1}{\tau_{pma}}$
  [τ_{pma} is the period of the periodic motion]

Chemical shift artefact:

- Occurs when two tissues, or components of tissue, have closely similar Larmor frequencies
- Can be mitigated using timing in, e.g., spin-echo sequence